Kinetic Roughening of Interfaces in Driven Systems

by

Bruno Grossmann
Department of Physics, McGill University
Montréal, Québec
Canada

A Thesis submitted to the
Faculty of Graduate Studies and Research
in partial fulfillment of the requirements for the degree of
Doctor of Philosophy

A la bidouce,

Abstract

We study the dynamics of an interface driven far from equilibrium in three dimensions. We first derive the equations of motion which describe this physics. Numerical results are then obtained for three models which simulate the growth of an interface: the Kardar-Parisi-Zhang equation, a discrete version of that model, and a solid-on-solid model with asymmetric rates of evaporation and condensation. We show that the three models belong to the same dynamical universality class by estimating the dynamical scaling exponents and the scaling functions. We confirm the results by a careful study of the crossover effects. In particular, we propose a crossover scaling ansatz and verify it numerically. Furthermore, the discrete models exhibit a kinetic roughening transition. We study this phenomenon by monitoring the surface step energy which shows a drastic jump at a finite temperature for a given driving force. At the same temperature, a finite size scaling analysis on the bond energy fluctuation shows a diverging peak.

Résumé

Nous avons etudié la dynamique d'une interface hors de son état à l'équilibre. Pour ce faire, nous avons utilisé trois modèles qui simulent la croissance d'une interface, soit l'équation de Kardar-Parisi-Zhang, une version discrète de cette même equation, et un modèle solide-sur-solide possédant un taux de croissance différent du taux d'évaporation. Nous montrons d'abord comment l'on obtient cette equation du mouvement. Nous prouvons que ces trois modèles appartiennent à la même classe dynamique d'universalité en montrant que leurs exposants et leurs fonctions d'échelle sont égaux. De plus, nous vérifions cette affirmation en estimant les exposants de transfert. Nous avons en particulier numériquement estimé la fonction de transfert, et vérifié qu'elle satisfaisait la forme que nous avions proposé. Par ailleurs, nous avons remarqué que les modèles discrets exhibaient une transition rugueuse cinétique. Nous avons étudié ce phénomène en calculant l'énergie d'un pas en fonction de la température. Nous avons ainsi détecté la présence d'une variation très importante de cette énergie à une température finie qui dépend du flux incident à la surface. Enfin, nous avons détecté la présence d'une divergence dans les fluctuations de l'énergie.

Acknowledgements

A long time ago, a student arrived in the prestigious department of physics of McGill university, where he hoped to end his quest by the completion of a mysterious Enchantment, otherwise known as Ph.D. Thesis. He was greeted by his Master-to-be, a benevolent, bright Enchantor, Martin Grant, known as the Wizard of nonequilibrium statistical mechanics; by other Enchantors, all very amiable; by more senior students: Chris, the Master of spinodal decomposition, Diane, the voronoi Enchantress, Loki, the Wizard of dendrites, Mohamed, the Magician of surfactants, Ross, the Master of visual cortex, Ahmed, the mesoscopic Sorcerer,Tony, the Master of X-rays and Bertrand, the unfortunate third floor student (since then turned into a more fortunate fourth floor student by the magic of Phase Transitions); and by the Helpers of the Enchantors. All were very nice to him and made him feel comfortable. Then started the long period of the Enchantment, during which he slowly learned the trades of being a physicist. He met many obstacles, but was greatly helped by other students, in the department for the same purpose as he was: Eugenia, the Princess of lipid bilayers, Ian, the multispin Coder, Jianhua, the Master of nucleation, Ken the Wizard of models A, B and C, Martin, the Prince of Monte Carlo renormalization group in space and time, Tao the Magician of Feynman diagrams; and also Geoff the guitar-playing Thinker, Jacques the Master of Physics at night, Ming,Yan and Tianqu the badminton Sorcerers, Steve the Experimentalist, Nick the Questionner, Philippe the Singer and "animal Impersonator", and many, many others. Ultimately, after a long struggle, the end was near. Yet, another quest is to come... more important and difficult than the ones he has had to face before... the quest for a job. Will the student *ever complete this last quest successfully?*

Cast

The student..........Bruno
The princess..........Delphine
The other actors..........Themselves

Special thanks to: Martin Grant for being bright <u>and</u> nice to me; Chris, Ross, Diane, Loki, Ahmed, Mohamed,Tony and Bertrand for welcoming me upon my arrival; Eugenia, for her intellectual honesty and the heated discussions that accompany this quality; Jianhua, for introducing me to some elements of the Chinese culture and at the same time becoming my friend; Martin, for not treating me as a "maudit francais" (and, I hope, not regretting it afterward!); Ian and Ken, for being postdocs that actually interact with students; Tao and Hong for introducing me to the subtilities of the renormalization group method. And of course, all the other people whose names are not in this list.

The financial support of NSERC, FCAR and my wife was greatly appreciated.

Contents

Abstract iii

Résumé iv

Acknowledgements v

List of Figures ix

1 Introduction 1

2 Models of a Growing Interface 11
- 2.1 Introduction to the statistical mechanics of equilibrium interfaces . . 12
- 2.2 The Kardar-Parisi-Zhang (KPZ) equation 16
  - 2.2.1 Derivation of the equation of motion 17
- 2.3 The asymmetric Solid-On-Solid (SOS) model 22
- 2.4 Exact Results 27
- 2.5 Discussion 39

3 Numerical Results for the Interface Width 42
- 3.1 The finite difference method 43
- 3.2 The Monte Carlo method 48
- 3.3 Results in two dimensions 51
- 3.4 Crossover scaling in two and three dimensions 54
- 3.5 Roughening exponents for the driven interface in three dimensions . . 59

4 The Equilibrium Roughening Transition 64
- 4.1 Introduction to phase transitions 65
- 4.2 The equilibrium roughening transition 67
  - 4.2.1 Theory 68
  - 4.2.2 Roughening temperature 74
  - 4.2.3 Surface tension 74
  - 4.2.4 Correlation length 75
  - 4.2.5 Step free energy 75
- 4.3 Experimental observation of the roughening transition 76

5 The Roughening Transition in Driven Systems **80**
5.1 Roughening transition in driven systems 81
5.1.1 The discrete Kardar-Parisi-Zhang equation 81
5.1.2 Solid-on-solid model with asymmetric rates of evaporation and condensation 84
5.2 Discussion 91

6 Conclusion **94**
6.1 Summary and Discussion 94

References **96**

List of Figures

1.1 Ising model representation of an interface 4

2.1 Width of an interface 15
2.2 Zeros of the interface 19
2.3 The SOS model 24
2.4 Coexistence curve 25
2.5 Self-similarity of KPZ interfaces 31
2.6 Diagramatic representation of the variables 33
2.7 Diagramatic representation of the KPZ equation 34
2.8 Diagramatic representation of high- and low-wavenumber variables . . 34
2.9 Diagramatic representation of the KPZ equation for high and low frequencies 35
2.10 Diagramatic represention of the first-loop perturbation results for the KPZ equation 36

3.1 Testing of finite size effects 45
3.2 Sum rule test 47
3.3 Sum rule relation in $d = 2$ 47
3.4 Sum rule relation in $d = 3$ 48
3.5 Growth exponent for the KPZ equation in $d = 2$ 52
3.6 Saturation exponent in $d = 2$ 52
3.7 Saturation exponent in $d = 2$ 53
3.8 Growth exponent for the SOS model in $d = 2$ 54
3.9 Crossover behavior of the KPZ equation in $d = 2$ 57
3.10 ln W vs ln λ for various values of λ. 58
3.11 Crossover behavior of the asymmetric SOS model in $d = 2$ 59
3.12 Crossover behavior of the three-dimensional KPZ equation 60
3.13 Growth exponent β 61
3.14 Saturation exponent χ for the three-dimensional KPZ equation 62
3.15 Saturation exponent χ for the three-dimensional SOS model 62

4.1 Roughening transition in a lead crystallite 77

5.1 Transition from discrete to continuous growth 82
5.2 Smooth interface below T_R 83

5.3 Rough interface above T_R 84
5.4 Dynamic roughening transition in a dendrite 85
5.5 Step free energy E_{step} vs L for various temperatures 87
5.6 Step free energy E_{step} vs T for various system sizes 88
5.7 Fluctuations in the energy bond C vs T for various values of the driving force λ 89
5.8 Finite size scaling plot of the energy bond fluctuations 90
5.9 Ising model of the interface 92

Chapter 1

Introduction

The physics of condensed matter surfaces and interfaces has been studied for a long time. One can, for example, cite the discovery of catalytic action by Michael Faraday in 1833, the rectification of electrical resistance through the presence of a thin surface layer at the interface of a sandwich of Fe and Cu by Karl Ferdinand Braun, and the publication by J. Willard Gibbs of his memoir (Gibbs 1948), where he completely describes the thermodynamics of surface phases. Despite these early studies, it is only in the 20^{th} century that surface science has been recognized as a discipline in its own right. Since the 1950's, interface phenomena has been a major research area for physicists, chemists, and material scientists.

The physical behavior of interfaces is often interesting and intricate. This is because interfaces are low dimensional systems, that is , $(d-1)$-dimensional objects evolving in a d-dimensional world, which makes them particularly sensitive to the fluctuations that are always present in any thermodynamic system. Furthermore, interfaces are present in many physical systems of interest, whose properties they often effect significantly. This reason, and others, has led physicists to study more closely the behavior of interfaces, first in simple cases, then in more complicated circumstances. The discovery that the equilibrium interface between a liquid and its vapor is not microscopically flat, as one would expect, but rather rough, is an example which is particularly relevant to this work. Even though this roughness can be very small (the thickness of the interface of a glass of water is of the order of tens of angstroms), the consequences associated with this discovery have had repercussions in various fields of physics.

In another connection, the study of phase transitions plays a central role in modern condensed matter physics. Changes of phase are dramatic events which require careful study for a complete understanding. In addition, the fundamental concepts and methodology developed to study phase transitions have far-reaching utility in other area of physics. One often has to simplify the problem dramatically while still retaining the fundamental properties of the system, to be able to solve it. Both first-principles and phenomenological methods are often used.

The physical phenomena associated with both interfaces and phase transitions is complex and has been the subject of many years of research. Indeed, it is not surprising that systems involving both areas pose challenging problems. The roughening transition is such a phenomenon.

The roughening transition is a phase transition taking place in interfacial systems. It had been known that some of the interfaces observed experimentally were microscopically flat in a certain range of parameters, and rough outside this range. This type of phenomenon -called the roughening transition - had already been conjectured by theorists. The existence of a roughening transition in an equilibrium interface separating two coexisting phases was first put forward in 1951 in a now famous paper by Burton, Cabrera and Frank (Burton, Cabrera and Frank 1951). They argued that below a certain temperature T_R, thermal fluctuations could not overcome the barrier provided by surface energy, so that the interface remained microscopically flat. However, above T_R, the surface tension would not be strong enough to prevent fluctuations on all wavelengths. These fluctuations would then delocalize the interface, whose height would then exhibit long wavelength variations. The interface would then become rough. Their argument, which we now briefly review, makes use of the Ising model.

The Ising model was devised to describe the statistical mechanics of classical spins, and to explain the behavior of ferromagnets. The model makes use of a d-dimensional array of spins $\{S_i\}$ with only two possible spin values, namely +1 and -1. The interactions of these spins are described by the following Hamiltonian:

$$\mathcal{H} = -J\Sigma_{i,j}S_iS_j, \tag{1.1}$$

where J is the coupling constant and the indices i and j run over every nearest-neighbor pair of spin. If $J > 0$, $\mathcal{H}$ descibes the interactions of spins in a ferromagnet and, if $J < 0$, of an antiferromagnet. This model involves many assumpticns: localization of the spins, uniform interactions, coupling extending only to nearest neighbors. Nevertheless, it serves as a landmark in the field of statistical mechanics because it was the first model exhibiting a phase transition for which an exact solution (in $d = 2$) was found. In $d = 3$, its properties, including its phase transition, have been carefully investigated. In addition, at this phase transition, it has universal properties identical to that of, for example, liquid-gas, ferromagnetic and binary alloy phase transitions. Let us finally point out that the Ising model suitably transformed into a lattice gas model can also describe the behavior of a solid-gas or liquid-gas system, as in the original argument of Burton et al. Essentially, the transformation involves associating $S_i = +1$ with a solid and $S_i = -1$ with a gas.

The argument concerning the roughening transition is most transparent for the (100) facet separating $S = +1$ and $S = -1$ phases of the three-dimensional simple-cubic Ising model (Fig. 1.1). The low temperature excitations of the facet correspond to one-block (one-spin) fluctuations either up or down. However, on looking "down" at the facet and its excitations, one recognizes that it is equivalent to the one-phase state of the *two-dimensional* Ising model with low-temperature one-block (one-spin) excitations. One can also consider a ledge in the three-dimensional system, which is equivalent to coexisting phases in two dimensions. This low-temperature mapping shows the stability of the smooth facet, and suggests that T_R of that facet is approximately the critical temperature of the second-order phase transition in the two-dimensional Ising model.

Since that original study, much theoretical and experimental work has been done

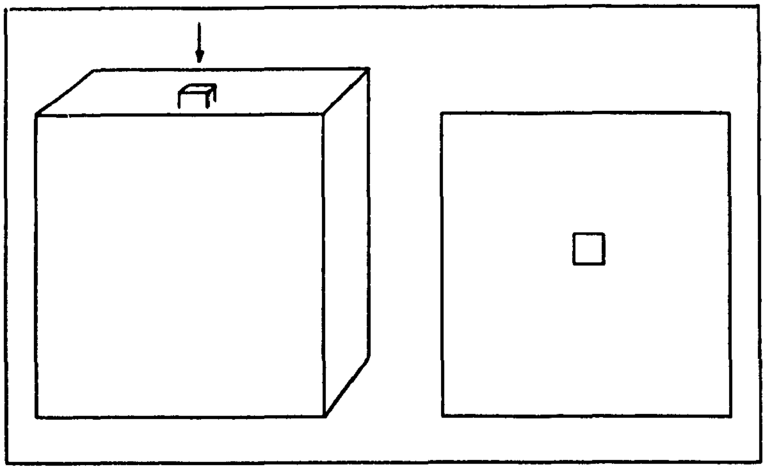

Figure 1.1: a) Global view of an interface in a three dimensional Ising model. b) Top view of the same interface. In a), the filled region on the bottom, including the one-block excitation, corresponds to $S = +1$ while the empty region above corresponds to $S = -1$. In b), it is useful to think of the big region as corresponding to $S = -1$ with a one-spin excitation of $S = +1$; i.e the "two-dimensional Ising model" corresponds to the layer immediately above the $S = +1$ region in a).

(Van Beijeren and Nolden 1987; Weeks and Gilmer 1979; Gilmer 1982; Zia 1984; Jasnow 1986). It is now understood that the Burton-Cabrera-Frank idea was incomplete since it did not take into account the possibility of clusters growing on other clusters as T approaches T_R from below. These give rise to capillary-wave excitations of the surface. As a consequence, the roughening transition, rather than being a second-order transition, is a Kosterlitz-Thouless transition (Kosterlitz and Thouless 1974; Kosterlitz 1974; Chui and Weeks 1976). Despite the fact that the transition is therefore of infinite order, signs of it have been observed experimentally (Wolf et al. 1985; Rottmann et al. 1984). Furthermore, renormalization-group techniques, in particular that used by Kosterlitz and Thouless to analyze the two-dimensional Coulomb gas system, have been successfully applied to the problem (Kosterlitz and Thouless 1974; Kosterlitz 1974). Also, many computer simulations of interface models have been performed to confirm the presence of the transition and quantitative results have been obtained (Swendsen 1977; Swendsen 1978; Mon et al. 1988; Van Beijeren and Nolden

1987). Consequently, the roughening transition occurring in equilibrium interfaces is now well understood.

However, most interfaces observed in nature are not in equilibrium. The interfaces of snowflakes and rapidly quenched crystals are good examples of such nonequilibrium systems. Furthermore, it is difficult, even in laboratory conditions, to obtain an interface which is in its equilibrium state. Nevertheless, the nature of the roughening transition in systems which are far from equilibrium has received less attention (Gilmer 1982). This is unfortunate since roughening transitions play an important role in three-dimensional crystal growth (Van Beijeren and Nolden 1987; Weeks and Gilmer 1979; Zia 1984; Rottmann and Wortis 1984). In experiments on epitaxy and sputtering (Chang and Ploog 1985; Vossen and Kern 1978; Mazor et al. 1988), where an interface grows at a constant rate, it is of interest to determine how a constant driving force affects the transition. For example, one would like to know the roughness of the interface above the transition temperature T_R, as well as the conditions, if any, under which an interface can be grown in the smooth faceted phase which exists below T_R.

Experiments on crystal growth (Dougherty and Gollub 1988; Maurer et al. 1989; Bilgram, Firmann and Hürlimann 1989; Gallet, Balibar and Rolley 1987) find that one can go from a smooth to a rough phase by increasing the driving force beyond a particular strength, at a fixed temperature $T < T_R$. The effect of interface roughening on the process of crystal growth is that below T_R the growth occurs layer by layer, whereas above T_R the growth is continuous (Gilmer 1982; Rottmann and Wortis 1984; Müller-Krumbhar 1979). A more dramatic indication of this is that, when a crystal grows into a metastable supercooled liquid, the shape of the dendrite tip formed after a Mullins-Sekerka instability (which is important in crystal growth if the length scale over which heat diffuses is small compared to the edge length of the system) can be faceted or rounded depending on the supercooling strength (Dougherty and Gollub 1988). Furthermore, in sputtering experiments, the interface is usually rough, and columnar growth can be observed (Vossen and Kern 1978), while in epitaxial growth, very smooth interfaces can be produced (Chang and Ploog 1985). Thus at a fixed temperature, rough or smooth interfaces can be grown by adjusting the external driving force (Chang and Ploog 1985; Vossen and Kern 1978; Dougherty and Gollub 1988). Given the experimental and technological relevance of these systems, it is important to understand the basic physics of interface dynamics far from equilibrium. It should also be noted that the dynamics of a growing interface separating two phases is a fundamental problem in condensed-matter physics.

An important step in this direction was made by the work of Kardar, Parisi, and Zhang (KPZ) (Kardar, Parisi and Zhang 1986; Medina et al. 1989). They proposed a nonlinear differential equation, given below, to model a growing interface driven by an external flux of particles. By applying a dynamical renormalization-group technique, a scaling form of the interface correlation is obtained along with the scaling exponents for a two-dimensional system. The width W obeys (Family and Vicsek 1985)

$$W(L,t) \sim L^{\chi} f(tL^{-z}), \tag{1.2}$$

where L is the linear size of the growing substrate, t is time, and f is a scaling function. For dimension $d = 2$ [the interface grows on a $(d-1)$-dimensional substrate], a fluctuation-dissipation theorem allows one to calculate the interface exponents, $\chi = \frac{1}{2}$ and $z = \frac{3}{2}$. These are consistent with numerical simulations (Plischke and Rácz 1985; Jullien and Botet 1985; Meakin, Jullien and Botet 1986; Zabolitzky and Stauffer 1986; Wolf and Kertész 1987a; Meakin 1987; Family and Vicsek 1985; Meakin et al. 1986; Plischke, Rácz and Liu 1987; Kim and Kosterlitz 1989; Huse and Henley 1985; Kardar 1985; Bovier, Fröhlich and Glaus 1986; Nattermann and Renz 1988), and are different from the equilibrium roughening exponents $\chi_o = \frac{3-d}{2}$ and $z_o = 2$, where the subscript o implies no driving force. In three dimensions, namely the critical dimension d_c of the model where the nonlinear driving force is irrelevant by power counting, no direct result was found due to the failure of perturbation theory for $d < d_c$, although a hyperscaling relation enforces $\chi + z = 2$ when the nonlinear driving force is relevant. Given this unclear situation, in the experimentally most important dimension, there have been several conjectures for the values of the growth exponents as a function of

d. If $\beta \equiv \chi/z$, with $\chi + z = 2$, the conjectures for dimension d are $\beta = \frac{1}{3}$, due to Kardar, Parisi and Zhang (Kardar, Parisi and Zhang 1986); $\beta = 1/(2d-1)$, due to D.E. Wolf and J. Kertesz (Wolf and Kertész 1987a); and $\beta = 1/(d+1)$, due to J.M. Kim and J.M. Kosterlitz (Kim and Kosterlitz 1989).

Like all interface models with translational invariance, in the KPZ equation there is a capillary-wave Goldstone mode due to the broken translational invariance normal to the interface. This causes the poles of response functions to be massless, and the frequency-dependent fluctuations around equilibrium to be $1/f$-like, where f is frequency. One novelty of the nonlinear Kardar-Parisi-Zhang equation is the appearance of anomalous dimensions in correlation functions (although we re-emphasize that power-law correlations exist even for the linear case).

Computer simulations of lattice-based models, such as deposition models (Family and Vicsek 1985; Meakin et al. 1986), Eden models (Plischke and Rácz 1985; Jullien and Botet 1985; Meakin, Jullien and Botet 1986; Zabolitzky and Stauffer 1986; Wolf and Kertész 1987a; Meakin 1987), solid-on-solid (SOS) models (Meakin et al. 1986; Plischke, Rácz and Liu 1987; Kim and Kosterlitz 1989), and directed polymer models (Huse and Henley 1985; Kardar 1985; Bovier, Fröhlich and Glaus 1986; Nattermann and Renz 1988), agree with the results for the KPZ equation in two dimensions, suggesting that all these models belong to the same universality class. In three dimensions, however, the lattice models do not give consistent results (Jullien and Botet 1985; Wolf and Kertész 1987b; Meakin, Jullien and Botet 1986; Meakin 1987; Devillard and Stanley 1989; Meakin et al. 1986; Meakin 1987; Baiod et al. 1988; Liu and Plischke 1988; Kim and Kosterlitz 1989; Forrest and Tang 1990; Kardar and Zhang 1987).

Driven interfaces are also closely related to self-organized critical phenomena, recently introduced by Bak *et al.* (Bak, Tang and Wiesenfeld 1988) through the study of dynamical models that evolved automatically to a critical state without tuning any parameter. Such a self-organized critical state is characterized by the absence of length and time scales, and was argued to be responsible for long-range temporal correlations in many dissipative dynamical systems. These new critical phenomena are fundamentally different from that near a second-order phase transition, or that due to the equilibrium capillary-wave fluctuations on an interface (Grossmann, Guo and Grant 1990). In the first case, the critical point can only be reached by tuning parameters such as pressure and temperature in the phase diagram. In the second-case, the argument goes as follows: interface equation describe a system's behavior after tuning onto, say, a line of liquid-vapor or solid-liquid coexistence in the phase diagram of a pure substance: Gibb's phase rule forbids an inhomogeneous state in thermal equilibrium, except on, say, lines and points ina two-dimensional phase diagram. In this sense, interface equations are self-critical. However, they represent a zero-fraction of the equilibrium two-dimensional phase diagram since they are only valid on phase transition *lines* and *points*. Since they only describe an infinitesimal portion of the phase diagram, they are not valid examples of self-organized criticality.

Driven interfaces in crystal growth *do not* correspond to equilibrium or close-to-equilibrium states. Instead, for a solid growing into a supercooled liquid melt, one can supercool the liquid to a range of different temperatures below the melting temperature, for a given pressure. If one insists on identifying these states within an *equilibrium* phase diagram, the far-from-equilibrium states correspond to the limits to which one can, say, supercool a liquid or superheat a solid. Driven interface equations are thus valid on a *surface* of the equilibrium two-dimensional phase diagram. In this sense, the critical state is truly reached without tuning, since it involves a nonzero fraction of the equilibrium phase diagram. However, this point of view concerning self-organized criticality implies strong bounds on the nature of the nonequilibrium state, since, in the example above, the liquid is only metastable. The eventual decay of this state by droplet nucleation implies limits on interface models which we shall discuss below, where we present a derivation of the driven interface equation from the Langevin equation for full space.

In this thesis we report original contributions to the issues discussed above. Firstly, we give a derivation for the KPZ equation. Secondly, we numerically determine the roughening exponents at the critical dimension, $d_c = 3$. Thirdly, we study the nature of the roughening transition in the driven system (Guo, Grossmann and Grant 1990a; Guo, Grossmann and Grant 1990b; Grossmann, Guo and Grant 1991a; Grossmann, Guo and Grant 1991b).

In Chapter 2 we introduce and discuss the origin of the KPZ equation. We derive that equation from the Langevin equation for a system with a nonconserved scalar order parameter, when an external field is present, and when an asymmetric coupling to a conserved variable exists. We also describe a model we expect to be in the same universality class, the asymetric Solid-On-Solid (SOS) model. We then give a summary and a brief derivation of some exact results that are of some use for the analysis of our results. We discuss the connection of this class of models with nucleation phenomena. The idea of droplet nucleation implies limits on the long-time and long-length-scale applicability of the KPZ equation to this class of problems, which we examine.

In Chapter 3, we present the results of a numerical integration of the KPZ equation at $d_c = 3$; we also performed a study of crossover phenomena in this model, where the system crosses over from the zero-driving-force case to a finite-driving-force situation (Guo, Grossmann and Grant 1990b). We report numerical studies of models which we expect to be in the same dynamical universality class in the rough phase. In particular, the growth and crossover exponents were numerically determined for the KPZ equation, and via Monte Carlo simulation on the solid-on-solid (SOS) model with asymmetric rates of evaporation and condensation, which we expect to be in the same universality class. Our results for both models are consistent with $\chi/z \approx 0.13$, and $\chi + z \approx 2$, for the KPZ equation and the SOS model in the rough phase (Chakrabarti and Toral 1989; Guo, Grossmann and Grant 1990a).

In Chapter 4, we review the extensive results obtained for the equilibrium roughening transition. We examine the behavior of relevant phyrical quantities, such as the surface tension and the step free energy, at the transition point. We also mention some examples of experimentally observed roughening transitions.

Chapter 5 studies the possibility of a kinetic roughening transition. This was investigated through the study of variants of two important models used to study it in the past: the discrete Gaussian model, and the SOS model (Van Beijeren and Nolden 1987; Weeks and Gilmer 1979; Zia 1984; Chui and Weeks 1976; Swendsen 1977; Swendsen 1978; Rottmann and Wortis 1984; Saito 1978; Saito 1980; Nozières and Gallet 1987). We find that our data for both a discrete KPZ model, and an asymmetric SOS model can be interpreted in terms of a roughening transition occurring at a nonzero T_R, which appears to be stronger than the usual Kosterlitz-Thouless transition. We characterize it with a simple finite-size-scaling ansatz, as is used for second-order phase transitions. The transition here corresponds to a nonequilibrium phase transition such as has been studied for driven diffusive systems (Katz, Lebowitz and Spohn 1983; Leung et al. 1988). Furthermore, we present results from a simulation of the nonequilibrium SOS model in which we compute the surface step energy (Leamy and Gilmer 1974) as a function of temperature at a given driving force, for different system sizes. For the equilibrium roughening transition, the step energy has been shown to be a useful indication of the transition (Leamy and Gilmer 1974; Swendsen 1977; Swendsen 1978; Mon et al. 1988). In our study, a strong jump in the value of the step energy at a nonzero temperature T_R is observed. The value of T_R agrees with that of a finite-size scaling analysis of the bond-energy fluctuations of the model. We also give arguments in parallel to the original Burton-Cabrera-Frank work to discuss the nature of the transition.

Chapter 2

Models of a Growing Interface

The process involved in creating a model which faithfully represents a physical system can be subtle. The canonical example is the Ising model, which well simulates a number of important phenomena. When creating a model, or modifying existing models, one has to carefully select the elements of reality that will be kept, and the ones that will be discarded, to avoid unnecessary complications while ensuring that the model describes the system appropriately. As we will see later, the choice of the model plays an important role in deciding how the physical system will be studied.

In the present case, the physical system we have in mind is one containing two phases, one possibly metastable and the other stable, separated by an interface. The stable phase then grows into the other phase and the interface moves at a constant speed. The interface is smooth on a macroscopic scale, and can be faceted or rounded, where it should be noted that interfaces that look smooth on a macroscopic scale can still be rough. Thus, we are not dealing with large scale instabilities encountered in out-of-equilibrium processes such as dendritic growth and directional solidification. Also, we shall not consider the interface's microscopic structure. We assume that the interface is simply a low dimensional object which separates two phases. This is because we shall not be concerned with physical phenomena involving dynamics of the interface's microscopic structure, such as surface reconstruction, in this work.

2.1 Introduction to the statistical mechanics of equilibrium interfaces

The use of statistical mechanics to obtain the physical properties of bulk systems can seem magical. How can one draw valid conclusions from approximations involving 10^{23} atoms? It is now fairly well understood that the success of statistical mechanics is related to the fact that most of the (irrelevant) microscopic quantities obey simple Gaussian probability statistics. Only a small number of relevant variables determine a system's asymptotic, long wavelength, late time properties. These thermodynamic variables are those with which we shall be concerned.

The statistical mechanics of interfaces is more involved than that of bulk systems. There are many reasons for this: interfaces exist between two phases and are thus difficult to treat separately from the bulk; their properties can be of considerable importance, especially close to the critical point, where the correlation length diverges; they are low-dimensional objects; and their presence is often closely associated with a phase transition in the system. Furthermore, interfaces are very sensitive to fluctuations in the bulk. This stems essentially from the fact that they break translational symmetry in the system. Thus, for example, in a bulk phase, a fluctuation in the pressure is immediately counterbalanced by diffusion phenomena, restoring the system's pressure toward its equilibrium value. However, if an interface is present and the fluctuation occurs close to it, the restoring force now is the surface tension, but it is not strong enough to prevent long wavelength distortions of the interface, as will be shown later.

A first principle approach is to consider the interface as decoupled from the bulk, and thus as a separate entity. One can then study a $(d-1)$-dimensional object. We shall assume that the energy of the interface is proportional to its $(d-1)$-dimensional area. One can thus write the following equation:

$$\mathcal{F} = \alpha L^{d-1}, \tag{2.1}$$

where $\mathcal{F}$ is the free energy of the interface, L is its length and α is the surface tension. Now,

$$\mathcal{F} = \alpha \int_0^{L_0} d^{d-1}x \left[1 + \left(\frac{\partial h}{\partial x}\right)^2\right]^{\frac{1}{2}} \tag{2.2}$$

where the interface position is given by $y = h(x)$. Expanding in a Taylor series in $(\nabla h)^2$,

$$\mathcal{F} \approx \alpha L_0^{d-1} + \frac{\alpha}{2}\int_0^{L_0} d^{d-1}x \left(\frac{\partial h}{\partial x}\right)^2 . \tag{2.3}$$

Thus, the $(\nabla h)^2$ is the elastic energy associated with the elongation of the interface. The latter term will often appear in our dynamical equations for the interface's motion. Even though this free energy is simple, it allows us to calculate the thickness of the interface, as will be seen in the section below on exact results.

As was mentioned in the introduction, numerous theoretical and numerical studies of the equilibrium roughening transition have been made. Those studies made use of various types of models that can be classified into two broad classes: the continuous or macroscopic models and the microscopic models. Both classes have some advantages and some disadvantages.

The continuous models describe the dynamics of the interface by a stochastic partial differential equation, known as a Langevin equation. This type of equation is usually obtained by postulating the form of the free energy functional that describes the system and applying certain operators to it. Although the equation is phenomenological, it can be shown that it describes the system well if it satisfies a certain relation called the fluctuation-dissipation theorem. A well-studied example of such a model is the roughening equation which represents the roughening of an equilibrium interface as a function of time. It has the following form:

$$\frac{\partial h(\vec{x},t)}{\partial t} = \nu \frac{\partial^2 h(\vec{x},t)}{\partial \vec{x}^2} + \eta(\vec{x},t), \tag{2.4}$$

where $h(\vec{x},t)$ represents the height of the interface at position $\vec{x}$ and time t,and $\eta(\vec{x},t)$ is the stochastic term mimicking the presence of thermal noise in the system, and obeys the following properties

$$\langle \eta(\vec{x},t) \rangle \;=\; 0 \tag{2.5}$$

$$\langle\eta(\vec{x},t)\eta(\vec{x}',t')\rangle \;=\; 2D\delta^{d-1}(\vec{x}-\vec{x}')\delta(t-t') \tag{2.6}$$

The $\langle\rangle$ symbols denote a spatial averaging of the quantity contained in between. The second relation is the fluctuation-dissipation relation for the system, ensuring that the model behaves in a physical way. The fluctuation-dissipation relation is enforced by requiring $D/\nu = k_B T/\alpha$, where k_B is Boltzmann's constant and T is the temperature. These models give a very good description of the late-time long-wavelength behavior of the roughening interface. However, they do not describe the roughening transition because they are continuum models, and the roughening transition is present because of the underlying discreteness due to the lattice.

The microscopic models describe the interface at a more microscopic level. Although there are many such models, the most successful ones are the Solid On Solid (SOS) model and the discrete Gaussian (DG) model. Those two models describe the interface as a set of discrete-valued variables h_i, where i spans a $(d-1)$dimensional space. The h_i represent the height of the interface at the coordinate i. Thus, this representation neglects the presence of overhangs and bubbles. We will see that this can be of some relevance in the case of the growing interface. Nevertheless, those models describe the roughening transition well. Their disadvantage lies in the fact that they are more difficult to solve analytically. Also, they are not as convenient as the continuum models to describe the late-time long-wavelength behavior of the interface. The models we have just discussed describe an interface in equilibrium. However, as we will see later, the same distinction in two classes can be made in the case of models for driven interfaces.

To quantitatively describe an interface, one can use the following quantity

$$W = \sqrt{\langle(h(\vec{x},t) - \langle h(\vec{x},t)\rangle)^2\rangle} \tag{2.7}$$

which corresponds to the width of the interface (see Fig. 2.1).

This quantity exhibits scaling, that is to say, it can be described by power laws. For example, at late times, but sufficiently early that finite-size effects are unimportant,

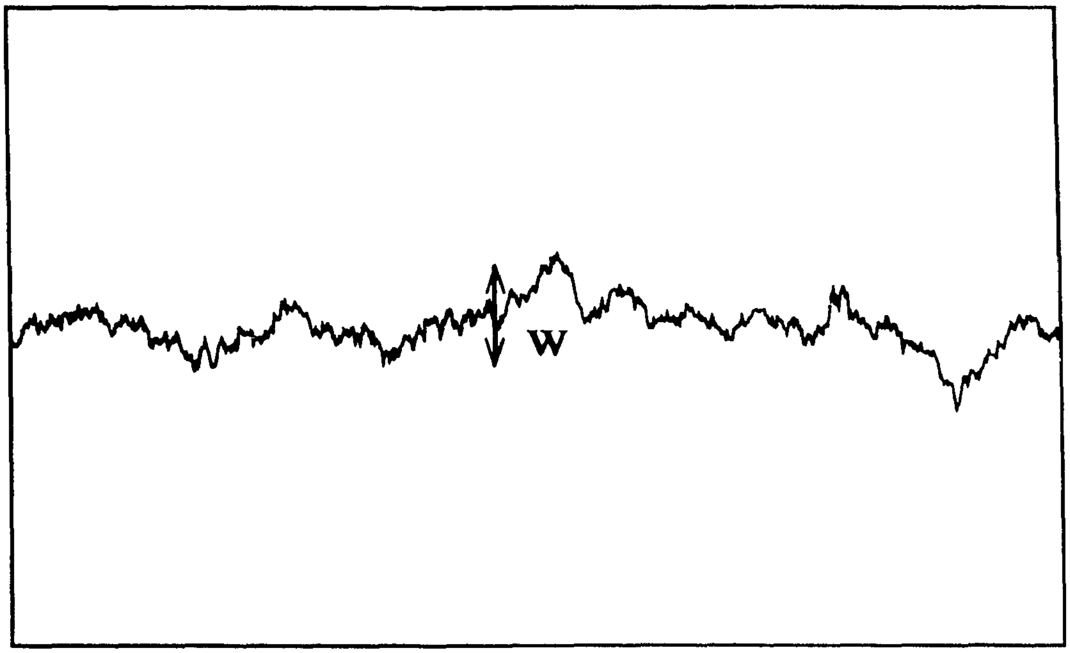

Figure 2.1: Width of an interface. The width is the root mean square deviation of the curve from its average value.

the interface width can be described by the following expression:

$$W(L,t) \sim t^{\beta} f_1(tL^{-z}), \tag{2.8}$$

where t is the time and f_1 is a scaling function. On the other hand, it can be more conveniently written as:

$$W(L,t) \sim L^{\chi} f_2(tL^{-z}), \tag{2.9}$$

where f_2 is another scaling function. The quantities β and χ, which determine the roughness of the interface, are called the scaling exponents. It can be shown that they obey the scaling relation

$$z = \chi/\beta \tag{2.10}$$

2.2 The Kardar-Parisi-Zhang (KPZ) equation

Let us now introduce the far-from-equilibrium counterparts of the above models. The KPZ equation was first introduced to model the dynamical behavior associated with the lateral growth of an interface. It is a nonlinear stochastic differential equation for the time evolution of the interface height variable $h(\vec{x},t)$,

$$\frac{\partial h}{\partial t} = \nu \frac{\partial^2 h}{\partial \vec{x}^2} + \frac{\lambda}{2}\left(\frac{\partial h}{\partial \vec{x}}\right)^2 + \eta, \tag{2.11}$$

where ν and λ are constants, and η is a random noise $\langle\eta\rangle = 0$, which is assumed to satisfy Gaussian statistics with

$$\langle \eta(\vec{x},t)\eta(\vec{x}',t')\rangle = 2D\delta^{d-1}(\vec{x}-\vec{x}')\delta(t-t'), \tag{2.12}$$

where D is a constant. The vector $\vec{x}$ determines positions in a $(d-1)$-dimensional plane of a full space $\vec{r} = (\vec{x}, y)$. Since it has been assumed that h is a single-valued function of $\vec{x}$, overhangs and bubbles are not considered. We will argue below that bubbles are relevant, for very late times, for some important experimental representations of the KPZ equation. The nonlinear term cannot be obtained from a simple Hamiltonian and has a kinetic origin (Kardar, Parisi and Zhang 1986; Medina et al. 1989); a derivation will be presented below. This term breaks the symmetry of positive and negative h and provides a driving force which causes the interface to grow in time. Without the stochastic term, it can be transformed into the well-known Burger's equation, a simplified version of the Navier-Stokes equation, where h becomes the velocity potential (Burgers 1974). As was mentioned above, with $\lambda = 0$, the equation describes the dynamics of interface roughening near equilibrium, where many investigations have been performed (Chui and Weeks 1978; Saito 1980; Edwards and Wilkinson 1982; Nozières and Gallet 1987; Grant 1988). We first present a derivation of the KPZ equation and then give a summary of exact results.

2.2.1 Derivation of the equation of motion

To derive the KPZ interface equation of motion, we require an equation for the full space, where the interfaces correspond to regions of rapid variation of an order-parameter field (Some of our remarks in this section are implicit in the original work of Kardar *et al.* (Kardar, Parisi and Zhang 1986)). The order-parameter field is simply a measure of the ordering of the system, like the magnetization for a ferromagnetic system or the density for a liquid-gas system. A dynamical equation can be prescribed at low temperatures in an ordered state by assuming that the time dependence of a slowly varying nonconserved order parameter is due to the minimization of the local free energy. All other degrees of freedom are modeled by a random noise whose intensity is determined in part by the temperature. This is a consequence of the fact that the time scale associated with the order parameter field is widely separated from the time scales associated with the other degrees of freedom. The equation we need is the following,

$$\frac{\partial\psi(\vec{r},t)}{\partial t} = -\Gamma\left[H + \frac{\delta F[\psi(\vec{r},t)]}{\delta\psi}\right] + \mu, \tag{2.13}$$

where $F[\psi]$ is the free energy functional, Γ is the mobility, and H is the external field. The transport coefficient is related to the intensity of the random noise μ by a fluctuation-dissipation relation:

$$\langle\mu(\vec{r},t)\mu(\vec{r}',t')\rangle = 2\Gamma T\delta(\vec{r}-\vec{r}')\delta(t-t'), \tag{2.14}$$

where Boltzmann's constant has been set to unity. The free energy functional F is the sum of all the exchange interactions plus the sum of the local free energies f at all sites $\vec{r}$,

$$F[\psi] = \int d\vec{r}\left[c(\nabla\psi)^2 + f(\psi)\right], \tag{2.15}$$

where $f = -m\psi^2 + u\psi^4$, and c, m, and u are positive constants. The Langevin equation 2.13 is well known from critical dynamics (Hohenberg and Halperin 1977; Gunton, San Miguel and Sahni 1983; Gunton and Droz 1983), where it corresponds to the universality class of model A, the nonconserved Ising model. It is straightforward to derive Eq. 2.13 from the microscopic spin-flip kinetic Ising model (Gunton and Droz 1983).

One can also recover the Langevin equation above from a modification of model C of critical dynamics (Hohenberg and Halperin 1977; Collins and Levine 1985; Jörgensen, Harris and Grant 1989; Harris and Grant 1990; Caginalp 1989; Caginalp 1990), where a nonconserved order parameter ψ is coupled to a conserved field, called e. The field e must be coupled asymmetrically to ψ (so that e's equilibrium value differs in the two phases, say $\psi = \pm 1$) and, for our purposes, the length scale for diffusion of e, L_T, must be larger than all other lengths in the system. With an asymmetric coupling, this provides a model for the liquid-solid interface, which can be used to study the Mullins-Sekerka instability and dendritic growth. By requiring $L_T \gg L$, we consider length scales much smaller than those of that instability, implying our analysis is only valid, for example, near the tip of a large growing dendrite, where curvature is small.

In equilibrium, the order parameter ψ will equal its time-independent value ψ_o. If equilibrium is characterized by coexisting phases separated by a flat diffuse interface located around $y = 0$, which requires $H = 0$, then, by solving Eq. 2.13, we obtain

$$-c\frac{d^2\psi_o(y)}{dy^2} + \frac{\partial f}{\partial \psi_o} = 0. \qquad (2.16)$$

The mean-field surface tension is given by

$$\sigma = \frac{1}{2}c\int dy \left(\frac{d\psi_o}{dy}\right)^2 . \qquad (2.17)$$

Far from equilibrium, the interface may be convoluted and time dependent. Instead of being located at $y = 0$, it is useful to write it as the zeros of an auxiliary function (see Fig. 2.2)

$$u = 0. \qquad (2.18)$$

To determine the equation of motion for u, we impose the solvability condition:

$$\psi(\vec{r}, t, H) \simeq \psi_o(u(\vec{r}, t, H)). \qquad (2.19)$$

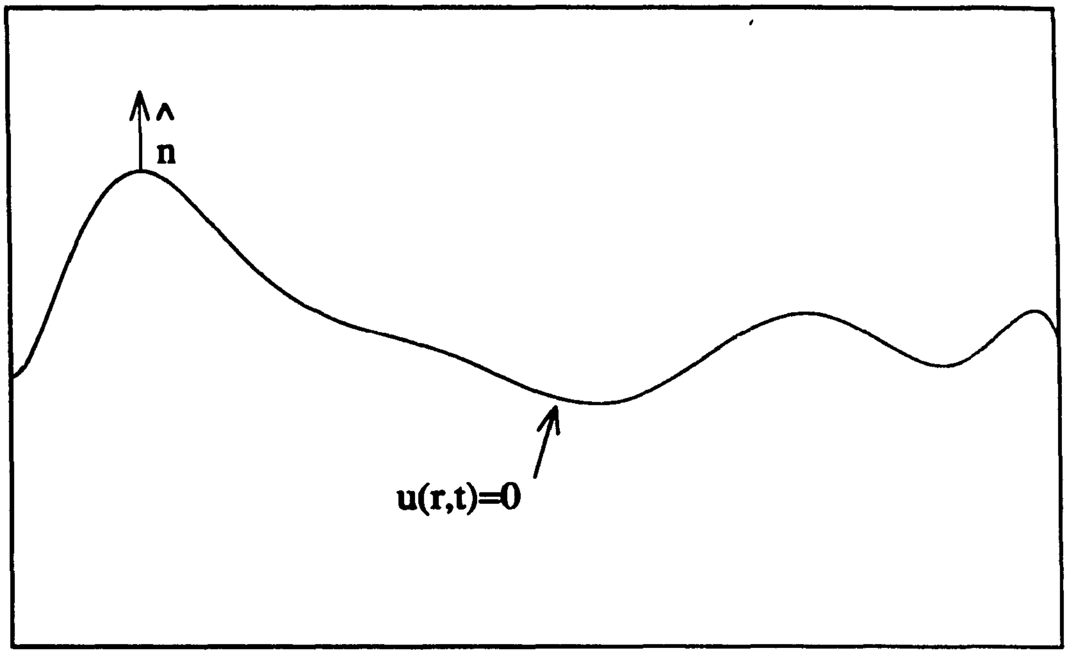

Figure 2.2: Schematic representation of the zeros of the interface by the auxiliary function u.

This means that the shape of the nonequilibrium interface is approximately the same as the equilibrium shape. This is reasonable for a gently-curved surface. Note that writing the interface as $u = 0$ implies that bubbles are not considered (although overhangs have not yet been excluded), since the interface does not interact with other surfaces. In the presence of a field, there can be many nucleated droplets, whose interfaces would eventually interact as the droplets grow to macroscopic size. Thus our analysis is restricted to the time regime when the interfaces can be considered independent. The implications of this will be discussed below.

Using Eq. 2.20, the Langevin equation transforms into

$$\frac{\partial u}{\partial t}\frac{\partial\psi_o(u)}{\partial u} = -\Gamma\left[H - c\nabla^2\psi_o(u) + \frac{\partial f}{\partial\psi_o}\right] + \mu. \qquad (2.20)$$

But from Eq. 2.16, one can eliminate $\partial f/\partial\psi_o$ in terms of second derivatives of ψ_o,

$$\frac{\partial u}{\partial t}\frac{d\psi_o(u)}{du} = -\Gamma\left[H - c\nabla^2\psi_o(u) + c\frac{d^2\psi_o(u)}{(\ell du)^2}\right] + \mu, \qquad (2.21)$$

where $\ell = |\vec{\nabla} u|^{-1}$ is the differential length in the u direction. Decomposing the

Laplacian on the right-hand-side of the equation gives

$$\frac{\partial u}{\partial t}\frac{d\psi_o(u)}{du} = -\Gamma\left[H + cK\frac{d\psi_o(u)}{\ell du}\right] + \mu, \tag{2.22}$$

where $K = -\vec{\nabla}\cdot\hat{n}$ is the differential curvature, and $\hat{n} = \ell\vec{\nabla}u$ is the unit normal vector to the interface. Let us now project the equation onto the interface with the operator

$$\mathcal{P}(\cdots) = \frac{1}{\Delta\psi_o}\int \ell du\frac{d\psi_o}{\ell du}(\cdots) \tag{2.23}$$

where $\Delta\psi_o$ is the miscibility gap. We obtain

$$-\ell\frac{\partial u}{\partial t} = \frac{\Gamma H\Delta\psi_o}{\sigma} + \Gamma cK + \eta \tag{2.24}$$

where $\eta = -(c/\sigma)\int \ell du d\psi_o/(\ell du)\mu$ is the noise at the interface. Finally, since the velocity normal to the interface at $u = 0$ is given by $v = -\ell\partial u/\partial t$, from continuity of flux at $u = 0$, we obtain:

$$v = \lambda + \nu K + \eta, \tag{2.25}$$

where,

$$\lambda = \frac{\Gamma H\Delta\psi_o}{\sigma}, \tag{2.26}$$

$$\nu = \Gamma c, \tag{2.27}$$

the noise satisfies

$$\langle\eta(\vec{s},t)\eta(\vec{s}\,',t')\rangle = 2D\delta^{d-1}(\vec{s}-\vec{s}\,')\delta(t-t'), \tag{2.28}$$

where $\vec{s}$ is a vector determining positions on the $u = 0$ surface, and

$$D = \nu\frac{T}{\sigma}. \tag{2.29}$$

This equation can be written in terms of a free energy:

$$v = -\frac{\nu}{\sigma}\frac{\delta F_s}{\ell\delta u} + \eta, \tag{2.30}$$

where

$$F_s = \int d\vec{r}\left[-H\psi_o(u) + \sigma\frac{\delta(u)}{\ell}\right]. \tag{2.31}$$

The first term is essentially a step function on the interface, and gives the volume energy, while the second is a delta function on the interface, giving the surface energy. Equations of this kind are well known in other contexts (Allen and Cahn 1979; Bausch et al. 1981; Kawasaki and Ohta 1982a; Kawasaki and Ohta 1982b; Grant and Gunton 1983; Caginalp 1989; Caginalp 1990). For example, the equation of motion for the case where the field H is a random quenched variable was derived several years ago (Boyanovsky and Cardy 1983; Grant and Gunton 1984).

The form of Eq. 2.25 can also be obtained from a simple phenomenological argument (Zia 1990). A similar approach has been given by Krug and Spohn (Krug and Spohn 1990). In the presence of a field, a flat interface will translate at a constant velocity $v = \lambda$, since velocity is proportional to thermodynamic force. If the interface is curved, the velocity should be a function of the natural thermodynamic variables of the system. An interface is best described, if it is very thin, by asking how curved it is, i.e., what is its local curvature K. Thus we have $v = v(K)$, in the most simple case. Now, if in addition the interface is only gently curved, so that K is small, to leading order in a Taylor series expansion, one obtains $v = \lambda + \nu K$ as above, and ν must be positive if the motion is so as to reduce curvature.

To recover the KPZ equation, we consider an interface which is almost flat, without overhangs, i.e., $u(\vec{r}, t) = y - h(\vec{x}, t) = 0$. One then obtains:

$$\frac{\partial h}{\partial t} = \frac{1}{\ell}\left[\lambda + \nu\ell^3 \frac{\partial^2 h}{\partial \vec{x}^2} + \eta\right]. \tag{2.32}$$

where $1/\ell(h) = [1 + (\partial h/\partial \vec{x})^2]^{1/2}$. Thus to leading order in $(\partial h/\partial \vec{x})^2$, letting $h \rightarrow h - \lambda t$ for convenience (note this implies the KPZ equation is invariant under a Galilean transformation), one obtains the KPZ equation,

$$\frac{\partial h}{\partial t} = \nu \frac{\partial^2 h}{\partial \vec{x}^2} + \frac{\lambda}{2}\left(\frac{\partial h}{\partial \vec{x}}\right)^2 + \eta, \tag{2.33}$$

where the noise satisfies Eq. 2.14 to this order.

This derivation implies that the KPZ equation can be used to describe a flat growing interface in the nonconserved Ising universality class in the presence of a field, or a solid growing into a supercooled liquid, subject to the restrictions mentioned above (Jörgensen, Harris and Grant 1989). We should also note that there are many experimental representations of models A and C (It may be that derivations can be given of the KPZ equation for other situations, without these restrictions (Krug and Spohn 1990).). Thus, the KPZ equation is especially relevant to dendritic growth. It can be used to describe the behavior of the solid-liquid interface at the tip of the dendrite, where the curvature is small.

2.3 The asymmetric Solid-On-Solid (SOS) model

As mentioned above, there are many advantages to using microscopic models. Firstly, their microscopic description of the interface is more appealing. Moreover, if properly constructed, they contain the essential elements necessary for any roughening transition to take place. Consequently, there have been many such models developed. The crude and simple microscopic model of a crystal is that of a compact structure packed together out of rigid elementary building blocks, which may, for instance, be of cubic shape, corresponding to lattice cells or parts thereof. This model is known as the Kossel crystal (Kossel 1927). As it is, this model completely ignores lattice vibrations, electronic structure, dislocations and other essential features of realistic crystals, but in spite of this, it yields a good qualitative picture of realistic crystal surfaces in some cases. A slightly more refined description of a crystal in equilibrium with its vapor is provided by the lattice gas version of the three-dimensional Ising model. In this model, the unit building blocks are replaced by lattice cells which may be either empty or occupied by a single particle. In a typical two-phase equilibrium state, there is a dense component which can be identified as the crystal phase with a small concentration of vacancies, and a dilute phase which can be identified as the vapor phase. The latter component consists predominantly of empty sites with a small concentration of vapor particles, mostly monomers, but some united in small clusters. The crystal surface can be defined microscopically as the contour separating the crystal phase from the vapor. Even though the description of the vapor phase by a lattice structure is unrealistic, it is expected to be reasonable at low temperatures. If, in such a model, one neglects the presence of bubbles - that is compact inclusions of one phase in the other - and overhangs - that is a portion of the interface where the height $h(x)$ is multivalued - , one arrives at the Solid-On-Solid (SOS) model (see Fig. 2.3).

The SOS model has been extensively studied both theoretically and with the aid of computer simulations, and its equilibrium properties are well understood (Van Beijeren and Nolden 1987). Consider for simplicity the case of a (100) face of an impurity-free simple cubic crystal in equilibrium with its vapor. We can model this situation using the lattice gas model, in which every site is either vacant or occupied by a single atom which in turn can only interact with its nearest neighbors with an interaction strength J. At sufficiently low temperatures, it is assumed that one can neglect the presence of crystal defects, such as vacancies, and particularly bubbles and overhangs. The surface of the crystal can then be represented by a set of discrete variables $h_{i,j}$ representing the height of the interface at a lattice position (i,j), with an appropriate energy assigned to different configurations. The Hamiltonian is defined as

$$\mathcal{H}[h_{i,j}] = \sum_{i,j}(|h_{i,j} - h_{i+1,j}| + |h_{i,j} - h_{i,j+1}|). \tag{2.34}$$

Dynamics is introduced into the model by creating or annihilating atoms at random positions on the surface. This process simulates the molecular exchange between the solid and vapor phases. It is worth mentioning that simulations of the SOS model at high temperature describe the same physical phenomenon - namely the equilibrium roughening of an interface - as Eq. 2.4. There exists another model, the discrete Gaussian (DG) model, which is also of interest for us. It uses the same microscopic description of the crystal surface as the SOS model, but its energetics are slightly different. The Hamiltonian used for the dynamics is

$$\mathcal{H}[h_{i,j}] = \sum_{i,j}((h_{i,j} - h_{i+1,j})^2 + (h_{i,j} - h_{i,j+1})^2). \tag{2.35}$$

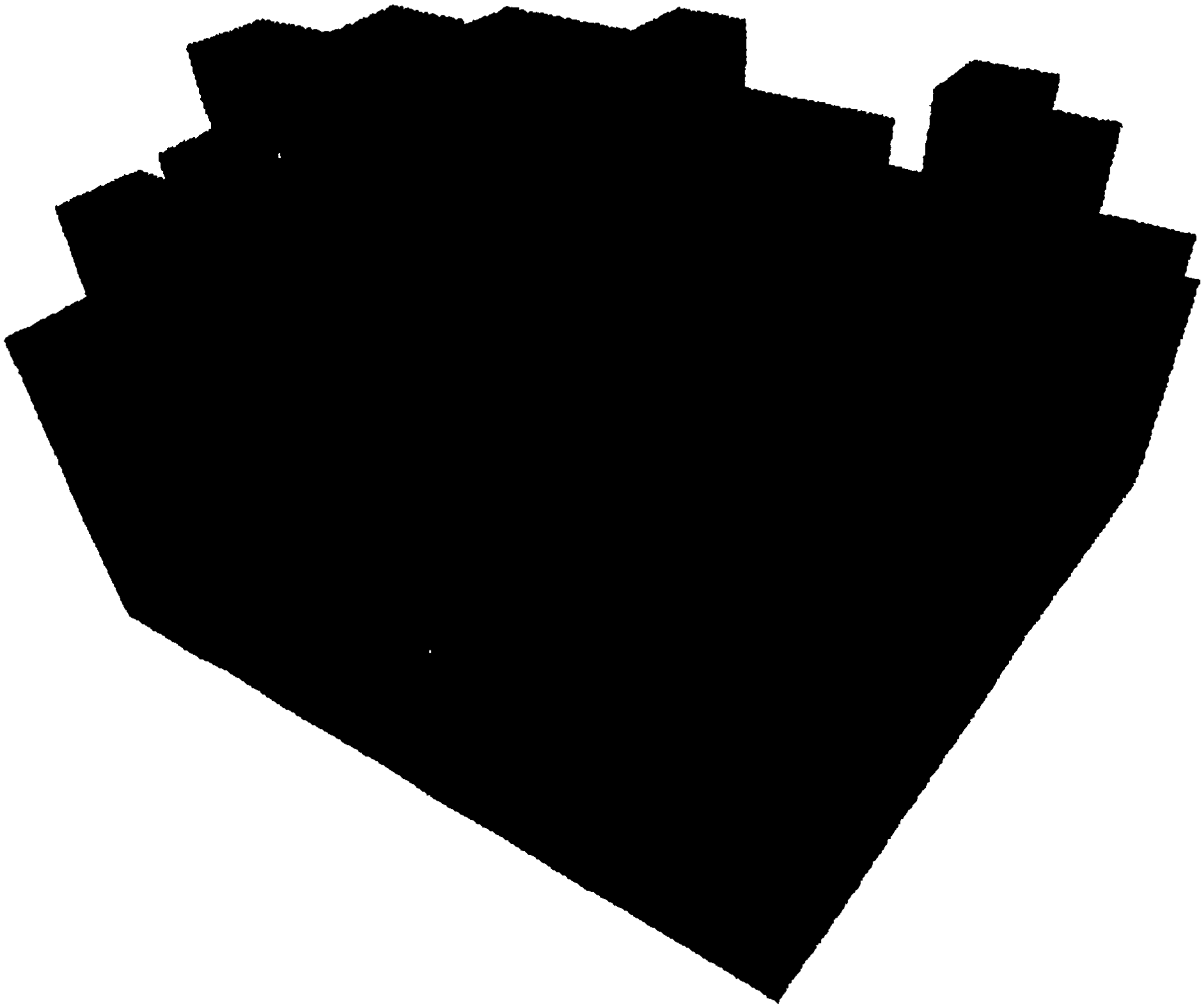

Figure 2.3: A typical configuration of the SOS model. Note the absence of overhangs and bubbles.

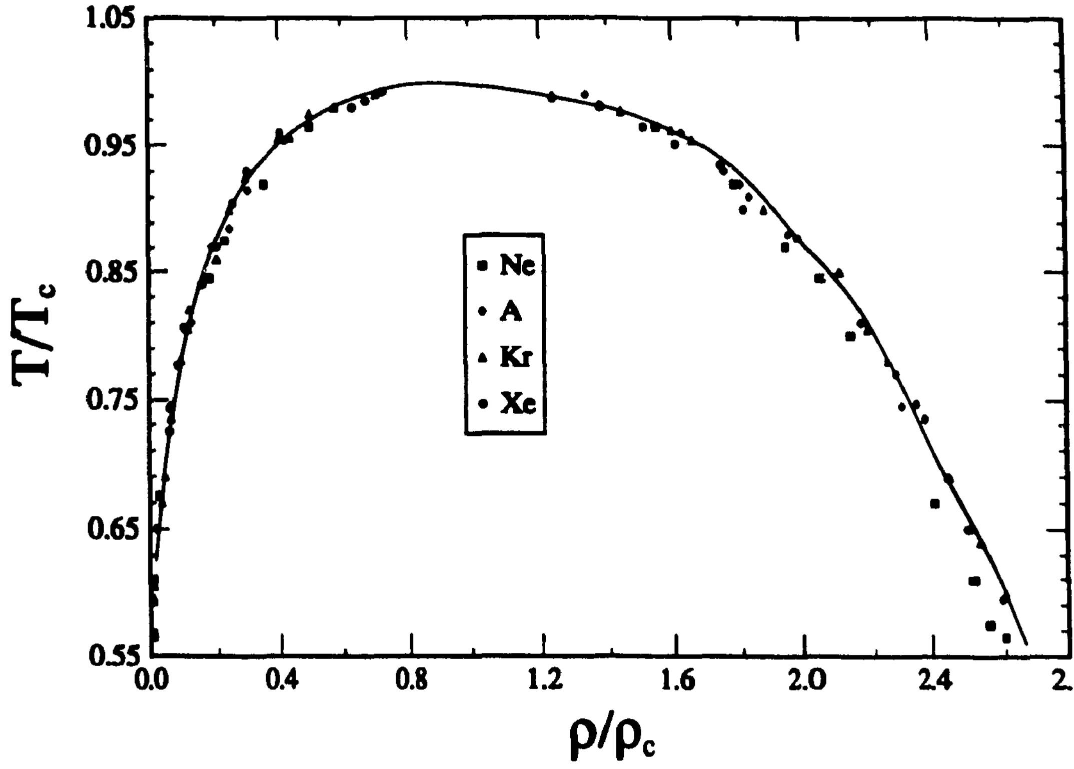

Figure 2.4: Coexistence curves of 4 different fluids close to their critical temperatures. The curve is a cubic fit to the data (Guggenheim 1945).

To first order, the square terms in this Hamiltonian mimic the finite-difference version of a Laplacian operator. Indeed, analysis of this model is sometimes simpler than in the absolute value model. This is why this model has been used to perform various calculations.

If the difference in the Hamiltonians translates into a difference in the short wavelength regime, we have to remember that, at low temperatures, the difference between neighboring sites is small, that is, is equal to zero or unity in most of the cases. Thus, in this case, the two models are equivalent, at least so far as long length scale and long time properties are concerned. To be precise, for our purposes, models are equivalent if they share common asymptotic properties, like the scaling exponents χ and z, and the scaling function defined in Eq. 1.2. One then says that the two models share the same universality class.

The concept of universality is closely related to the field of critical phenomena. A good example of universal behavior is well illustrated by Fig. 2.4. On this figure, the rescaled densities as a function of the rescaled temperature overlay perfectly, indicating all the compounds considered scale in the same way. The universal behavior of many systems is well known experimentally. For example, it has been found that the behavior of some ferromagnetic systems and some liquid systems are described by the same critical exponents. As a consequence of these observations, it was conjectured that diverse physical systems behave identically near their critical points. This universality hypothesis states that only two quantities determine the critical behavior of most systems: the dimensionality of space d and the dimensionality of the order parameter D. All systems having the same values of d and D are said to be in the same universality class.

As we will see in Chapter 4, the study of the SOS and DG models was instrumental in finding a proper description for the equilibrium roughening transition. Furthermore, if one is far enough from the transition temperature, one can recover the scaling behavior of the roughening equation (Eq. 2.4). Those and other reasons have led many people to devise microscopic models that exhibit the same critical exponents as the two dimensional KPZ equation. Examples of such models are the Eden model, the ballistic deposition model and the KK model (Kim and Kosterlitz 1989).

In the Eden model (Eden 1961), given a cluster of N particles, the $(N+1)^{th}$ particle is added at a randomly chosen perimeter site of the cluster. In the ballistic deposition model, spheres are dropped sequentially above randomly chosen positions of the horizontal substrate, move towards the surface along ballistic trajectories and stick permanently at the point of first contact with the substrate or a previously deposited sphere. There are many variations on this model. One can allow the sphere to "roll downhill" until it reaches a stable equilibrium. One can also perform on- and off- lattice simulations. Finally, one can use various angles of incidence for the trajectories.

The Kim and Kosterlitz model is a restricted SOS (RSOS) model. The energetics are still governed by the SOS Hamiltonian, but the model restricts every nearest neighbor height difference to a maximum value of one lattice constant.

Although the growth exponents obtained from simulations performed on those models agree with the KPZ equation in $d = 2$, the situation in $d = 3$ is much less clear. This led us to devise a model which we thought would contain the same feature as the KPZ equation, and consequently, would be in the same universality class. This model, which we named the asymmetric SOS model, is described by the same Hamiltonian as the equilibrium SOS model. To study the nonequilibrium properties of a driven interface, we use $\mathcal{H}$ for Monte Carlo attempts, but bias those attempts by an amount λ_a, which is the fractional amount of extra attempts made on one side. Thus λ_a gives the asymmetry of rates of evaporation and condensation on the interface corresponding to λ in the KPZ equation, while the temperature T for Monte Carlo moves approximately corresponds to D/ν in the KPZ equation. This implies that $\lambda_a = 0$ represents the equilibrium case, while $\lambda_a > 0$ causes a constant velocity of the interface. We expect this asymmetry to allow terms even in $\partial h/\partial \vec{x}$ to appear in long-wavelength equations of motion, so that this model would be in the same universality class as the KPZ equation. We point out here that the procedure introducing asymmetry, and thus, allowing us to use the "new" model to study interface growth, is associated with minimal changes from the standard SOS model.

2.4 Exact Results

Exact results for the models simulating the equilibrium roughening of an interface are available. Most of them stem from a renormalization group analysis. This technique has been widely used in statistical physics, because it is particularly successful at handling the various singularities that occur at a second order phase transition. Since some of those results are useful for the analysis of the nonequilibrium systems, we describe them here. Let us first review a simple method that allows us to calculate the critical exponents related to the roughening equation (Eq. 2.4).

As mentioned above, the roughening equation and the equilibrium SOS model both describe the roughening of an interface. Above the roughening transition, the renormalization group calculations performed on those two models predict that the height-height correlation, that is the width of the interface defined by Eq. 2.7, diverges. Furthermore, the way it diverges depends on the dimensionality of the model. To see this in an easy way, let us make use of the roughening equation. Let us Fourier transform this equation and rewrite it in momentum and frequency space

$$i\omega h(\vec{q},\omega) = -\nu q^2 h(\vec{q},\omega) + \eta(\vec{q},\omega), \tag{2.36}$$

where $\vec{q}$ is the momentum, ω is the frequency and $\eta(\vec{q},\omega)$ satisfies the following relations

$$\begin{aligned} \langle \eta(\vec{q},\omega) \rangle &= 0, & (2.37) \\ \langle \eta(\vec{q},\omega)\eta(\vec{q}\,',\omega') \rangle &= 2D\delta^d(\vec{q}+\vec{q}\,')\delta(\omega+\omega'). & (2.38) \end{aligned}$$

One can thus write

$$h(\vec{q},\omega) = \frac{1}{\nu q^2 + i\omega}\eta(\vec{q},\omega) \tag{2.39}$$

From this equation, one can immediately infer that the interface does not move, that is, that its average position is time independent and equal to zero. This result is simply obtained by taking the spatial and temporal average of the whole equation. One can also find the width of the interface. We first write

$$\langle h(\vec{q},\omega)h(\vec{q}\,',\omega') \rangle = \frac{1}{(\nu q^2 + i\omega)(\nu q'^2 + i\omega')}\langle \eta(\vec{q},\omega)\eta(\vec{q}\,',\omega') \rangle \tag{2.40}$$

We then take the Fourier transform of this equation to obtain the width in real space. Taking the $t \to \infty$ limit, we obtain

$$W(L) \sim L^{\frac{(3-d)}{2}}, \tag{2.41}$$

for $d < 3$, where L is the linear size of the system and d is the dimension of space. Thus, the width of the interface diverges in the thermodynamic limit, that is, when $L \to \infty$. This fact is a consequence of the Goldstone theorem. The free energy of the interface (Eq. 2.15) is translationally invariant; it has an infinite number of energetically equivalent positions. By placing the interface at a particular position in space, one breaks this translational symmetry. As a consequence, there emerges an excitation which makes the interface vary slowly in space. This excitation is called a Goldstone mode. It has a very low energy which goes to zero as the wavelength associated with it goes to infinity. The interface is unstable against such long wavelength perturbations and its width increases to infinity in the thermodynamic limit. However, note that the interface width remains small compared to the dimensions of the system, since $W/L \sim 1/L^{\frac{(d-1)}{2}}$ as $L \rightarrow \infty$, for $d > 1$.

The above method has the advantage of allowing us to find precisely how the interface diverges as a function of the space dimensionality much more easily than the renormalization group technique. However, as was mentioned before, the continuum model does not allow us to find the roughening temperature, or any of the quantities of interest associated with the roughening transition. Nevertheless, one is able to extract the critical exponents z_o and χ_o from this analysis. From above, $\chi_o = (3-d)/2$, and it can be easily shown that $z_o = z$ for $d < 3$. In $d = 3$, the situation is a bit more delicate, because it corresponds to the upper critical dimension, that is, the dimension above which mean field results become exact. One then finds that the width of the interface diverges very weakly as

$$W \sim \sqrt{\ln L}, \qquad t/L \gg 1, \tag{2.42}$$

$$W \sim \sqrt{\ln t}, \qquad t/L \ll 1. \tag{2.43}$$

It is often difficult to obtain information on the dynamics of a system by such simple methods. One usually has to use more involved analytic methods to obtain such results. The renormalization group method is such a scheme. The reason it has attracted the attention of many researchers is because it has been quite successful at handling various analytical problems other methods could not. The philosophy behind this method is closely associated with scaling and universality. Indeed, this universal behavior shared by all systems at their critical points led people to think that most of the microscopic characteristics of the system were not useful in describing the behavior of the system - in other words, they were associated with irrelevant variables. A few parameters were crucial to obtain the right description - the variables associated with these parameters were relevant variables. The renormalization group method consists of rescaling the system, and, in so doing, integrating the irrelevant variables away while keeping the relevant variables. Even though there are very few rigorous proofs for doing such a thing, it can be phenomenologically justified by the scaling behavior of critical systems. The success of the renormalization group method in equilibrium problems prompted people to try the same type of analysis on driven systems, and in particular on the KPZ equation. Forster, Stephen and Nelson (Forster, Nelson and Stephen 1977) have applied the dynamical renormalization group method to the noisy Burgers equation, and their results are also valid for the KPZ equation, as shown by Kardar, Parisi and Zhang (Kardar, Parisi and Zhang 1986).

We illustrate their method. Consider the KPZ equation:

$$\frac{\partial h}{\partial t} = \nu\frac{\partial^2 h}{\partial \vec{x}^2} + \frac{\lambda}{2}\left(\frac{\partial h}{\partial \vec{x}}\right)^2 + \eta, \tag{2.44}$$

$$\langle \eta(\vec{x},t)\eta(\vec{x}',t')\rangle = 2D\delta^{d-1}(\vec{x}-\vec{x}')\delta(t-t'). \tag{2.45}$$

Next, we Fourier transform those equation. We thus define $h(\vec{k},\omega)$ and $\eta(\vec{k},\omega)$ such that

$$h(\vec{k},\omega) = \int_{x<\frac{2\pi}{\Lambda}} d^{d-1}x \int_{-\infty}^{+\infty} dt h(\vec{x},t)e^{-i\vec{k}\cdot\vec{x}+i\omega t}, \tag{2.46}$$

$$\eta(\vec{k},\omega) = \int_{x<\frac{2\pi}{\Lambda}} d^{d-1}x \int_{-\infty}^{+\infty} dt \eta(\vec{x},t)e^{-i\vec{k}\cdot\vec{x}+i\omega t}. \tag{2.47}$$

Here, Λ is a short wavelength cut-off corresponding to the lattice constant or the interatomic distance. Conversely,

$$h(\vec{x},t) = \int_{k<\Lambda} \frac{d^{d-1}k}{(2\pi)^{d-1}} \int_{-\infty}^{+\infty} \frac{d\omega}{2\pi} h(\vec{k},\omega)e^{i\vec{k}\cdot\vec{x}-i\omega t}, \tag{2.48}$$

$$\eta(\vec{x},t) = \int_{k<\Lambda} \frac{d^{d-1}k}{(2\pi)^{d-1}} \int_{-\infty}^{+\infty} \frac{d\omega}{2\pi} \eta(\vec{k},\omega)e^{i\vec{k}\cdot\vec{x}-i\omega t}. \tag{2.49}$$

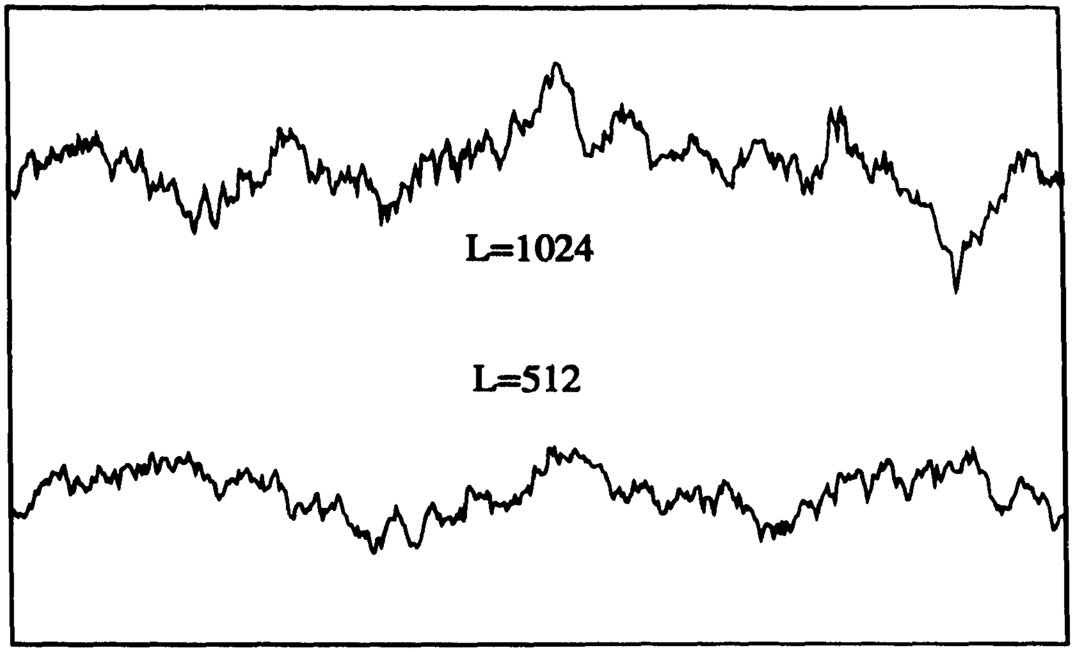

Figure 2.5: Self-similarity of KPZ interfaces.

One can substitute the above expressions in the KPZ equation, which then assumes the following form:

$$\begin{aligned} h(\vec{k},\omega) &= h^0(\vec{k},\omega) \\ &\quad -\frac{\lambda}{2}G_0(k,\omega)\int_{q,\Omega}\vec{q}\cdot(\vec{k}-\vec{q})h(\vec{q},\Omega)h(\vec{k}-\vec{q},\omega-\Omega), \end{aligned} \tag{2.50}$$

$$\langle\eta(\vec{k},\omega)\rangle = 0, \tag{2.51}$$

$$\langle\eta(\vec{k},\omega)\eta(\vec{k}',\omega')\rangle = 2D(2\pi)^d\delta(\vec{k}+\vec{k}')\delta(\omega+\omega') \tag{2.52}$$

with

$$G_0(k,\omega) = \frac{-1}{-i\omega+\nu k^2}, \tag{2.53}$$

$$h^0(\vec{k},\omega) = G_0(k,\omega)\eta(\vec{k},\omega), \tag{2.54}$$

$$\int_{q,\Omega} \equiv \int_{q<\Lambda} \frac{d^{d-1}q}{(2\pi)^{d-1}} \int_{-\infty}^{+\infty} \frac{d\Omega}{2\pi}. \tag{2.55}$$

The way the KPZ equation is now written allows us to iterate the equation up to any order. However, this is not quite what we are going to do. Although our goal here is not to review the mathematical and physical background associated with the renormalization group method, let us outline the arguments validating the procedure. In most of the cases encountered in statistical physics, the usual perturbation theories used to calculate any of the relevant physical quantities will work well enough. However, there is one point in the phase diagram of most compounds where this methods fails. It is the critical point. The reason for this failure is that, at this point, the correlation length diverges in the thermodynamic limit, thermodynamic quantities become singular, and the perturbation expansion becomes uncontrolled, so that the higher order a perturbation term is, the more relevant it is. Another important and simplifying thing happens at the critical point: All the singular quantities exhibit scaling. For example, in the present case, the width obeys the following equality:

$$W \approx L^{\chi}, \tag{2.56}$$

where L is the linear size of the system. What this means physically is well represented by Fig. 2.5. One can hardly distinguish one figure from another - statistically, they are equivalent - and yet one is represented on a scale which is twice the other.

Another important fact associated with the behavior of systems at the critical point is the divergence of the correlation time - that is, the time Δt it takes for $W(\vec{x}, t+\Delta t)$ to become uncorrelated with $W(\vec{x}, t)$:

$$\lim_{\Delta t \to +\infty} \langle W(\vec{x}, t) W(\vec{x}, t+\Delta t) \rangle = const. \tag{2.57}$$

The fact that the correlation time and correlation length diverge means that *the rapidly-varying wavelengths in the system are averaged out, and that only the long wavelength behavior of the system is relevant. The renormalization-group technique involves a controlled averaging or "coarse-graining" of these rapidly-varying quantities.*

In the case that is of interest here, the diverging quantity is the width of the interface W. The scaling laws obeyed by W have been given by Eqs. 2.8 and 2.9. The first step in the renormalization group procedure is a coarse-graining procedure. It corresponds to applying a perturbation method to this equation, that is, to iterate the equation to first order, to replace the exact h terms in the integrals by their unperturbed counterparts h^0 and to integrate over the small wave vector region, that is, over the wave vectors forming the stochastic noise described above. Using the notation in Fig. 2.6, we can represent Eq. 2.48 by the diagram in Fig. 2.7. We then split the integration into two parts using the symbols represented in Fig. 2.8. Note the change in scale $e^l > 0$, by which the rapidly-varying short-wavelengths quantities are integrated out. We then obtain the perturbed equations represented in Fig. 2.9. After some tedious calculations, one obtains, to first order, the representation the corrections to Eq. 2.48 in Fig. 2.10, which translate into the following equations:

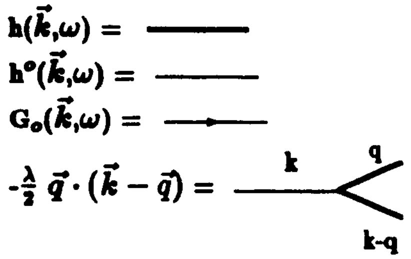

Figure 2.6:

$$h^<(\vec{k},\omega) = G_I^<(\vec{k},\omega)\eta_I^<(\vec{k},\omega)$$

$$-\frac{\lambda_I}{2}G_I^<(k,\omega)\int_{q,\Omega}\vec{q}\cdot(\vec{k}-\vec{q})h^<(\vec{q},\Omega)h^<(\vec{k}-\vec{q},\omega-\Omega), \quad (2.58)$$

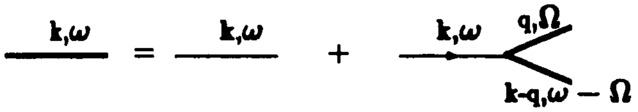

Figure 2.7:

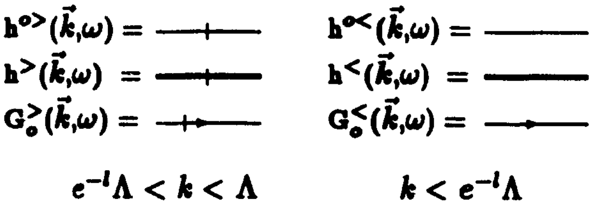

Figure 2.8:

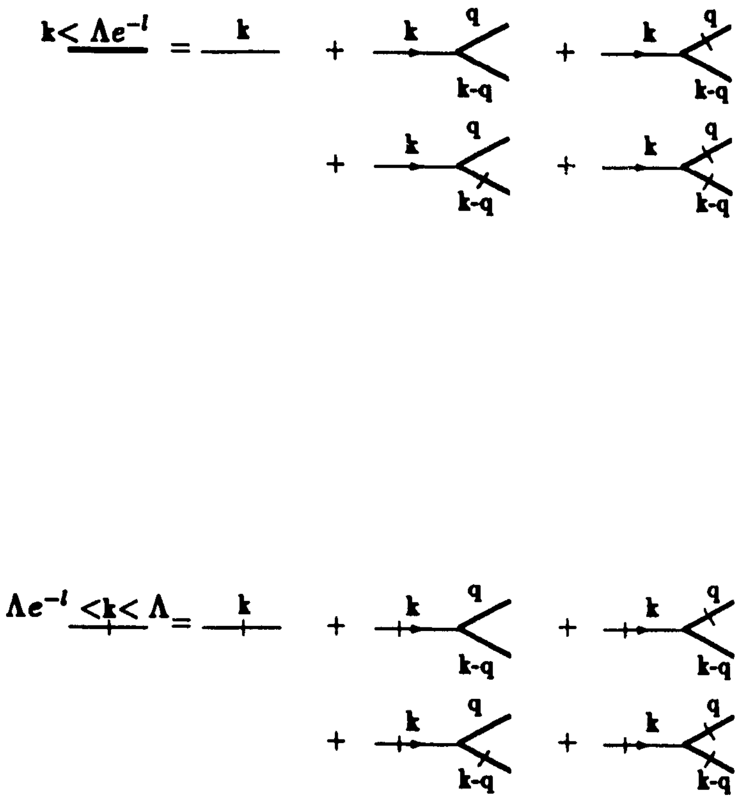

Figure 2.9:

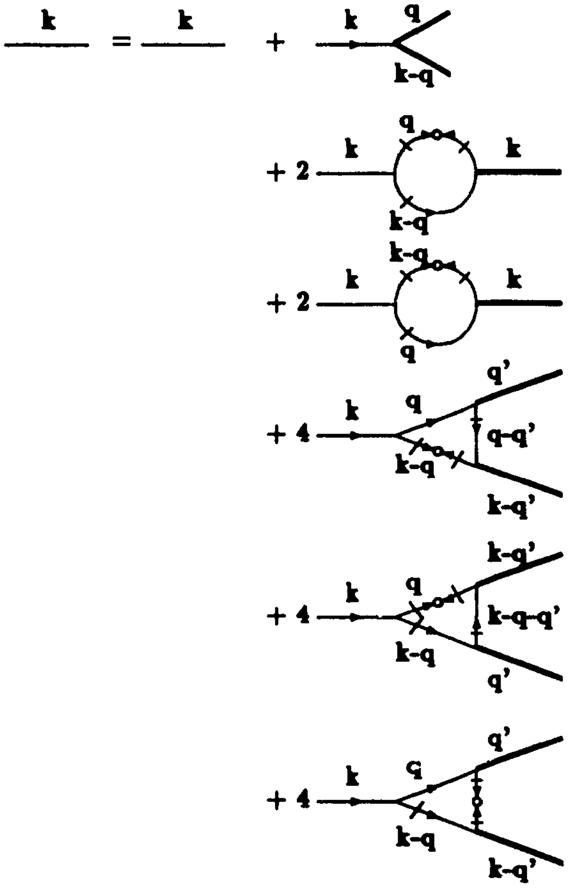

Figure 2.10:

with

$$\nu_I = \nu\left\{1 + \frac{\bar{\lambda}_0^2 K_{d-1}}{4}\frac{1}{d-1}\left[e^{-l(d-3)} - 1\right]\right\} \tag{2.59}$$

$$D_I = D\left\{1 - \frac{\bar{\lambda}_0^2 K_{d-1}}{4}\frac{1}{d-3}\left[e^{-l(d-3)} - 1\right]\right\} \tag{2.60}$$

$$\lambda_I = \lambda \tag{2.61}$$

$$\langle \eta_I^<(\vec{k},\omega)\eta_I^<(\vec{k}',\omega')\rangle = 2D_I(2\pi)^{d-1}\delta(\vec{k}+\vec{k}')\delta(\omega+\omega') \tag{2.62}$$

where $h^<$ refers to relevant wavectors heights, as opposed to the wavectors forming the stochastic noise, $K_{d-1} = 1/2^{d-2}\pi^{\frac{d-1}{2}}\Gamma(\frac{d-1}{2})$ is a constant of integration corresponding to a $(d-1)$-dimensional surface and $\bar{\lambda}_0 = \lambda^2 D/\nu^3$. The second step is then to ensure that the above equations obey scaling laws which are observed in the system. One thus introduces the following scale transformations:

$$\vec{k}' = e^{l}\ \vec{k} \tag{2.63}$$

$$\omega' = e^{zl}\ \omega \tag{2.64}$$

$$h'(\vec{k}',\omega') = e^{-zl-(d-1+\chi)l}\ h_I^<(\vec{k},\omega) \tag{2.65}$$

$$\eta'(\vec{k}',\omega') = e^{-(d-1+\chi)l}\ \eta_I^<(\vec{k},\omega). \tag{2.66}$$

Substituting those expression in Eqs. 2.56-2.60, we obtain the following:

$$\nu(l) = e^{(z-2)l}\ \nu_I \tag{2.67}$$

$$D(l) = e^{(z-2\chi-d+1)l}\ D_I \tag{2.68}$$

$$\lambda(l) = e^{(z-2+\chi)l}\ \lambda_I. \tag{2.69}$$

Finally, taking l as an infinitesimal length, one obtains the following results:

$$\frac{d\nu(l)}{dl} = \nu(l)\left[-2 + z + \frac{\bar{\lambda}^2 K_{d-1}}{4}\frac{3-d}{d-1}\right] \tag{2.70}$$

$$\frac{dD(l)}{dl} = D(l)\left[z-d+1-2\chi+\frac{\bar{\lambda}^2 K_{d-1}}{4}\right] \tag{2.71}$$

$$\frac{d\lambda(l)}{dl} = \lambda(l)\left[z-2+\chi\right] \tag{2.72}$$

To ensure that these equation satisfy the scaling relations, one has to enforce that $\nu(l), D(l)$ and $\lambda(l)$ are independent of l. This gives the following flow equations:

$$z = 2-\frac{\bar{\lambda}^2 K_{d-1}}{4}\frac{3-d}{d-1}, \tag{2.73}$$

$$\chi = 1-\frac{d-1}{2}+\frac{\bar{\lambda}^2 K_{d-1}}{4}\frac{d-2}{d-1}, \tag{2.74}$$

$$\frac{d\bar{\lambda}}{dl} = \frac{3-d}{2}\bar{\lambda}+K_{d-1}\frac{2d-5}{4d-4}\bar{\lambda}^3. \tag{2.75}$$

to leading order in $\bar{\lambda}$.

The important result that comes out of these equations is that there are no stable fixed points to the order we have calculated the critical exponents. As a matter of fact, for $d \leq 3$, $\bar{\lambda}(l)$ diverges exponentially with l. When $d > 3$, one finds that the perturbation term $(\nabla h)^2$ is irrelevant, and one recovers the equilibrium roughening critical exponents. The reason one obtains exact results when $d = 2$ is suggested by the equation describing χ. The last term in the flow equation vanishes in this particular dimension, and one is left with $\chi = 1/2$. In fact, it can be shown that this occurs to all order in $\bar{\lambda}$. From the hyperscaling relation $\chi + z = 2$, one can then find $\beta = 1/3$. However, even though those results are exact, it does not mean that we did find a fixed point. Furthermore, we do not have any such "luck" in $d = 3$. This can be seen from the behavior of $d\bar{\lambda}/dl$. In $d = 3$, the first term vanishes, but the second term is positive. Thus, the value of $\bar{\lambda}$ increases as the system is rescaled. It does not flow towards a stable fixed point. This is one reason why numerical work is required to obtain growth exponents in $d = 3$.

2.5 Discussion

The derivations given above (particularly in Section 2.2.1) clarify the physical picture represented by these models: the far-from-equilibrium states described by the KPZ equation are regions in an equilibrium phase diagram corresponding to the limits to which one can, say, supercool a liquid or superheat a solid. The theoretical counterpart of this process is the quenching of an Ising model with a field applied below its ordering temperature, or the off-critical quench of a binary liquid into the nucleation region. The limits we refer to above also translate into limits on the range of validity of the above models, related to a combination of the strength of the field and the time scale of the description.

There are strong bounds on the nature of the nonequilibrium state, since, in the example above, the liquid is only metastable. The state eventually decays by droplet nucleation, which implies limits on driven interface models, since there is a time regime for which bubbles are relevant. Nucleation is a subtle problem in nonequilibrium theory, involving the nature of metastable states in the hydrodynamic limit. (By hydrodynamic limit, we mean the late-time, large-system-size analog of the thermodynamic limit for nonequilibrium systems). However, the nucleation rate is easy to obtain within the classical approach of Becker and Döring (Becker and Döring 1935; Gunton and Droz 1983). Nucleation occurs when droplets of a stable phase form by spontaneous thermal fluctuations from a metastable matrix. Small nucleated droplets disappear, thus the metastability, while large droplets grow. The rate-limiting process for the formation of the stable phase involves droplets which barely grow, called critical droplets. Classical nucleation theory has two main parts, a quasi-equilibrium theory of the critical droplet, and a kinetic theory of its growth.

Assume the system is ordered with spins up, and an infinitesimal uniform external field is applied which favors spins down. The free energy of a domain of down spins is assumed to be,

$$F_s(R) \approx -HR^d + \sigma R^{d-1}, \tag{2.76}$$

where R is the size of the domain and factors of 2 and π have been ignored for convenience. The first term corresponds to the volume energy of a droplet, while the second to its surface area, so that $F_s(R)$ is a simplified form of Eq. 2.15. The free energy has a maximum $R^* = [(d-1)/d]\sigma/H$. Domains with radii $R > (<)R^*$, grow (shrink) respectively, where R^* is the critical droplet radius. The rate of nucleation I is proportional to the probability of such a droplet appearing by a fluctuation, i.e., $I \propto \exp[-F_s(R^*)/T]$ or

$$I = \frac{L^d}{t^*} e^{-F_s(R^*)/T}, \tag{2.77}$$

where L^d is the volume of phase space accessible for such a fluctuation, and the time scale is given by

$$t^* \equiv (\partial \ln R^*/\partial t)^{-1}, \tag{2.78}$$

so that $1/t^*$ is the linearized growth rate of the critical droplet. The characteristic time scale for a droplet fluctuation is $\tau \sim I^{-1}$, or

$$\tau \propto \exp[\frac{\sigma}{H^{d-1}} + \ln L^d], \tag{2.79}$$

where some numerical factors have been ignored. Note that τ is only weakly dependent on system size and dimension of space for $d > 1$, e.g., $\tau_{d=2} \approx \exp(\ln \tau_{d=3})^{1/2}$.

Thus, for the systems mentioned above, the KPZ equation is useful on time scales $t \ll \tau$, since droplets (i.e., bubbles) are neglected by assuming $h(\vec{x}, t)$ is single-valued. It is known from the study of the kinetics of first-order transitions that droplet nucleation becomes appreciable at the cloud point in experimental systems (Gunton, San Miguel and Sahni 1983; Gunton and Droz 1983), when $\tau = \mathcal{O}(1)$. For even larger field strengths, the system's state can become completely unstable; for example, in long-range-force systems (where the critical droplet is of the system size), this occurs at the spinodal curve $H = H_{sp}(T)$, which is a line of mean-field second-order transitions. It should be emphasized that the nature and formal definition of a metastable state in the hydrodynamic limit is as yet unresolved, except for the relatively uninteresting case of systems with long-range forces. Even with this restriction, the KPZ equation is quite useful for describing the growth of interfaces in non-equilibrium

systems. It is applicable to the interface of a growing bubble if the system meets the conditions stated above. A particularly good example of such a system is dendritic growth, where the time scale for growth of a dendrite is on a much faster scale than the nucleation rate in the undercooled liquid. Given the restrictions discussed above, the KPZ equation describes dynamical roughening at the tip of such a growing dendrite.

Chapter 3

Numerical Results for the Interface Width

As we have seen in the previous section, it is not clear how to make further progress analytically. At this point, we resort to numerical work. In this particular case, as we mentioned in the previous chapter, there are no exact results available for the critical exponents related to the roughening of the interface in $d = 3$. These exponents are not only relevant to theorists, but can also be estimated experimentally, and are of potential use in materials problems: for example, for controlling the speed at which an interface grows. Furthermore, as we will see in the next chapter, the knowledge of those exponents can help us analyze the dynamical roughening transition.

Based on the fact that many models yield the same results as the KPZ equation in $d = 2$, people have conjectured values of those exponents as a function of d. However, none of the models that yielded the same scaling exponents as the KPZ equation in $d = 2$ have been shown to belong to the same universality class as the latter in *any* dimension. Thus we felt it worthwhile to directly integrate the KPZ equation using a finite difference scheme. This method has its advantages and its disadvantages.

The major advantage is that we obtain some values of the scaling exponents for the KPZ equation, rather than some model that might belong to a different universality class. There are also disadvantages with this method. It is always delicate to perform a finite difference calculation using an ordinary differential equation, because of the many parameters one has to vary to obtain optimal results. However, in the case of a nonlinear stochastic differential equation, things are even worse. One then has to worry about the stability of the solution, the range of validity of the various parameters. Furthermore, the presence of noise does not make things easier. Finally, one has to be confident of having reached the scaling regime to evaluate meaningful scaling exponents.

As was mentioned in Chapter 2, we expect that the asymmetric SOS model belongs to the same universality class as the KPZ equation in *any* dimension. In parallel to the numerical integration of the KPZ equation, we thus performed a Monte Carlo simulation of this model.

In this chapter, we present the integration method we have used, and the various tests we have performed to verify the robustness of our results. We also describe the Monte Carlo simulations performed on the asymmetric SOS model. We then present some two dimensional results, some crossover results, and close the chapter with the three dimensional results for the scaling exponents and the crossover exponent.

3.1 The finite difference method

The finite difference method (or Euler method) is the simplest method to simulate differential equations. It consists in making the following approximation for the spatial and temporal derivatives

$$\begin{aligned} \frac{\partial h(\vec{x},t)}{\partial \vec{x}} &= \frac{h(\vec{x}+\Delta\vec{x},t)-h(\vec{x},t)}{\Delta\vec{x}}, && (3.1) \\ \frac{\partial h(\vec{x},t)}{\partial t} &= \frac{h(\vec{x},t+\Delta t)-h(\vec{x},t)}{\Delta t}. && (3.2) \end{aligned}$$

Using this scheme, one can approximate the KPZ equation by the following form

$$\begin{aligned} h(\vec{x},t+\Delta t) &= h(\vec{x},t)+\Delta t\left[\nu\frac{(h(\vec{x}+\Delta\vec{x},t)+h(\vec{x}-\Delta\vec{x},t)-2h(\vec{x},t))}{(\Delta x)^2}\right. \\ &\left.+\frac{\lambda}{2}\left(\frac{h(\vec{x}+\Delta\vec{x},t)-h(\vec{x},t)}{\delta x}\right)^2+\eta(\vec{x},t)\right] \qquad (3.3) \end{aligned}$$

There are of course conditions to be fulfilled for this approximation to be valid and to give the right solution to the equation. First, Δx and Δt have to be chosen small enough so that the length and time scales of interest are larger than them. That is

$$\begin{aligned} \Delta x &\ll L, && (3.4) \\ \Delta t &\ll t && (3.5) \end{aligned}$$

where L and t are respectively the length scales and time scales associated with the problem. Furthermore, Δx and Δt cannot be chosen independently. This is seen easily if one examines closely the Euler approximation. The equations to be solved involve both temporal and spatial derivatives. Thus, not only are there certain length and time scales present in the system, but the two are related (for example, through speed in the case of a wave equation). Thus, the choice of the time and space increments must be made judiciously, first of all to avoid wasting (computer) time, but more importantly to avoid numerical instabilities. For example, it is well known that, in the case of the diffusion equation

$$\frac{\partial h(\vec{x},t)}{\partial \vec{x}} = D\nabla^2 h(\vec{x},t), \tag{3.6}$$

Δx and Δt have to be chosen so that $\Delta t/(\Delta x)^2 \leq 0.5$. This constraint is obtained by taking the difference between the exact solution - that is, the whole expansion -and the approximate solution and chosing $\Delta t/(\Delta x)^2$ such that this difference converges to a finite bound. Furthermore, we are interested in differential equations which incorporate an additive noise piece. This should make things worse, because it introduces an additional deviation of the numerical results from the exact results. Finally, the presence of a nonlinear piece introduces the possibility of bifurcation problems, which can only be detected by careful inspection of the data. All the concerns above must be appropriately treated in the numerical scheme.

To test the robustness of our results, we performed various tests. We first varied Δt and Δx to detect any changes in the results. We used $\Delta t = 10^{-2}, 5\times10^{-3}, 10^{-3}$ and

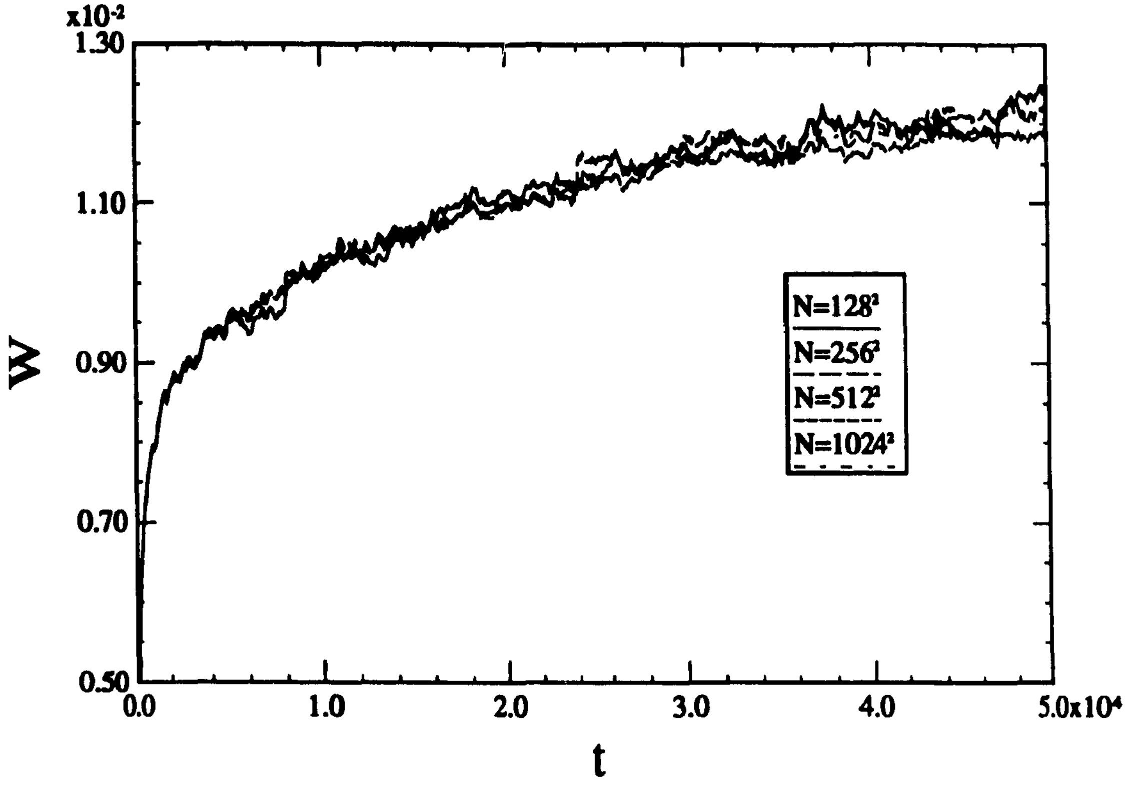

Figure 3.1: Check for the presence of finite size effects in the KPZ simulations. t is the time, W is the width of the interface

$\Delta x = 1, 0.5$ for $d = 2$, and $\Delta t = 10^{-3}, 5\times10^{-4}, 10^{-4}$ and $\Delta x = 1, 0.5$ for $d = 3$. For all those different parameters, our results did not change. We then varied the sizes of the systems we simulated, to check for any size dependence in the growth of the width. We used sizes of $L = 4096, 8192, 16384$ for $d = 2$ and $N = 128^2, 256^2, 512^2, 1024^2$ for $d = 3$ (see Fig. 3.1). Again, the width did not exhibit any size dependence.

All those tests were performed with white noise, that is

$$\forall(\vec{x},t), \eta(\vec{x},t) \in [-1,1], \tag{3.7}$$

$\eta(\vec{x},t)$ satisfying Eqs. 2.6 and 3.7. We also used a seed-shuffling algorithm to avoid possible correlations. To further test our algorithm, we simulated the KPZ equation with the same parameters but with gaussian noise

$$\forall(\vec{x},t), \eta(\vec{x},t) \in [-\infty,+\infty] \tag{3.8}$$

and

$$\mathcal{P}(\eta(\vec{x},t)) \propto \exp(-(\eta(\vec{x},t))^2). \tag{3.9}$$

Again, no differences were found between various runs.

To check the accuracy of our integration scheme, we made use of sum rules derived by Fox (Fox 1990) for the KPZ equation. If one makes use of the nonlinear change of variable $w(\vec{x},t) = \exp[\lambda h(\vec{x},t)/2\nu]$, one then obtains the following differential equation:

$$\frac{\partial w(\vec{x},t)}{\partial t} = \nu\nabla^2 w(\vec{x},t) + \frac{\lambda}{2\nu}\eta(\vec{x},t)w(\vec{x},t). \tag{3.10}$$

This is a diffusion equation plus a multiplicative noise term. This equation is thought to represent directed polymers, as well as quenched disorder (Krug and Spohn 1990). The white noise assumption allows us to make use of the Furutsu-Novikov theorem (Furutsu 1963; Novikov 1965) to obtain the following equation:

$$\frac{\partial}{\partial t}\langle w(\vec{x},t)\rangle = \nu\nabla^2\langle w(\vec{x},t)\rangle + \left(\frac{\lambda}{2\nu}\right)^2 D\delta^{d-1}(0)\langle w(\vec{x},t)\rangle, \tag{3.11}$$

where $\delta^d(0)$ is the d-dimensional delta function. We can get rid of this divergence by introducing an ultraviolet cut-off; that is, a lattice constant which is present in any real system. Then, the noise correlation assumes the following form

$$\langle\eta(\vec{x},t)\eta(\vec{x}',t')\rangle = 2D(2\pi\sigma^2)^{-\frac{(d-1)}{2}}\exp\left(-\frac{(\vec{x}-\vec{x}')^2}{2\sigma^2}\right)\delta(t-t') \tag{3.12}$$

Taking the average of Eq. 3.10, we then obtain

$$\frac{\partial}{\partial t}\langle w(\vec{x},t)\rangle = \nu\nabla^2\langle w(\vec{x},t)\rangle + \left(\frac{\lambda}{2\nu}\right)^2 D(2\pi\sigma^2)^{-\frac{(d-1)}{2}}\langle w(\vec{x},t)\rangle. \tag{3.13}$$

Solving for $\langle w(\vec{x},t)\rangle$, we find

$$\begin{aligned}
\langle w\rangle &= \exp\left[t\left(\frac{\lambda}{2\nu}\right)^2 D(2\pi\sigma^2)^{-\frac{(d-1)}{2}}\right]\exp(t\nu\nabla^2)w(0) && (3.14)\\
&= \exp\left[t\left(\frac{\lambda}{2\nu}\right)^2 D(2\pi\sigma^2)^{-\frac{(d-1)}{2}}\right] && (3.15)
\end{aligned}$$

We can thus say that $\langle w(\vec{x},t)\rangle$ is an exponential function of time. More precisely,

$$\ln\langle w\rangle = c\left(\frac{\lambda}{2\nu}\right)^2 t \tag{3.16}$$

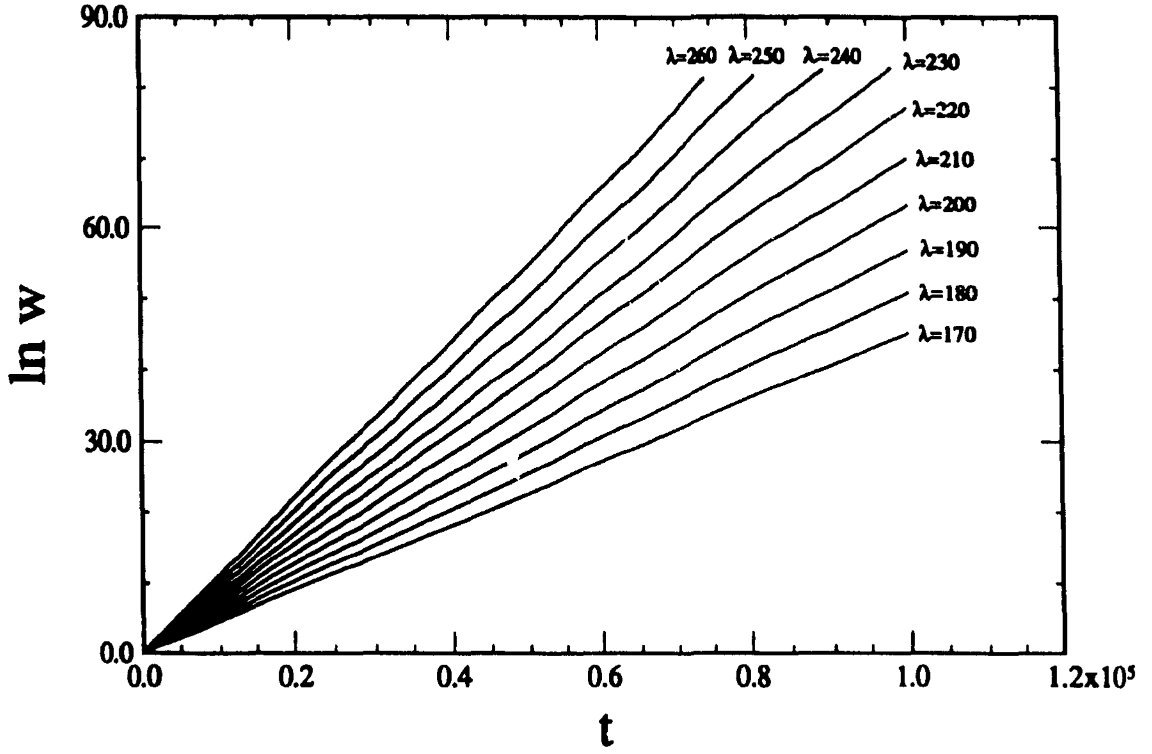

Figure 3.2: Sum rule test on the KPZ equation. t is the time, w is defined in Eq. 3.15

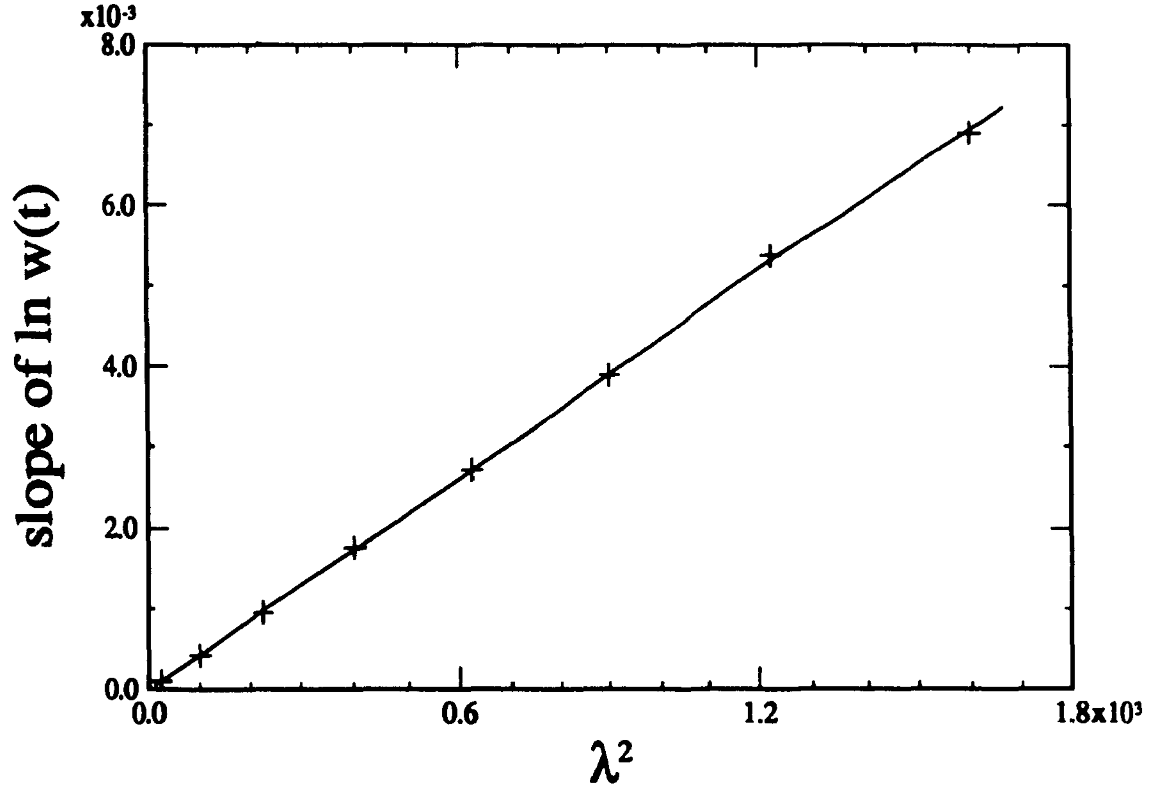

Figure 3.3: Sum rule relation in $d = 2$. λ is related to the strength of the driving field, w is defined in Eq. 3.15

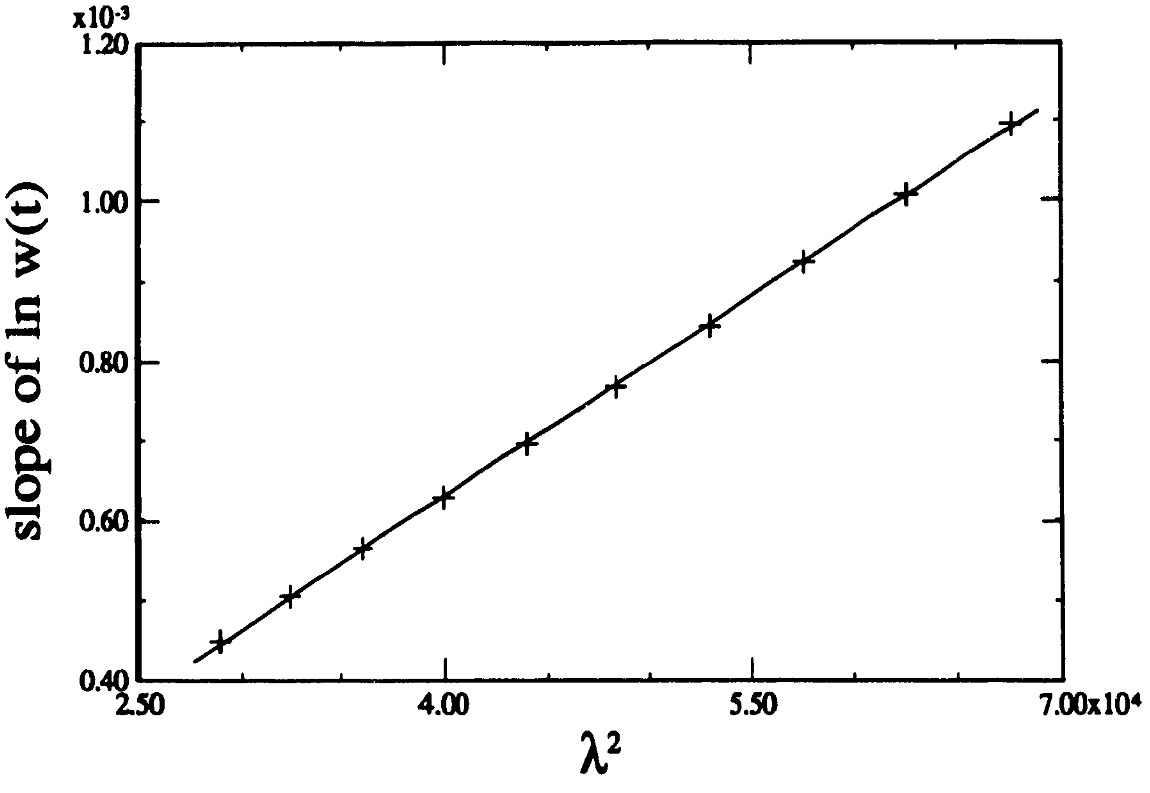

Figure 3.4: Sum rule relation in $d = 3$.

where c is a constant. Thus, $ln\langle w\rangle$ is a linear function of time and the slope of the line is proportional to λ^2.

We then tested these predictions by calculating $\langle w(\vec{x},t)\rangle$, taking the logarithm of the data and plotting the variation of the slope as a function of λ^2 (since ν is held constant). As can be seen from Figs. 3.2, 3.3 and 3.4, this exact property of the KPZ equation is well-obeyed by our numerical integration results.

3.2 The Monte Carlo method

The Monte Carlo method has been known for a long time, but only with the recent advent of powerful computers has it been possible to fully utilize its advantages. Our purpose here is not to review extensively its applications, but rather to concentrate on the points essential to our work.

The Monte Carlo method in statistical physics permits the study of models of equilibrium and nonequilibrium thermodynamic system by stochastic computer simulation. Starting from the description of the desired physical system by a model Hamiltonian, one uses random numbers to construct the appropriate probability with which the various generated states of the systems have to be weighted. In the classical equilibrium case, the Monte Carlo simulation allows for the calculation of the phase space integrals associated with the following expression:

$$\langle A \rangle = \frac{\int_{\Omega} dx A(x) \exp[-\mathcal{H}(x)/k_B T]}{\int_{\Omega} dx \exp[-\mathcal{H}(x)/k_B T]}, \tag{3.17}$$

where A is an observable,$\mathcal{H}(x)$ is the Hamiltonian of the model with phase space variables x, k_B is the Boltzmann constant and T is the temperature. We thus want to calculate the statistical mechanics average of A. It was quickly realized that this *random sampling* method was not of great use for problems in statistical mechanics, because it gives the same probabilistic weight to any configuration occurring in the phase space. Consequently, Metropolis et al. introduced the idea of *importance sampling*. Instead of chosing the points in the phase space completely at random, they are selected according to a probability $P(\vec{x}_i)$. Then, Eq. 3.17 is approximated by

$$\langle A \rangle \approx \frac{\Sigma_{i=1}^{M} A(x_\nu) P^{-1}(x_i) \exp[-\mathcal{H}(x_i)/k_B T]}{\Sigma_{i=1}^{M} \exp[-\mathcal{H}(x_i)/k_B T]}, \tag{3.18}$$

where M is the number of phase space points we use for the averaging procedure. The simplest and most natural possibility is choosing $P(x_i) = P_{eq}(x_i) \propto \exp\left[-\mathcal{H}(x_i)/k_B T\right]$. Since $P_{eq}(x_i)$ is not known explicitly in the case of interest here, the realization of Eq. 3.18 is not completely obvious. Nevertheless, it is possible to construct a random walk of points x_i via a Markov process – that is, a process which probability distribution for any future realization of a state only depends on its present probability distribution – such that $P(x_i)$ tends towards $P_{eq}(x_i)$ as the number of points generated to calculate the integral goes to infinity. This Markov process is defined by specifying a transition probability $W(x_i \longrightarrow x_j)$ from one phase space point x_i to another point x_j. In order that the Markov process has the desired convergence property, it is sufficient to impose the detailed balance condition

$$P_{eq}(x_i)W(x_i \rightarrow x_{i'}) = P_{eq}(x_{i'})W(x_{i'} \rightarrow x_i), \tag{3.19}$$

which means that the ratio of transition probabilities depends on the change in energy $\delta\mathcal{H} = \mathcal{H}(x_j) - \mathcal{H}(x_i)$ only, that is

$$\frac{W(x_i \rightarrow x_{i'})}{W(x_{i'} \rightarrow x_i)} = \exp[-\delta\mathcal{H}/k_B T]. \tag{3.20}$$

One choice for $W(x_i \rightarrow x_j)$ is

$$W(x_i \rightarrow x_{i'}) \quad = \quad \frac{1}{\tau}\exp[-\delta\mathcal{H}/k_B T] \qquad \delta\mathcal{H} > 0 \tag{3.21}$$

$$= \quad \frac{1}{\tau} \qquad \delta\mathcal{H} < 0 \tag{3.22}$$

where τ is an arbitrary factor which does not affect detailed balance. Thus, one takes $\tau = 1$.

The procedure above is applied to obtain static quantities of systems that are in equilibrium. The application of the Monte Carlo method to calculate dynamical quantities is more problematic. This is because many systems considered do have a time evolution in terms of deterministic kinetic equations for their variables. However, some important models do not have a time associated with their dynamics. The equilibrium SOS model belongs to the latter class. Then, the kinetics associated with Eqs. 3.21-3.22 provide a measurement of time.

Up to now, we have been focusing on equilibrium systems. It is clear that the asymmetric SOS model does not describe an interface at or close to equilibrium. However, we have to remember that it is a microscopic model, describing interactions down to a very small length scale. Our assumption is that the energetics at those length scales do not change, or, equivalently, that the interface exhibits local equilibrium. With this assumption, it is then reasonable to use the Monte Carlo method, on recalling that the biggest changes in the nonequilibrium model with respect to the equilibrium one occur in the small wavevector region, on large length scales.

Although Monte Carlo methods are quite different from numerical integrations, their results are hampered by similar problems: one still has to deal with finite size effects, and the simulation time still has to be long enough to ensure that we are in the scaling regime of interest. Furthermore, the constraints on the time step Δt of the numerical integration are replaced by constraints on the temperature T at which the Monte Carlo simulation is performed given an interaction strength J. We thus performed various test runs to satisfy ourselves that we were simulating the model in the right regime, and in particular, far enough away from the roughening transition.

3.3 Results in two dimensions

An important test of our algorithms and the validity of our microscopic model was the study of the KPZ equation and the asymmetric SOS model in $d = 2$. On integrating the KPZ equation, we recovered the exact results obtained previously (Forster, Nelson and Stephen 1977; Kardar, Parisi and Zhang 1986). The equilibrium roughening results were obtained when the driving force was zero. The equation was solved with systems of size $L = 4096$ and λ between 0 and 80, which we found was of sufficient size to avoid finite-size effects. A time mesh $\Delta t = 10^{-2}$ was used; smaller values gave essentially the same results. Results from over 100 independent integrations of the equation were averaged. The width of the interface W was monitored as a function of time t, where $W \sim t^{\beta}$. For $\lambda = 0$, we obtained $\beta = 1/4$. For large values of λ, e.g. $\lambda > 40$, the driven growth result, $\beta = 1/3$ was obtained (see Fig. 3.5). However, for values $0 < \lambda < 40$, effective exponents were observed, with values $1/4 < \beta < 1/3$, indicating the presence of crossover behavior.

To obtain the roughening exponent χ, the equation was integrated until a steady state was reached. We then estimated the steady-state exponent χ from $W \sim L^{\chi}$ as the system size was varied from $L = 50$ to 400. For all values of λ, $\chi = 1/2$ was consistently found, in agreement with both the dynamic roughening and the driven growth results (see Fig. 3.6).

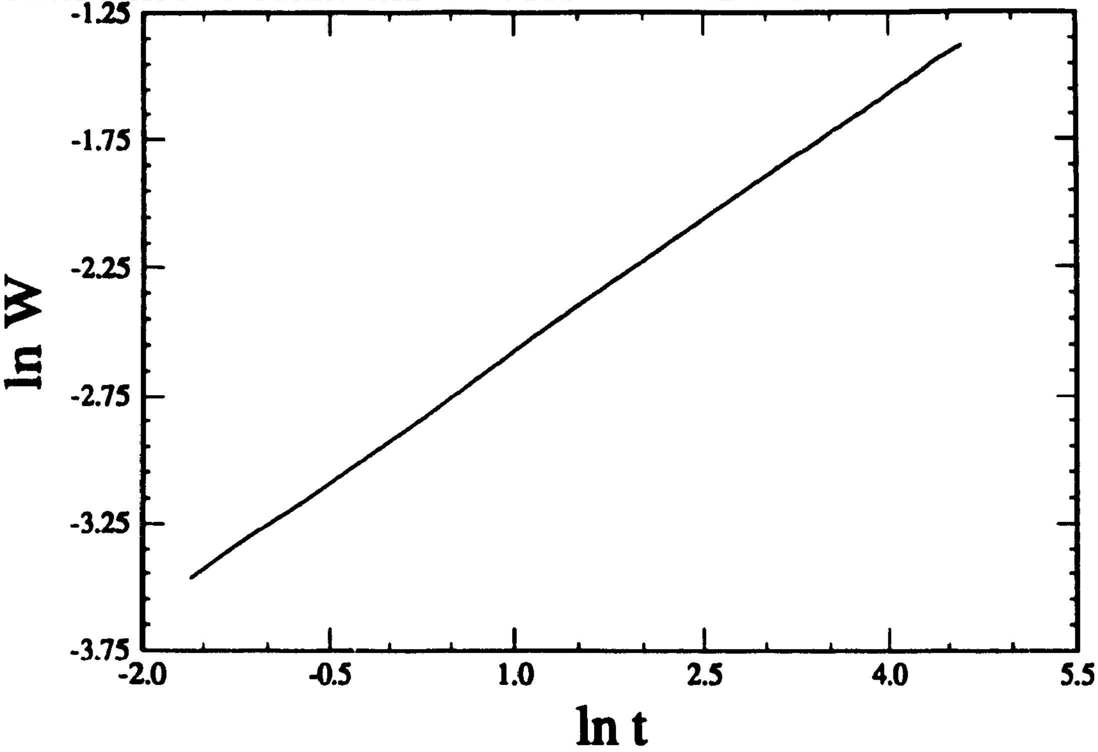

Figure 3.5: Behavior of the interface width related to the KPZ equation as a function of time $d = 2$. t is the time, W is the width of the interface. A fit of this curve yields a growth exponent $\beta = 1/3$.

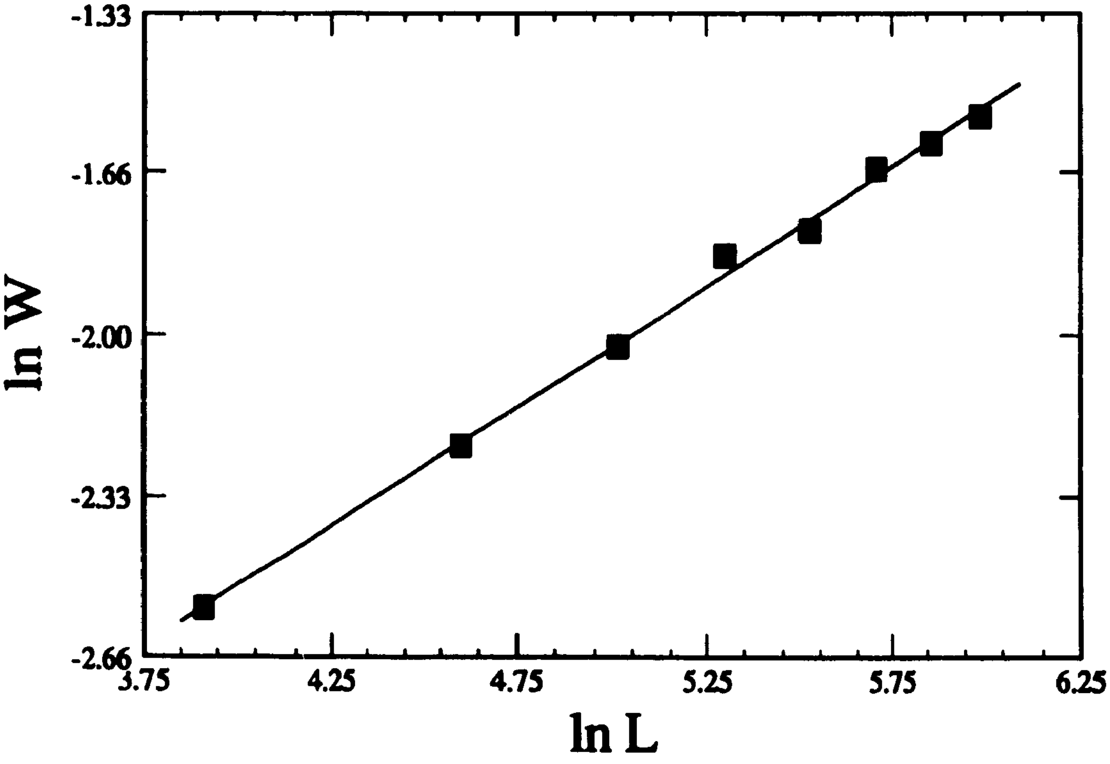

Figure 3.6: Behavior of the interface width of the KPZ equation as a function of size in $d = 2$. L is the linear system size, W is the saturated width of the interface. A fit of this curve yields a growth exponent $\chi = 1/2$.

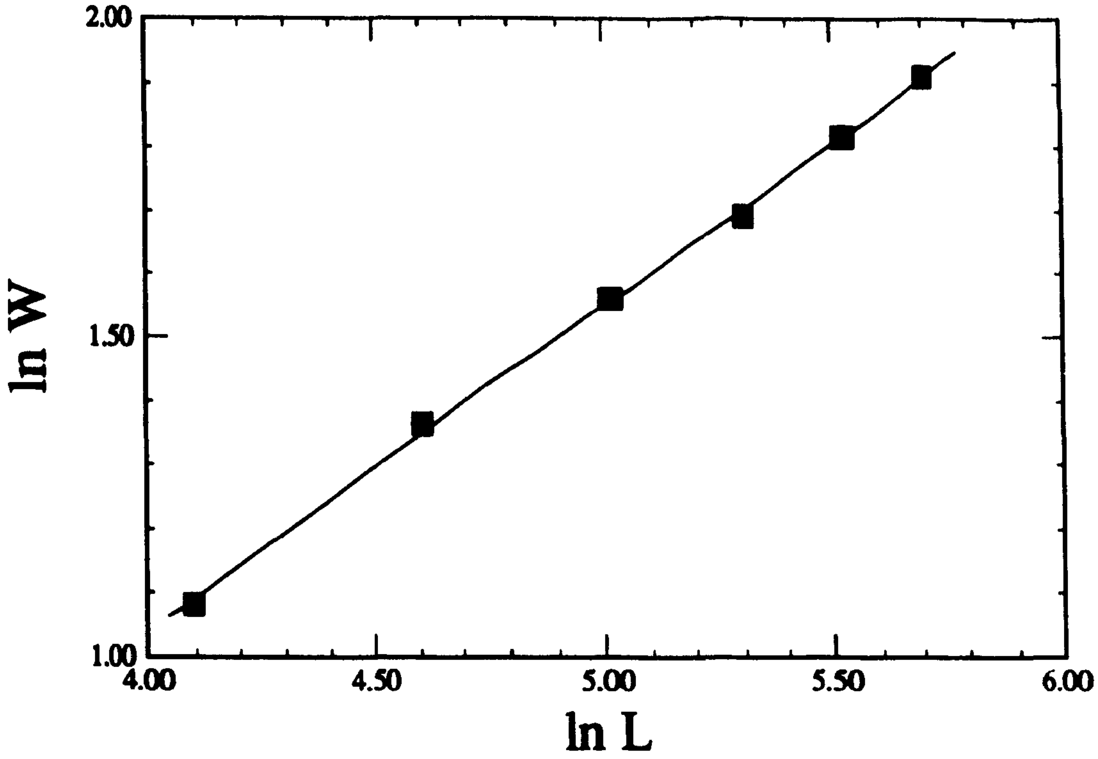

Figure 3.7: Behavior of the interface width of the SOS model as a function of size in $d = 2$. A fit of this curve yields a growth exponent $\chi = 1/2$.

Monte Carlo simulations of the nonequilibrium SOS model were performed with the system temperature, T, set to a convenient (reasonably large) value so as to observe a continuum-like behavior. The growth exponents were found to be independent of temperature. In $d = 2$, systems of size $L = 6\ 000$ and times of up to 40 000 Monte Carlo steps were used to obtain the growth exponent β, and smaller system sizes were used to calculate the growth exponent χ. For any nonzero λ_a, we expected $\chi = 1/2$ and $\beta = 1/3$ in the hydrodynamic limit. Indeed, $\chi = 1/2$ was obtained for all values of λ_a (Fig. 3.7). For $\lambda_a = 1.0$, i.e., when there are only growth attempts, we found $\beta = 1/3$ in agreement with the results for the two-dimensional KPZ equation (Fig. 3.8). For smaller values of λ_a, crossover effects were again observed, while at $\lambda_a = 0$, we observed $\beta = 1/4$ as expected.

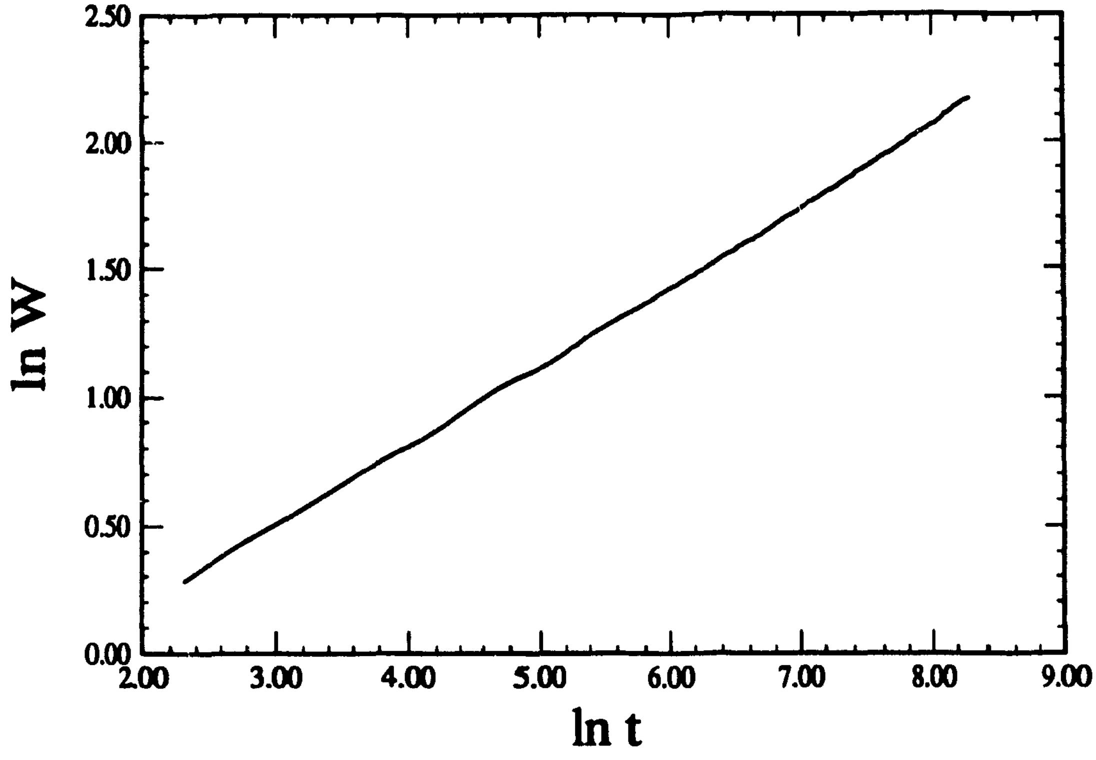

Figure 3.8: Behavior of the interface width of the SOS model as a function of time $d = 2$. A fit of this curve yields a growth exponent $\beta = 1/3$.

3.4 Crossover scaling in two and three dimensions

As is clear from the above, to extract reliable asymptotic results a careful analysis of crossover effects is needed (Guo, Grossmann and Grant 1990b). Since the presence or absence of the nonlinear driving force determines the dynamic universality class (driven or roughening), a natural analogy arises with critical phenomena. There, competing interactions lead to crossover behavior between different universality classes. For example, adding a cubic anisotropic interaction to the N-vector model can give crossover from Ising to Heisenberg fixed points (Brézin, LeGuillou and Zinn-Justin 1974). For the driven growth problem described above, a crossover regime is thus expected when the driving force is small, and either t or L is not asymptotically large. While the usual crossover phenomena occurs between two or more *stable* fixed points, we are now dealing with a situation where the crossover is to a strong-coupling fixed point where dimensional analysis is of little utility (since the $\epsilon = d_c - d$ expansion involves an unstable fixed point). As a consequence, the usual dimensional and scaling analysis cannot predict the crossover exponents. Thus a numerical study, as we present below, is required.

Guided by experience in critical phenomena, it is natural to propose an ansatz to account for crossover. In two dimensions it is

$$W(L,t,\lambda) \sim t^{\beta_0} f_2(tL^{-z_0}, t\lambda^{\phi}), \tag{3.23}$$

where $\beta_0 = 1/4$ and $z_0 = 2$ are the exponents for $\lambda = 0$, f_2 is the crossover scaling function, and the new exponent ϕ accounts for crossover to nonzero λ. Setting $\lambda = 0$, we recover the dynamical roughening results. When $t \ll L^{z_0}$ (or for $L = \infty$), the L dependence of f_2 can be dropped:

$$W \sim t^{\beta_0} f_2(t\lambda^{\phi}). \tag{3.24}$$

If $\lambda > 0$, the growth will eventually be controlled by the unknown strong-coupling fixed point which is characterized by the driven growth exponents β and z. Hence we must have $W \sim t^{\beta}$, so that $f_2(u) \sim u^{\beta-\beta_0}$ for large u. This gives

$$W \sim t^{\beta} \lambda^{\phi(\beta-\beta_0)} \approx t^{1/3} \lambda^{\phi/12}. \tag{3.25}$$

We expect Eqs. 3.24 and 3.25 to hold in the large L limit.

In $d = 3$, the above ansatz must be modified since dynamic roughening is marginal: $W^2 \sim A_0 \ln t$, where A_0 is a constant. Thus we propose the following crossover scaling ansatz

$$W^2(L,t,\lambda) \approx A_0[f_3(t\lambda^{\phi}) - \phi \ln \lambda] \tag{3.26}$$

where the scaling function satisfies $f_3(u) \sim \ln u$, for $u \to 0$; and $f_3(u) \sim u^{2\beta}$, for $u \to \infty$. Again, we require times $t << L^{z_0}$ so that any size dependence can be neglected. We do not consider the possibility of a logarithmic crossover, as has been suggested by Tang *et al.* (Forrest and Tang 1990). The arguments which lead to the logarithmic crossover was based on a fixed dimension calculation to one-loop order of the KPZ equation(Kardar, Parisi and Zhang 1986). Such a calculation is expected to be valid only for the nonlinear coupling constant $\bar{\lambda} << 1$, which is not the case for all the numerical solutions of the KPZ equation performed so far. For $\bar{\lambda} > 1$ the fixed dimension calculation does not give a controlled approximation and no satisfactory theory exists for the strong coupling regime at $d = 3$. We thus resort to a numerical study.

Although no perturbable strong-coupling fixed point has been found for the KPZ equation in $d \leq 3$, it is still worthwhile to show how to find ϕ by simple scaling arguments, if such a fixed point existed. First, we perform a scale transformation in space and time of the KPZ equation using the exponents for $\lambda = 0$: $\vec{x}' = e^{-l}\vec{x}$, $t' = e^{-z_o l}t$, $h' = e^{-\chi_o l}h$. Next, the transformed equation is restored to the original form by redefining the constants: $\nu \rightarrow \nu' = \nu e^{(z_o-2)l}$, $\lambda \rightarrow \lambda' = \lambda e^{(\chi_o+z_o-2)l}$, and $D \rightarrow D' = De^{(z_o-d+1-2\chi_o)l}$. Finally, the transformation $h'(\vec{x}', t', \lambda') = e^{-\chi_o l}h(\vec{x}, t, \lambda)$ implies

$$W(L, t, \lambda) \sim t^{\beta_o}F(Lt^{-1/z_o}, t\lambda^{z_o/(\chi_o+z_o-2)}) \tag{3.27}$$

where a choice of l has been taken such that $e^l = t^{1/z_o}$. This implies that the crossover exponent $\phi = z_o/(\chi_o + z_o - 2)$. Thus, for $d = 2$, this gives $\phi = 4$. However, our numerical results of the KPZ equation below give $\phi \approx 3$. This discrepancy is related to the absence of a stable fixed point in the strong coupling regime which is required for the scaling argument to work. Indeed, the dimensional analysis above is intimately related to the existence of a stable $\epsilon = d_c - d$ expansion, since power counting by the Ginzburg criterion, $\chi_o + z_o - 2 = 0$, determines the critical dimension.

To test the crossover scaling ansats and obtain the exponent ϕ, the numerical results of the previous section were used. In $d = 2$, data for those values of λ which gave $\beta < 1/3$ were analyzed. The inset to Fig. 3.9 shows $f_2 = W/t^{1/4}$ as a function of t for several values of λ. The curves, each representing an average of 100 independent runs, are well separated. If plotted as a function of $t\lambda^{\phi}$, as shown in Fig. 3.9, a good data collapse can be seen on using $\phi \approx 3.0$. This implies that our scaling ansatz is reasonable, with the curve of Fig. 3.9 corresponding to the crossover scaling function,

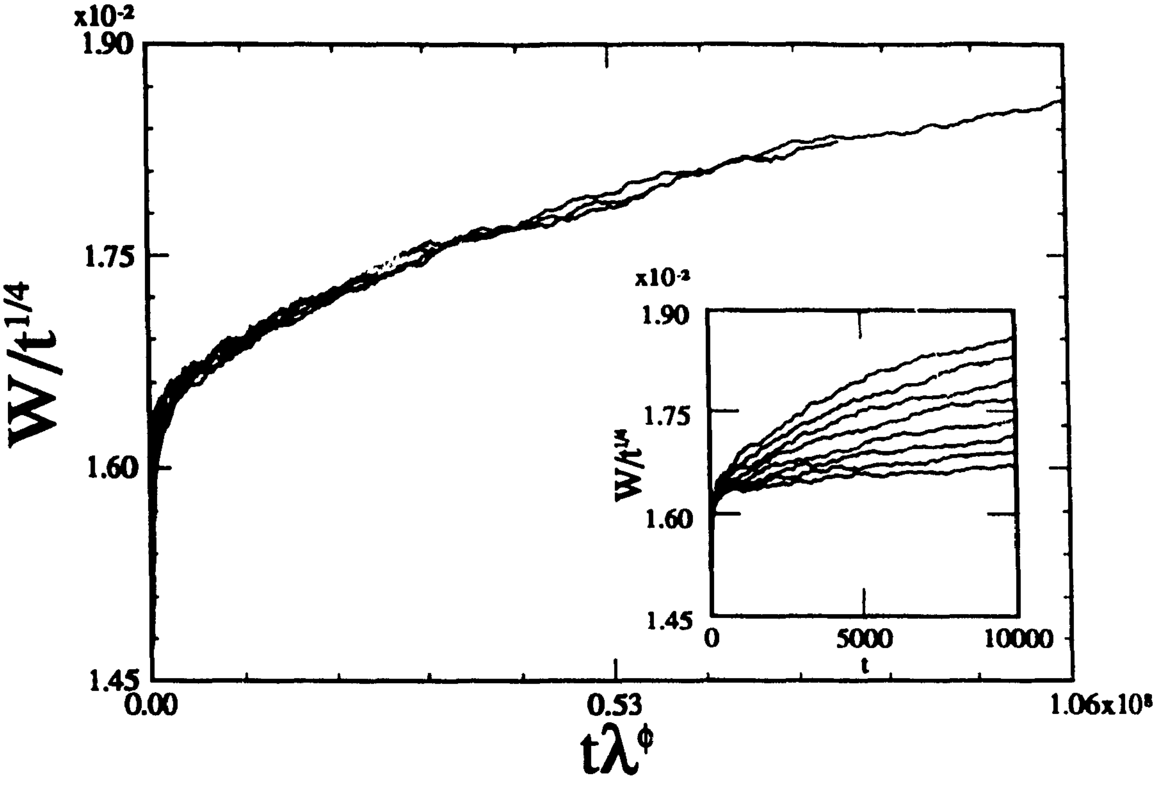

Figure 3.9: Crossover behavior of the KPZ equation in $d = 2$. ϕ is the crossover exponent. We find $\phi = 3.0$. Note that the curves are well-separated if not rescaled, as is shown in the insert.

f_2.

An independent check on the value of ϕ was performed by taking large values of λ, so that $\beta = 1/3$. We then monitored W versus λ for a fixed time. Our ansatz then predicts, as in Eq. 3.25, a power-law dependence, $W \sim \lambda^{\phi/12}$. Indeed, we found that $\ln\, W$ vs $\ln \lambda$ was well fitted by a straight line, as shown in Fig. 3.10, with a slope 0.23 ± 0.02 which is again consistent with $\phi \approx 3$. Combining the two independent calculations of ϕ, our best estimate for the crossover exponent is $\phi = 3.0 \pm 0.2$.

If the nonequilibrium SOS model shares a universality class with the KPZ model, we expect not only growth exponents, but also crossover behavior to be identical. Thus a crossover scaling analysis of our Monte Carlo data for small values of λ_a was performed. Keeping the system at a fixed temperature $T = 0.5$, we averaged results of 250 independent runs on systems of size $L = 2\ 000$, each with 4 000 Monte Carlo steps for different values of λ_a. Fig. 3.11 shows the crossover scaling function defined in Eq. 3.24 for the SOS model after data collapsing. This analysis gave a crossover

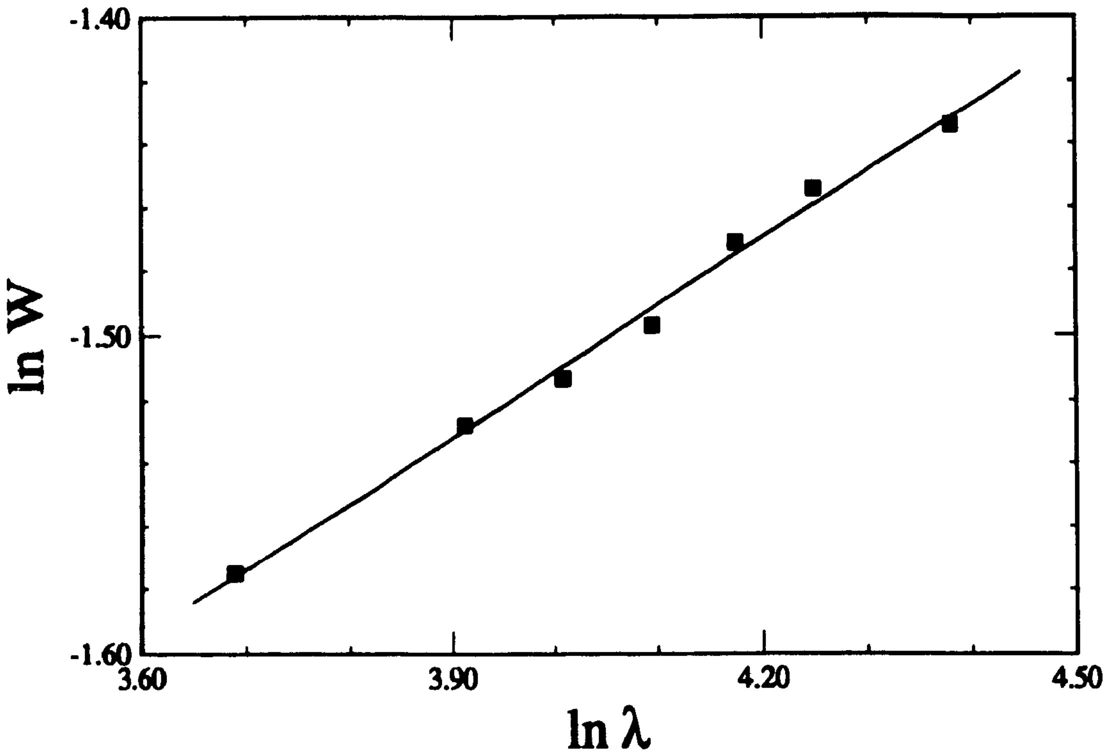

Figure 3.10: ln W vs ln λ for various values of λ.

exponent $\phi \approx 3.0$ which indeed agrees with that of the two-dimensional KPZ model.

In three dimensions, we integrated the KPZ equation using parameters discussed in the next section. Data with λ ranging from 120 to 240 by steps of 20 was used for the crossover analysis. For $\lambda < 120$, much longer runs were needed. Fig. 3.12 plots $f_3 = w^2/A_0 + \phi \ln \lambda$ versus $t\lambda^{\phi}$, where A_0 is obtained from the fit $W^2 = A_0 \ln t$ when $\lambda = 0$. As shown in the plot, with $\phi = 4.5$ excellent data collapsing is achieved. The behavior of f_3 at large values for $t\lambda^{\phi}$ was consistent with our results for β in three dimensions in the next section. Nevertheless, we caution that systematic errors could be present in our estimation of exponents in $d = 3$, because it is a marginal dimension. We did not perform a crossover scaling analysis on the three-dimensional SOS model due to the complications caused by the presence of a roughening transition.

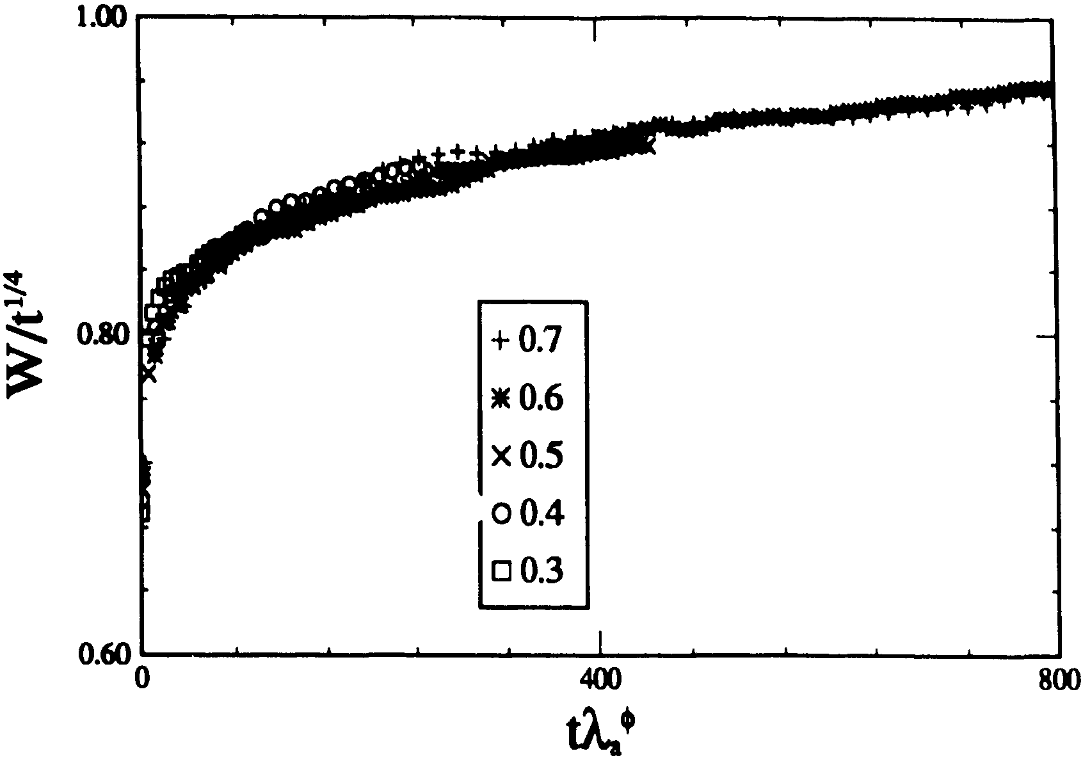

Figure 3.11: Crossover behavior of the asymmetric SOS model in $d = 2$. λ_a is the bias related to the difference between the probability of growing and the probability of evaporating.

3.5 Roughening exponents for the driven interface in three dimensions

The integration of the KPZ equation is hampered by large fluctuations and crossover effects. Besides large number of independent runs for average, one must study sufficiently large system sizes so that the growth of the width persists until the nonlinear term becomes important. Typically the following parameters were used: $\Delta t = 10^{-3}$, with 50 000 integration steps, and system sizes of 128^2 and 256^2. Test runs on 512^2 and 1024^2 systems were also performed which yielded the same value for β. Reducing the time mesh to $\Delta t = 2.5 \times 10^{-4}$ and integrating over 200 000 steps also gave the same results. As in the two-dimensional case, we varied λ to ensure the system was in the driven growth regime. Fig. 3.13 shows our results for W versus t with $\lambda = 240$, from averaging 50 independent runs. For late times, we estimate $\beta \approx 0.13 \pm 0.02$, in agreement with the value obtained by Chakrabarti and Toral

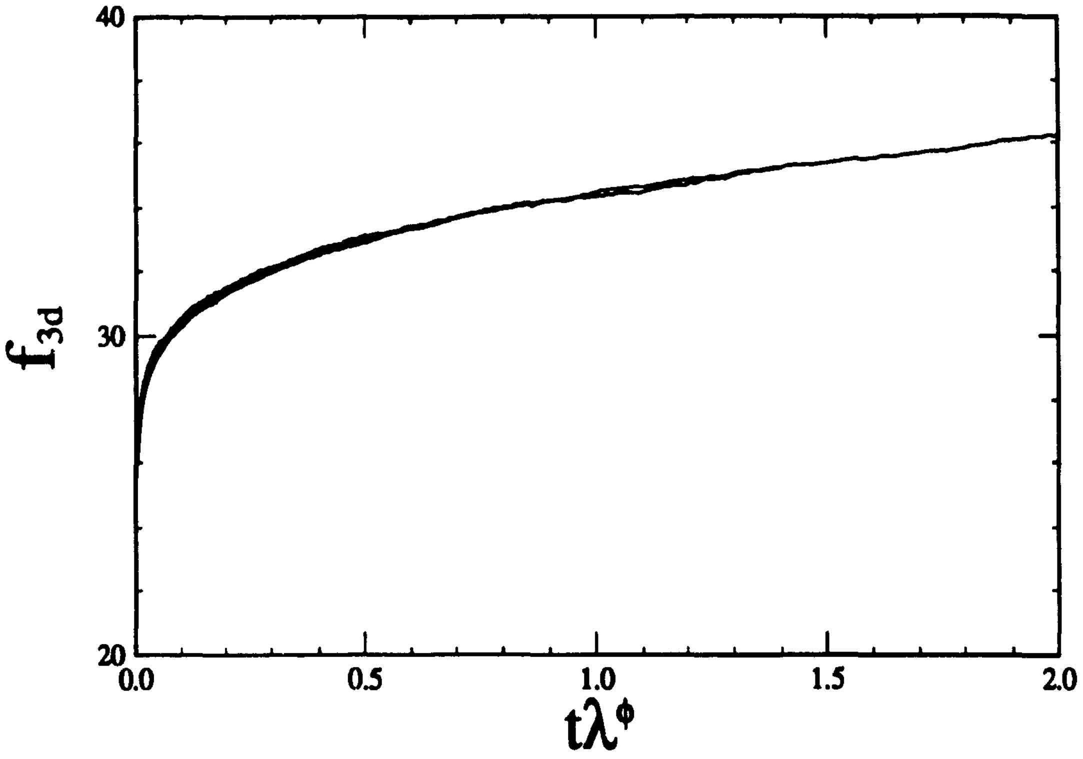

Figure 3.12: Crossover behavior of the three-dimensional KPZ equation. f_{3d} is the crossover scaling function.

(Chakrabarti and Toral 1989; Guo, Grossmann and Grant 1990a) but smaller than the value obtained by Amar and Family (Amar and Family 1989). Note that the effective exponent *drops* to that value from $\beta \sim 0.5$ for early times (due to the noise η). This phenomenon stems from the following analysis: at early times, the interface is only driven by noise. In this case it is well known that the exponent β must equal 1/2. As the interface length increases and long wavelength develop, the surface tension term becomes relevant. Finally, the non-linear piece comes into play, thus the crossover behavior described in the previous section. It is also worth mentioning that we have undertaken some selected analysis of larger systems, as well as larger values of coupling constants, and recover equivalent results. While for any nonzero λ we expect the dynamics in the asymptotic regime to be governed by the strong-coupling fixed point, for small values of λ crossover effects were important, as discussed above. Nevertheless, for $\lambda > 240$ we found the value quoted above.

The value for χ was more difficult to obtain because of large fluctuations, thus

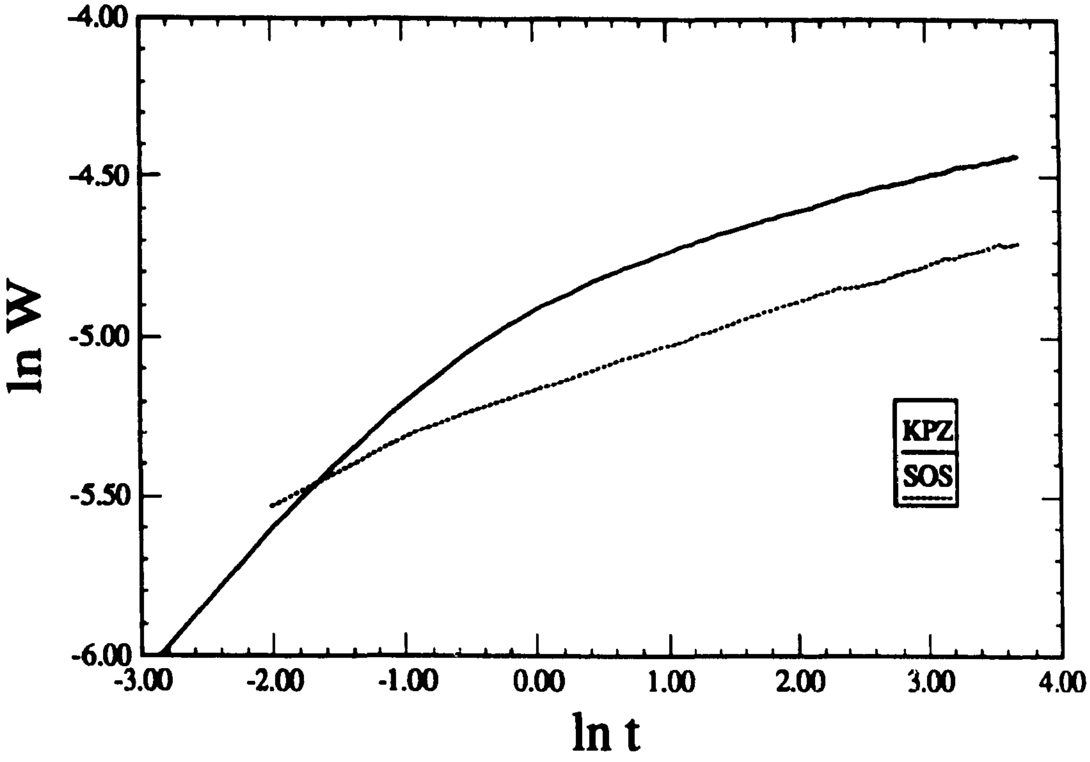

Figure 3.13: Growth exponent β for the three-dimensional KPZ equation and the SOS model. The latter data have been shifted down and left to compare them more easily to the KPZ data.

requiring a large amount of computing time. Nevertheless, data for $L \leq 30$ yielded $\chi = 0.24 \pm 0.04$ (Fig. 3.14). Noting that $z = \chi/\beta$, we thus verified numerically the hyperscaling relation (Kardar, Parisi and Zhang 1986) $\chi + z = 2$ in $d = 3$. Note that these exponents are distinctly different from those of dynamical roughening, $\beta_o = 0$ and $\chi_o = 0$, where W only diverges logarithmically.

As mentioned above, the interface dynamics represented by the KPZ equation is expected to account for that of a large universality class of lattice models, which we expect to include the asymmetric SOS model. In $d = 3$, Monte Carlo simulations of that model were done to extract the growth exponents β and χ. Systems of size 100^2 were used throughout, since they were found to be of sufficient size. In Fig. 3.13, the ln-ln plot of W versus t is shown along with that for the three-dimensional KPZ model. For $\lambda_a = 1$ and any reasonable T well above the roughening transition, we estimate $\beta \approx 0.13$ and $\chi \approx 0.25$, in agreement with the results obtained for the three-dimensional KPZ equation. From Fig. 3.15, we estimate $\chi \approx 0.25 \pm 0.02$,

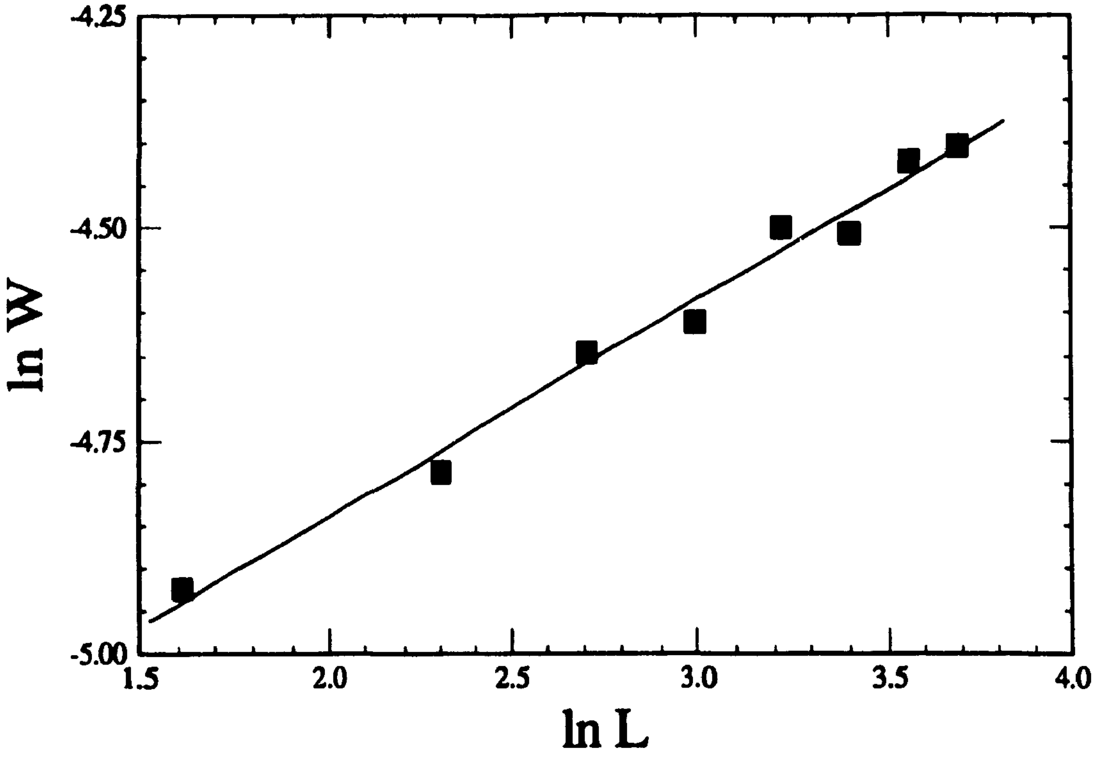

Figure 3.14: Saturation exponent χ for the three-dimensional KPZ equation

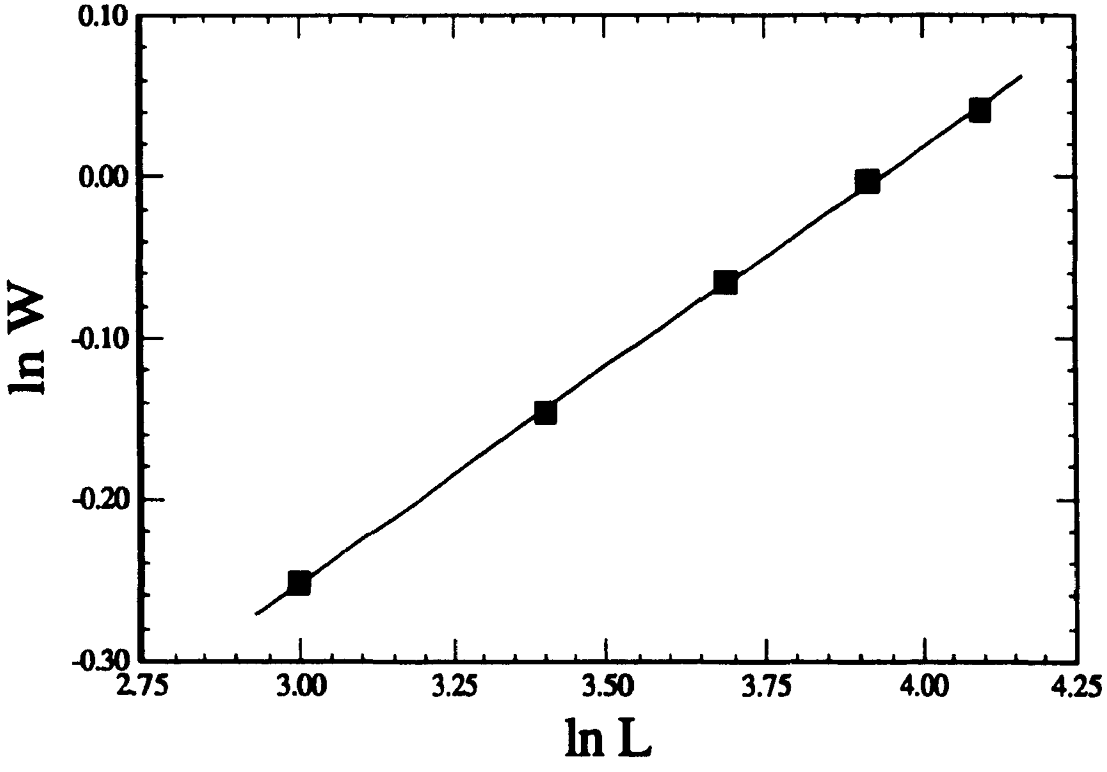

Figure 3.15: Saturation exponent χ for the three-dimensional SOS model

which again agrees with the hyperscaling relation. As in the two-dimensional case, smaller λ_s showed strong crossover effects, as discussed above. Nevertheless, the good agreement between the various exponents obtained in $d = 2$ and $d = 3$ make us confident that the KPZ equation and the nonequilibrium SOS model are in the same dynamic universality class in *both* two and three dimensions.

Thus, in $d = 3$, our best estimates for the growth exponents for both the KPZ equation and the asymmetric SOS model are $\beta \approx 0.13$, and $\chi \approx 0.25$. These results are not consistent with conjectures in the literature (Kardar, Parisi and Zhang 1986; Wolf and Kertész 1987a; Kim and Kosterlitz 1989). Those conjectures were, however, motivated by the study of simple models which, although they share similar features to the KPZ equation, are not obviously in the same universality class. Nevertheless, we again caution that crossover effects could play an important and subtle role in $d = 3$, because it is a marginal dimension, which may imply considerable systematic errors in our estimation of exponents. Further study is required to definitively determine the nature of growth in $d = 3$.

Chapter 4

The Equilibrium Roughening Transition

The study of phase transitions has played an important role in twentieth-century physics. At first, this interest might appear strange, since the phase transition lines represent only a very small portion of the phase diagram itself. Indeed, second order phase transitions often occur only at one point in the phase diagram. In the first part of this chapter, we will explain the importance of this phenomena.

The previous chapter was devoted to the study of interface dynamics, that is, the way the interface grows, its speed of growth, its roughness, and so on. However, this study did not take into account the behavior of the interface that is associated with its underlying microscopic structure. For example, it has long been known that below a certain temperature, the equilibrium interface should be microscopically flat. This stems from a microscopic study of the interface, which we will describe briefly below. Thus, there should be a certain temperature at which the interface changes state, and this change of state is associated with a phase transition. The nature of this phase transition has been the subject of much debate in the last 30 years. We now review the main results of the equilibrium roughening transition.

4.1 Introduction to phase transitions

Thermodynamic systems can exist in a number of phases, each of which can exhibit dramatically different macroscopic behavior. Generally, systems become more ordered as the temperature is lowered. Forces of cohesion tend to overcome thermal motion, and atoms rearrange themselves in a more ordered state. Phase changes occur abruptly at some transition temperature, although evidence that one will occur can sometimes be found on a microscopic scale as the transition temperature is approached.

The thermodynamics associated with phase transitions is relatively simple. At a transition point, two or more phases can coexist in equilibrium with each other, as stated by Gibb's phase rule. As a consequence of this, the chemical potential of the phases, and therefore the Gibbs free energy, must change continuously. However, phase transitions can be divided into two classes according to the behavior of the derivatives of the Gibbs free energy. Phase transitions which are accompanied by a discontinuous change of state – a discontinuous first derivative of the Gibbs free energy – are called first-order transitions. Phase transitions that are accompanied by a continuous change of state – the first derivative of the Gibbs free energy varying continuously – are called continuous or second-order phase transitions.

Phase transitions occur at, say, a critical point; a well-defined temperature above which one phase exists, and as the temperature is lowered a new phase appears. When a new phase appears, it often has different symmetry properties, and some new variable, called the order parameter, appears which characterizes the new phase. For first order phase transitions, there need not be a connection between the symmetries of the high- and low-temperature states. For a continuous phase transition, however, since the state changes continuously, there will generally be a well-defined connection between the symmetry properties of the two phases.

The field of critical phenomena is associated with continuous phase transitions. At the critical point one observes divergences in otherwise well-behaved thermodynamic quantities such as the specific heat for liquid-gas systems and the susceptibility for magnetic systems. Those divergences allowed people to define critical exponents. Indeed, it is now fairly well accepted that divergences occurring at the critical point are described by power laws. Thus, if $f(x)$ is a diverging thermodynamic function, one writes $f(x) \sim x^{-\alpha}$ as x goes to zero. This means that

$$lim_{x \to 0} \frac{\ln[f(x)]}{\ln x} = -\alpha \tag{4.1}$$

where x is the distance from the critical point. Usually, there are corrections to the power law behavior of thermodynamic functions, so that. one has to be in the asymptotic regime before calculating any meaningful critical exponent. The singularities at a critical point are related to fluctuation phenomena. Consequently, it is difficult to solve these kinds of problems exactly, because of the collective behavior of a large number of components of the macroscopic system studied. Instead, one uses appropriately chosen models which exhibit the right physical behavior. It is in this context of simplicity that the concept of scaling appeared. Scaling consists in describing the singular part of the various thermodynamic function near the critical point in terms of distance from the critical point, thus defining a set of critical exponents. The success of this description is because the correlation length diverges at the critical point. Scaling also explains why different systems nevertheless behaved in exactly the same way at their respective critical point, that is, they were described by the same sets of critical exponents. One then says that they belong to the same universality class. This latter concept can be very useful because it allows people to know what critical exponents describe a system without having to experimentally find them. It also allows various tests to be performed on theoretical models. Finally, scaling is the last step leading to renormalization group methods which have been introduced in Chapter 2.

As was mentioned at the beginning of this section, phase transitions occur in a variety of systems. The equilibrium roughening transition is a particularly fascinating example of phase transition. It also provides us with a very good example of how useful the concept of universality class can be. Let us now describe this transition in more detail.

4.2 The equilibrium roughening transition

In their now famous paper published in 1951, Burton, Cabrera and Franck were the first to suggest the existence of a roughening transition in crystal surfaces. They were actually interested by the behavior of solid surfaces in equilibrium with their vapor, and the growth that occurs in such systems. Based on energetic considerations, they showed that below a certain temperature, the growth due to the formation of nucleation droplets on the surface would in practice be replaced by the growth due to the presence of screw dislocations in the bulk. They then went on to identify the presence of a interface in $d = 3$ as being well-described by a two dimensional Ising model (Fig. 1.1). Their idea was that the surface layer was not influenced by the bulk or the vapor because of an exact cancellation taking place between the layers above and the layers below it. Then, as the two dimensional transition temperature for the Ising model was approached, large fluctuations would destroy the surface layer. According to this analysis, the roughening temperature would then have to be fairly close to the phase transition temperature of the two-dimensional Ising model.

While qualitatively correct in some aspects, the Burton-Cabrera-Franck argument is incomplete and not correct in detail. The main reason for the incorrectness of their reasoning lies in the fact that Burton *et al.* did not take into account the possibility of layers growing on the top of layers. By doing this, they then put a very strong constraint on the number of degrees of freedom describing the interface. Namely, from infinity this number was reduced to two. It is for the same reason that the exact cancellation of interaction taking place at the surface layer can only occur at $T = 0$. Fluctuations make the the behavior of interface between two coexisting phases more complicated than that given by the argument of Burton *et al.*.

Even though the analogy was incomplete, experimental facts confirmed that Burton *et al.* were still right in their prediction that some crystal surfaces would be rough above a certain temperature, and flat below it. Consequently, some experimentalists started looking for the roughening transition in various materials. However, this proved to be a very difficult task. In fact, theorists uncovered the solution to this problem before direct experimental observations of the transition were made. Since we want to keep the chronological order intact, let us first describe the theory before giving experimental facts.

4.2.1 Theory

As mentioned above, the theoretical study of the roughening transition started in the 50's with the paper by Burton *et al.*. Although their description is valid over a wide range of low temperatures, it breaks down close to the roughening transition temperature because it ignores the multilayer structure of the interface at (and above) this temperature. Nevertheless, it was only in the beginning of the 70's that people started to realize that there was a flaw in the argument put forward in their paper. Gallavotti and van Beijeren were the first to propose that in the three-dimensional Ising model a phase transition delocalizing the interface between phases of positive and negative magnetization might occur at a temperature below the bulk critical temperature. Weeks *et al.* found strong evidence for such a transition from low temperature expansions for moments of displacement of the interface. These expansions were found to become divergent at temperatures roughly 10 % above the critical temperature of the two-dimensional Ising model corresponding to a single layer, that is well below the critical temperature of the three-dimensional Ising model. A major advance in the theory took place in 1976, when Chui and Weeks successfully applied the renormalisation group method of Kosterlitz to study the roughening transition. Chui and Weeks introduced the discrete Gaussian (DG) model described in Chapter 2. Let us rewrite the Hamiltonian associated with it:

$$\mathcal{H}_{DG} = \tfrac{J}{2}\Sigma_{j,\delta}\,(h_j - h_{j+\delta})^2 \equiv \frac{J}{2}\Sigma_{jj'} h_j G_1^{-1}(jj') h_{j'}, \tag{4.2}$$

$$= \frac{J}{2}\Sigma_q |h_q|^2 G_1^{-1}(q) \tag{4.3}$$

where

$$G_1^{-1} = 4 - 2(\cos q_x + \cos q_y) \tag{4.4}$$

and

$$h_q = \frac{1}{\sqrt{N}}\Sigma_j h_j e^{iqj} \tag{4.5}$$

is the Fourier transform of the height variable h_j. Note that in Eq. 4.2, the interaction energy goes as $q^2|h_q|^2$ for small q's. This behavior is characteristic of surface tension (Buff, Lovett and Stillinger 1965), which determines the properties of interfaces at high temperatures. Thus the Gaussian model is thought to represent a wide class of column Hamiltonians.

The DG partition function can be written

$$Z_{DG} = \int dh_j \Pi_j W(h_j) \exp\left[-\frac{1}{k_B T}\mathcal{H}_{DG}\right] \tag{4.6}$$

where

$$\begin{aligned} W(h_j) &= \Sigma_{n_j=-\infty}^{\infty}\delta(h_j - n_j) &(4.7)\\ &= \Sigma_{k_j=-\infty}^{\infty}\exp[ik_j h_j]. &(4.8)\end{aligned}$$

The weighting function $W(h_j)$ in Eq. 4.6 restricts the integration in Eq. 4.5 so that only integer values of h_j contribute. Substituting Eq. 4.7 in Eq. 4.5, we obtain

$$Z_C \equiv \frac{Z_{DG}}{Z_0} = \Sigma_{k_j=-\infty}^{\infty}\left\langle \exp\left(i\Sigma_j k_j h_j\right)\right\rangle. \tag{4.9}$$

Here Z_0 is the unweighted Gaussian model's partition function (the partition function of Eq. 4.5 with $W(h_j) \equiv 1$), which can be evaluated exactly. The angular brackets indicate an ensemble average in the unweighted Gaussian ensemble.

In Eq. 4.8 we note the characteristic function for the Gaussian distribution. Hence the k_j also obey a Gaussian distribution given by the inverse matrix to G_1^{-1} and Eq. 4.8 becomes

$$Z_C = \Sigma_{k_j=-\infty}^{+\infty}\exp\left[-\frac{k_B T}{2J}\Sigma_{jj'}k_j G_1(jj')k_{j'}\right] \tag{4.10}$$

where, from Eq. 4.3, one find the inverse matrix $G_1(jj')$ to be

$$G_1(jj') = \frac{1}{2N}\Sigma_q \frac{e^{iq(j-j')}}{G_1^{-1}(q)}. \tag{4.11}$$

Eq. 4.9 is in fact the partition function for a neutral two-dimensional lattice Coulomb gas (Chui and Weeks 1976) in which the k_j represents the charges. Note the q^{-2} dependence at small q in this equation: this behavior characterizes the Coulomb interaction. Note also that the reduced temperature $k_B T/J$ has been inverted in going from the DG model in Eq. 4.5 to the Coulomb gas in Eq. 4.9. Finally, restrospectively, the fact that the Coulomb gas appears should not surprise us: the matrix $G_1^{-1}(jj')$ in Eq. 4.3 is the lattice analog of the Laplacian operator and hence its inverse matrix, $G_1(jj')$ in Eq. 4.10 is the two-dimensional lattice Green's function, that is the two-dimensional Coulomb potential.

Since Z_0 is analytic, the singularities in the DG partition function Z_D are identical with those in Z_C. These had already been discussed by Kosterlitz and Thouless (Kosterlitz and Thouless 1974; Kosterlitz 1974) in connection with their analysis of the XY model and a dislocation model for two-dimensional melting. They established that the Coulomb gas undergoes a phase transition from a low temperature dielectric phase with opposite charges tightly bound together in "diatomic molecules" to a high temperature metallic phase. The free charges in the metallic phase come from the now disassociated "molecules" and provide the usual Debye screening. The properties of this transition can thus be directly related to those of the roughening transition and differ greatly from those of the two-dimensional Ising model.

Let us now describe in more details the renormalization calculations and results. Chui and Weeks applied this method to an equation similar to Eq. 2.4, but with a periodic term simulating the lattice potential added:

$$\begin{aligned}\frac{\partial h}{\partial t} &= -\Gamma K^{-1}\Sigma_\delta\left(h_j - h_{j+\delta}\right) - \Gamma K^{-1} g^2 h_j + \Gamma\left(\frac{\Delta\mu_j}{T}\right) - \\ &\quad 2\pi K^{-1}\Gamma y_0 \sin 2\pi h_j + \eta_j, \end{aligned} \tag{4.12}$$

where $K^{-1} \equiv 2J/T$ and $\eta(\vec{x},t)$ is the stochastic noise obeying Eqs. 2.5-2.6 If $y_0 = 0$, we can solve the problem exactly (see Chapter 2). For non-zero y_0, we can take the Fourier transform of Eq. 4.11 and rewrite the equation as

$$h(q,\omega) = G(q,\omega)\left[\Delta u(q,\omega) + \eta(q,\omega)/\Gamma - 2\pi K^{-1} y_0 F \sin 2\pi h(s,t)\right]. \tag{4.13}$$

Here s is a dimensionless two-dimensional lattice vector (the unit of length being the lattice spacing) locating the center of a column, and F indicates a Fourier transform in space and time. The renormalization group method (Kosterlitz 1974; José et al. 1977) can then be applied to the linear response function χ^{-1} of the system, defined by the following equation

$$\chi^{-1}(q,\omega) = \chi_0^{-1}(q,\omega) + \Sigma(q,\omega), \tag{4.14}$$

with Σ given by

$$\Sigma(q,\omega) = \frac{4\pi^2 y_0 K^{-1} F\langle\cos[2\pi h_0(st)] h_1(st, s't')\rangle}{\langle h_1(q,\omega)\rangle} \tag{4.15}$$

The method consists in expanding the inverse linear response function $\chi^{-1}(q,\omega)$ in powers of y_0. Similar expansions have proven very useful in the static limit. The zeroth order term $[\chi_0^{-1}(q,\omega)]$ gives the limiting behavior ($T \to \infty$), and the higher-order terms give corrections arising from a non-zero weighting function. We can now use this expansion to generate differential recursion relations, as we have in Chapter 2, which relate the response in the original system with parameters K, Γ and y_0 to that in a system with renormalized parameters K', Γ' and y_0'. Integration of the recursion relations in fact provides a connection for all $T \geq T_R$ between the original system and the exactly solvable system with $y_0 = 0$.

We can expand h_0, h_1 and Σ in powers of y_0 in Eqs. 4.13-4.14 to obtain the following expansion for the inverse linear response function

$$\begin{aligned}
\chi^{-1}(q,\omega) \;=\; & \left[K^{-1} + \pi^3 K^{-2} y^2 \int_1^\infty ds\, s^{3-2\pi K}\right] q^2 \\
& -i\omega \left[\gamma^{-1} + \Gamma^{-1} \frac{\pi^4 y^2}{(\pi K - 1)} \int_1^\infty ds\, s^{3-2\pi K}\right] + O(y^4)
\end{aligned} \tag{4.16}$$

where $y \equiv y_0 \exp[-Kc]$ and c is a constant approximately equal to $\frac{1}{2}\pi^2$. We can now use the same trick we have used in Chapter 2. We divide the range of integration of each integral in Eq. 4.15 into to parts: one from 1 to b and the other from b to ∞, with $0 < \ln b \ll 1$ (that is, b is very close to unity). Now, the small s part of the integration can be combined with the original constant term (either K^{-1} or Γ^{-1}) to yield a new parameter value and the large s part of the integration rescaled so that the integrals again run from 1 to ∞. The scale factor is then absorbed in a redefined y variable. Eq. 4.15 can thus be rewritten in exactly the same functional form with K, y and Γ replaced by $K(l)$, $y(l)$ and $\Gamma(l)$, with $l \equiv \ln b$. This equivalence implies the following differential recursion relations

$$\frac{dK(l)}{dl} = -\pi^3 y^2(l) \tag{4.17}$$

$$\frac{1}{2}\frac{dy^2(l)}{dl} = -\left[\pi K(l) - 2\right] y^2(l) \tag{4.18}$$

$$\frac{d\ln\Gamma(l)}{dl} = -\frac{\pi^4 y^2(l)}{\pi K(l) - 1} \tag{4.19}$$

which are subject to the boundary conditions $K(l = 0) = K$, etc. The first two equations are essentially identical to the static recursion relation found by José *et al.* (José et al. 1977) and Nelson and Kosterlitz (Nelson and Kosterlitz 1977) in their analysis of the XY model and the two-dimensional Coulomb gas. We can define a new variable $x(l) \equiv \pi K(l) - 2$. Substituting this relation in Eq. 4.17, we obtain

$$\frac{1}{2}\frac{dx^2(l)}{dl} = -\pi^4 x(l) y^2(l). \tag{4.20}$$

Comparing this equation to Eq. 4.16 we see there is a conserved quantity

$$x^2(l) - \pi^4 y^2(l) = const = x^2(0) - \pi^4 y^2(0). \tag{4.21}$$

As long as $x(l) > 0$ Eq. 4.19 drives $y(l)$ to zero as $l \to \infty$. The roughening point can be thought of as the low temperature end point of this line of critical points with $y(\infty) = 0$ and at this end point we must have $x(\infty) = 0$ or $K(\infty) = \frac{2}{\pi}$. This value is universal (i.e. independent of the initial value of y and a number of other modifications in the initial Hamiltonian that could be envisioned (Nelson and Kosterlitz 1977)) and should hold for all roughening models.

Another feature comes from Eq. 4.20. when we evaluate it at $l = \infty$ for temperature greater than T_R. Then $y(\infty) = 0$ and

$$x^2(\infty) = \left[x^2(0) - \pi^4 y^2(0)\right] \qquad T \geq T_R. \tag{4.22}$$

Very near T_R we can expand the right hand side in a power series about $T - T_R$ noting that the constant term vanishes since at T_R, $x(\infty) = 0$. We then obtain to lowest order

$$x(\infty) = [A(T - T_R)]^{\frac{1}{2}}. \tag{4.23}$$

We can also obtain an estimate for T_R from Eq. 4.16. If we set $x(\infty) = 0$, recalling that $y = y_0 \exp[-\frac{1}{2}\pi^2 K]$, we obtain the equation

$$K = \frac{2}{\pi} + \pi^2 y_0 \exp[-\frac{1}{2}\pi^2 K] \qquad T = T_R. \tag{4.24}$$

Setting $y_0 = 1$ to approximate the DG model we solve Eq. 4.23 by iteration and find $kT_R/J \sim 1.45$.

Let us now turn our attention to the behavior of the dynamical parameter γ in Eq. 4.18. Eliminating $y^2(l)$ between Eqs. 4.16 and 4.18 and integrating, we obtain

$$\frac{\Gamma(\infty)}{\Gamma} = \frac{\pi K(\infty) - 1}{\pi K - 1}. \tag{4.25}$$

Hence Γ effectively scales with K whose behavior we have discussed above. This has immediate consequences for the statics and dynamics of the interface. For example, the average growth rate R of the crystal is related to the response to a spatially and temporally uniform driving force when the stabilizing field $g^2 = 0$. To first order in $\Delta\mu$ we obtain

$$\begin{aligned} R &= lim_{\omega \to 0} - i\omega\chi(q = 0, \omega)\frac{\Delta\mu}{T} & (4.26) \\ &= \Gamma(\infty)\frac{\Delta\mu}{T} \qquad T \geq T_R. & (4.27) \end{aligned}$$

Thus the theory predicts linear growth at and above T_R in agreement with conventional theories of crystal growth.

Below T_R, the situation is very different. Approaching the roughening temperature from below, the response function has the limiting form

$$\chi(q, \omega) = \left[K'(q^2 + \xi^{-2}) - i\left(\frac{\omega}{\Gamma'}\right)\right]^{-1} \tag{4.28}$$

with a finite correlation length ξ and renormalized coefficients K' and Γ'. Eq. 4.27 then predict a zero growth rate for $T = T_R$ to first order in $\frac{\Delta\mu}{T}$. This result is consistent with the fact that growth at low temperature occurs by a nucleation mechanism. Nucleation theory gives the result $R \propto \exp(-c/\Delta\mu)$ so in fact below T_R all terms in a power series about $\Delta\mu = 0$ should vanish.

One can carry the analysis of renormalization group results much further that this has been done in this short review. Nevertheless, we have the results we need to describe the characteristic behavior of the various quantities we are interested in. In the generic case, one is interested in the correlation length and the specific heat of the system. In the particular case of interfaces, one also wants to have some informations on the statistical width of the interface, the surface tension and the step free energy.

4.2.2 Roughening temperature

Although the roughening temperature is certainly not a universal constant, Kosterlitz's renormalization group method allows for its determination with remarkable accuracy. As seen from the analysis of flow equations, the predicted value for the discrete Gaussian model is of the order

$$T_R \approx 1.45 J/k_B, \tag{4.29}$$

where J is the strength of the coupling constant. This value is quite close to computer simulation estimates. The roughening transition temperature for the SOS model is approximately the same.

4.2.3 Surface tension

The surface tension exhibits a very weak singularity at the roughening transition. The singularity is of the following form:

$$\gamma \approx B \exp\left(-\frac{C}{|T - T_R|^{\frac{1}{2}}}\right). \tag{4.30}$$

This equation is only valid when T is close to T_R. Here we point out that all the derivative of γ taken with respect to the temperature are smooth functions of T and vanish at T_R. We will see this type of mathematical behavior in most of the thermodynamic quantities of interest. This is one of the reason why the experimental observation and even the detection of the transition through computer simulations is so difficult. The constants B and C are non-universal.

4.2.4 Correlation length

For temperatures below, but close to the roughening temperature, the correlation length, which is the characteristic length for correlations between thermal excitations of the crystal surface, behaves as

$$\xi \sim \exp\left(\frac{\pi}{y(0)}\right). \tag{4.31}$$

From Eq. 4.20, we know that $x(0) = y(0)$. Since we know the behavior of $x(0)$ close to the critical point, we find dependence of the correlation length ξ on the temperature to be

$$\begin{aligned} \xi &= \xi_0 \exp\left(\frac{A}{|T - T_R|^{\frac{1}{2}}}\right), \qquad T < T_R && (4.32) \\ &= +\infty, \qquad T \geq T_R && (4.33) \end{aligned}$$

where ξ_0 and A are non-universal constants. Here, we point out that ξ has very little to do with the correlation length of the bulk. The latter is only responsible for the intrinsic width of the physical interface, while the former is associated with the statistical width, which is much more important below the critical temperature.

4.2.5 Step free energy

The step free energy is defined as the difference of the free energy of an interface containing a step with that of a similar interface containing no steps at all. It follows the following form:

$$\begin{aligned} f_{step} &= f_0 \exp\left(-\frac{A}{|T - T_R|^{\frac{1}{2}}}\right), \qquad T < T_R && (4.34) \\ &= 0, \qquad T > T_R && (4.35) \end{aligned}$$

where f_0 is again a non-universal quantity and A is the same as in Eq. 4.32. This result is obtained by observing that f_{step} is the dual conjugate of the inverse correlation length in the XY model.

Thus, we can characterize the roughening transition by equating it to the facts that, at the roughening temperature and above, the step free energy f_{step} vanishes, and the statistical width of the interface,W, diverges.

4.3 Experimental observation of the roughening transition

There were initially few attempts to experimentally observe the roughening transition and determine the transition mechanism because it was thought that a crystal in equilibrium with its vapor would melt before the closest packed face would roughen. This belief was dismissed by experiments performed by Jackson and Miller (Jackson and Miller 1977), who found that for simple van der Waals crystals, the roughening point was well below the melting point. Furthermore, Jackson showed that it is possible to understand both the growth mechanisms (nucleated or continuous) and the crystal structure (faceted or isotropic) of a very wide variety of materials by determining whether the crystal as grown was below or above its surface roughening temperature. However, the direct experimental observation of the roughening transition is difficult for different reasons. First of all, it is generally very difficult to produce crystals with an equilibrium shape. Shapes produced during growth are generally metastable and their relaxation rate increases rapidly with crystal size. In experiments by Heyraud and Métois (Heyraud and Métois 1984) on lead crystallites of only a few micrometers in diameter at temperatures of a few hundred degrees Kelvin, they observed equilibration times of a few days (see Fig. 4.1).

In addition, it appears that most observable crystal faces do not exhibit a roughening transition within the physical range associated with their existence. Typically, the surfaces of crystals in equilibrium with their melt are rough all along the melting

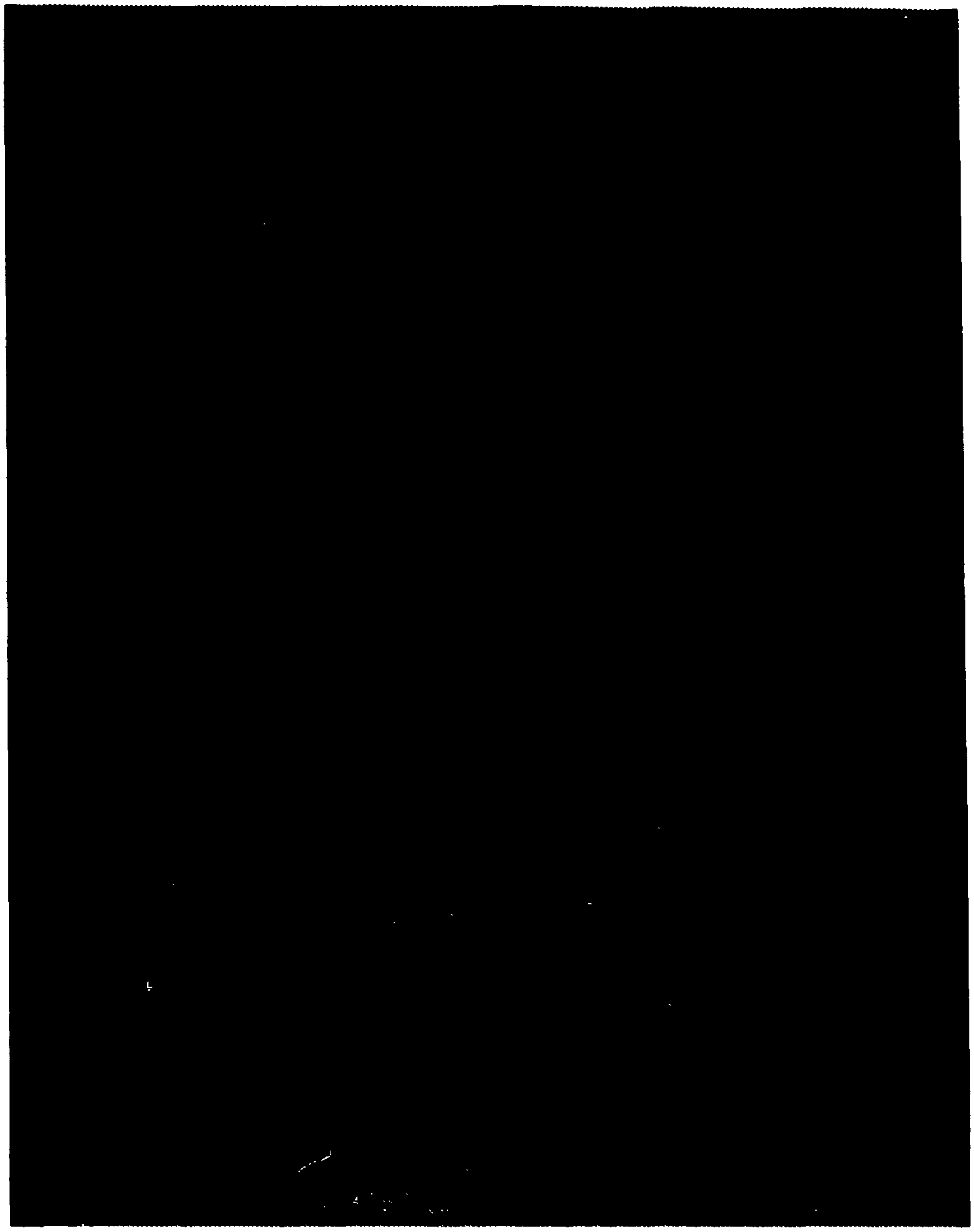

Figure 4.1: Roughening transition in a lead crystallite viewed from two angles reproduced from Heyraud and Métois, (Heyraud and Métois 1984).The size of the crystallite is a few millimeters, the temperature is 362°C. One can distinguish some facets corresponding to a microscopically flat interface in registry with the low index plane, while the rounded parts correspond to microscopically rough interfaces in a crystallographic orientation for which the roughening temperature is lower.

line, down to the triple point, whereas the principal facets of crystals in equilibrium with their vapor tend to remain smooth along the sublimation line up to the triple point. For crystal vapor interfaces, this difficulty can often be circumvented by considering higher index crystal faces, which are less tightly packed so they have lower roughening temperatures. But then the problem of the long relaxation times becomes important again, although relaxation times for the internal structure of existing facets are generally much shorter than the relaxation times for a full reconstruction of the crystal shape. Another experimental problem is the sensitivity of surface properties to impurities and dislocations, which may make it hard to decide whether an observed surface shape is really that of a pure crystal in equilibrium. Finally, even in cases where a roughening transition is observed, the nature of the transition makes it difficult to pin down the roughening temperature. Typically, facets disappear so gradually at the approach of the roughening temperature that they become practically unobservable already at temperatures distinctly below T_R.

In spite of these difficulties, roughening transitions have been observed experimentally in a number of systems. Pavlovska and Nemow (Pavlovska and Nemow 1977) studied the equilibrium shape of "negative crystals", that is, vapor bubbles included within a crystal in organic substances, and observed the disappearance of certain facets within well-reproducible temperature ranges. However, the best observations of the roughening transition so far have been made for helium crystals in equilibrium with superfluid helium (Wolf et al. 1985). This system is ideally suited for observing the roughening transition. This is because the relaxation to equilibrium is very fast, the heat and mass transport being extremely rapid in the superfluid. Crystal grown to the size of millimeters assume their equilibrium shape within periods ranging from milliseconds to minutes, depending on both external and internal parameters. In addition, these crystals are extremely pure because, with the exception of ^{3}He, all impurities can be filtered out from the superfluid very efficiently. Thus far, roughening transitions for three different types of facets have been observed. In addition, Wolf *et al.* (Wolf et al. 1985) have exploited the exceptional properties of the helium system in some beautiful experiments which confirm quantitatively the predicted Kosterlitz-Thouless character of the roughening transition.

Chapter 5

The Roughening Transition in Driven Systems

As was seen in the previous chapter, the properties of equilibrium interfaces have been extensively studied in the past fifteen years. On the other hand, the study of growing interfaces is a relatively new subject. While people have been interested in understanding the phenomenon for a long time, only in recent times have there been new developments in this topic. For example, new growth mechanisms have been uncovered, and new physical models have been put forward to explain the various growth phenomena observed in nature. It is only natural that people would try to apply the idea of a roughening transition to growing interfaces.

However, in doing this, one then faces a serious problem. The equilibrium roughening transition occurs in interfaces that are in equilibrium. The fact that they are in equilibrium means that one can in principle use classical statistical mechanics - partition function, entropy, etc - to solve the problem. On the contrary, growing interfaces are far-from-equilibrium systems, for which equilibrium or close-to-equilibrium statistical mechanics does not apply. Furthermore, as we have mentioned in Chapter 2, the two models we consider here are very closely related to nucleation phenomena, that is, to metastable states. Up to now, no satisfactory treatments of metastable states has been given in the framework of statistical mechanics. Thus, one has to be very careful in identifying any phase transitions in nonequilibrium systems. It is with this word of caution in mind that we shall discuss what we called the dynamical roughening transition, which is the subject of the second part of this chapter.

5.1 Roughening transition in driven systems

There have been some studies previously done on the roughening transition in driven system (Chui and Weeks 1976; Nozières and Gallet 1987). Those studies introduced a driving force in the problem by adding a constant field, and from the results it was concluded that the presence of such a field did not change the nature of the transition. However, both studies did not take into account the nonlinear term coming from the growth process, thus discarding a potentially relevant piece. Nevertheless, they are useful guides for further analysis.

As we have mentioned in Chapter 2, Langevin equation like the KPZ equation are not useful for describing phenomena coming from microscopic effects. However, it is possible to modify the KPZ equation so as to obtain the proper microscopic behavior. This is the subject of the next section. Nevertheless, treating discontinuities in space and time with continuous fields can be difficult. This is when the asymmetric SOS model comes into play. Since we know it belongs to the same universality class, we can use it to look for and probe the nonequilibrium roughening transition. This is the topic of the second section. We close the chapter with a discussion on our results.

5.1.1 The discrete Kardar-Parisi-Zhang equation

To investigate the possibility of a kinetic roughening transition, we introduce a model, motivated by the discrete Gaussian model of Chui and Weeks (Chui and Weeks 1976), which has been used to study the equilibrium roughening transition. It corresponds to Eq. 2.11 on a lattice, with the height variable h restricted to integer values of the lattice constant. We call this the discrete KPZ model, since choosing $\lambda \equiv 0$ gives the discrete Gaussian model. Making h integer valued implies a nonzero energy gap

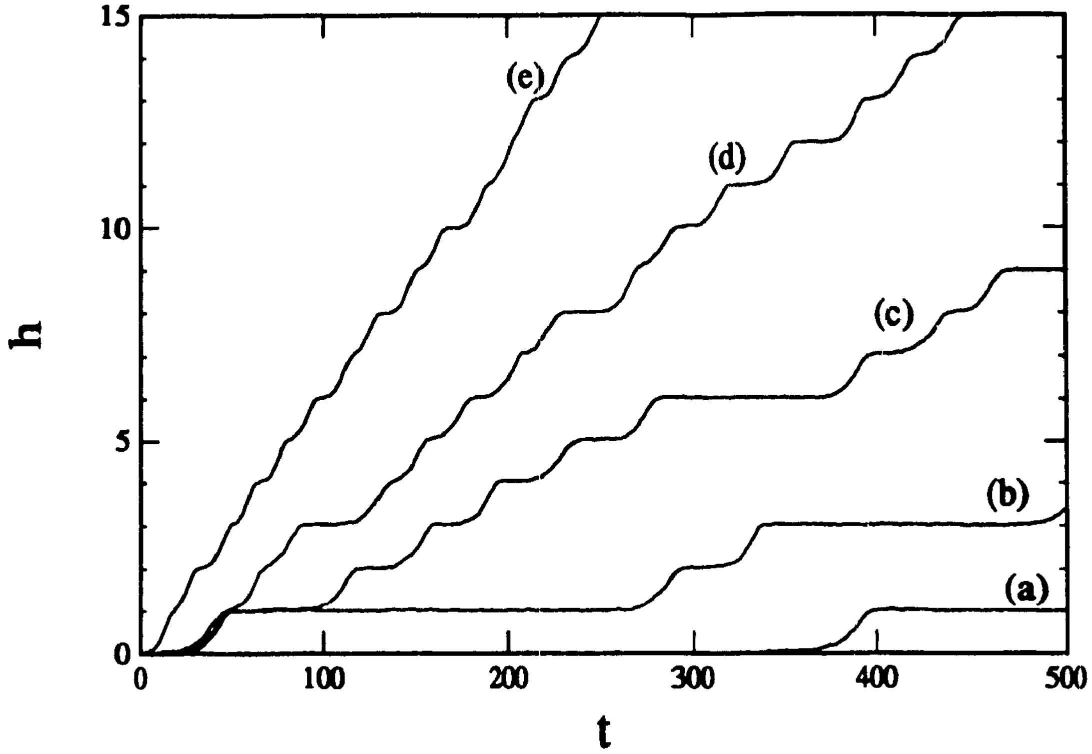

Figure 5.1: Growth of the three-dimensional KPZ equation by means of nucleation on the top layer. h is average height of the interface. The various curves correspond to different values of the driving force λ at fixed temperature.

at low temperatures, for small fluctuations on the interface, which is necessary for a roughening transition to take place. Thus translational invariance is not built into the model, and there can be a gap in the capillary-wave spectrum at low temperatures $T < T_R$. Above any roughening transition, the energy gap is irrelevant since the width diverges with system size. As a consequence, the asymptotic growth exponents in the rough phase of the discrete KPZ equation will be the same as those for the original model. The interest of the new model therefore lies in its low-temperature properties, where the discreteness of h could be relevant.

We again performed numerical integrations of Eq. 2.11, now with integer-valued h and edge length $L = 128$, as λ varied, keeping D and ν constant, in essence fixing T. The plots of the average height of the interface for various λ versus time are shown in Fig. 5.1.

Different curves are for varying driving forces λ with the temperature $T = D/\nu <$

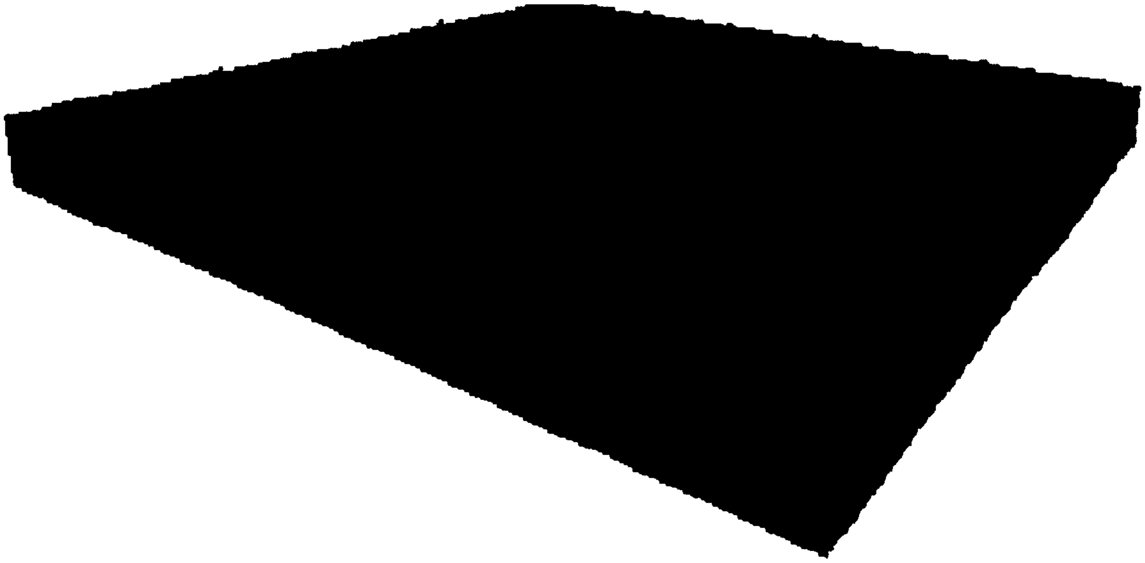

Figure 5.2: Example of a smooth interface below T_R. Notice the single block temperature excitations

$T_R(\lambda = 0)$ fixed. For small values of λ, the growth is one layer at a time (curves a and b), suggesting that the system is in its faceted phase. Beyond a large particular value of λ, the growth becomes continuous (curve c) signaling that the rough phase is reached.

Some configurations corresponding to these runs are shown in Figs. 5.2 and 5.3. We also verified that one could go from layer-by-layer growth to continuous growth by increasing temperature beyond a particular value, at a fixed nonzero driving force. Those observations are in essence very similar to what one would observe at a phase transition point. Thus, we decided to investigate the existence of a non-equilibrium roughening transition.

Unfortunately, the discrete KPZ model is numerically a difficult problem, so our observations are only qualitative. We could not, for example, get a precise value for the roughening temperature. To undertake a quantitative study, we again considered the SOS model with asymmetric rates of evaporation and condensation.

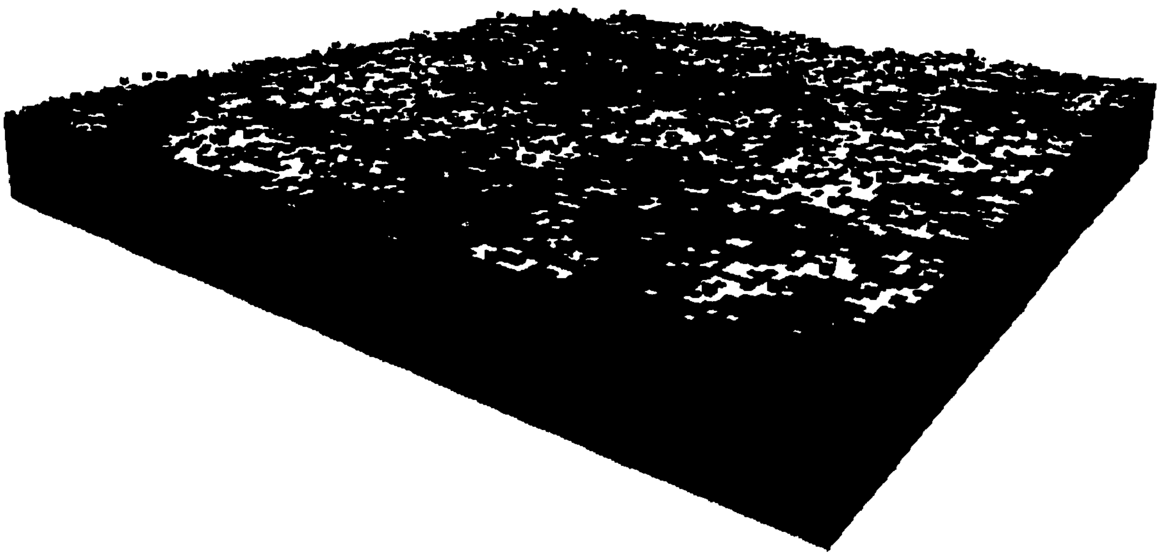

Figure 5.3: Example of a rough interface above T_R. Notice the multilayer excitations.

5.1.2 Solid-on-solid model with asymmetric rates of evaporation and condensation

As was mentioned in chapter 3, the SOS model has a roughening transition in equilibrium (Weeks and Gilmer 1979; Weeks 1980; Kosterlitz and Thouless 1974; Kosterlitz 1974; Swendsen 1977; Swendsen 1978), and its nonequilibrium properties have been previously studied by many authors (Weeks and Gilmer 1979; Weeks 1980). Analytic work, within linear response, has been done by Chui and Weeks (Chui and Weeks 1978), Saito (Saito 1978), and Nozières and Gallet (Nozières and Gallet 1987). Here we wish to determine the conditions, if any, under which the interface can be grown layer by layer in the smooth faceted phase which exists below T_R. While signs of such a kinetic roughening transition have been observed in experiments (Fig. 5.4) (Dougherty and Gollub 1988; Franck and Jung 1986; Maurer et al. 1989; Bilgram, Firmann and Hürlimann 1989; Gallet, Balibar and Rolley 1987), there is little theoretical understanding of the phenomena.

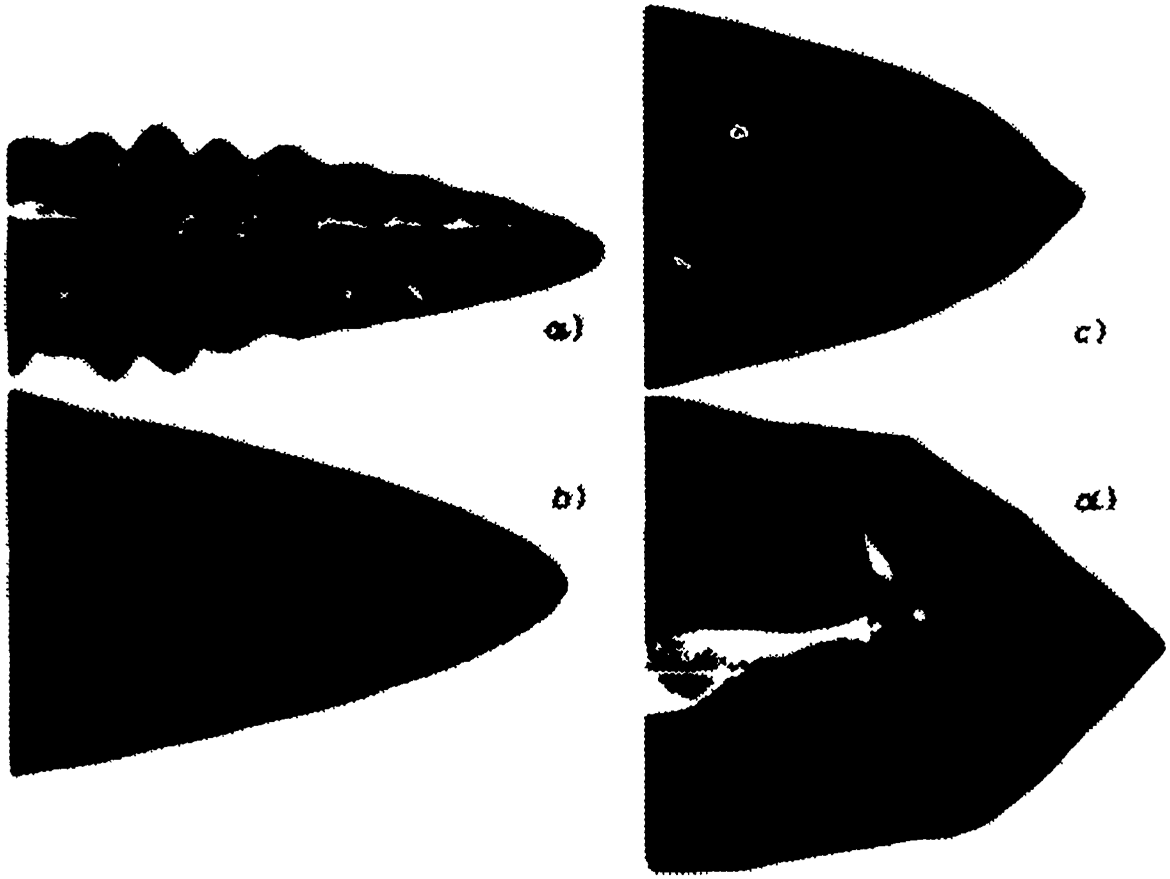

Figure 5.4: Dynamic roughening transition in a dendrite as the speed of growth is decreased reproduced from Maurer *et al.*,(Maurer et al. 1989).The compound used is NH_4Br. The speed of growth of the dendrite decreases from a) to d):a)$v=0.43$ $\mu m.s^{-1}$; b)$v=0.042$ $\mu m.s^{-1}$; c)$v=0.015$ $\mu m.s^{-1}$; d)close to equilibrium. One clearly sees the faceted interfaces in the last two pictures.

The properties of the equilibrium roughening transition, on the other hand, have been much more thoroughly investigated; many numerical studies of the SOS, Gaussian, and three-dimensional Ising models (Swendsen 1977; Swendsen 1978; Mon et al. 1988), have been performed. A quantitative description of the roughening transition is difficult to obtain since the transition is of infinite order. One useful approach, due to Leamy and Gilmer (Leamy and Gilmer 1974), is to determine the extra energy associated with the presence of a step on the interface, E_{step}. This should vanish at the roughening temperature T_R in the thermodynamic limit. This idea, combined with finite-size scaling, can accurately determine T_R (Mon et al. 1988).

Motivated by the success of that work for the equilibrium roughening transition, we have applied these ideas to the nonequilibrium asymmetric SOS model. We computed the step energy for a given driving force λ_a, at different temperatures for several system sizes. It exhibits a strong transition from a large value to a much smaller value at a given temperature. Another quantity which shows a strong transition is the bond-energy fluctuations, a quantity similar to the specific heat. We note here that the specific heat does not have any divergence in the *equilibrium* roughening transition, since that transition is of infinite order. However, in the equilibrium case, the width of the interface diverges at T_R as $\sqrt{\ln L}$ for $L \to \infty$, whereas in driven growth the width diverges as a power law in the steady state, $W \sim L^{\chi}$ as shown in the previous section. Thus we expect the kinetic roughening transition to be stronger than its counterpart in equilibrium. Indeed, our finite-size scaling analysis shown below finds that the bond-energy fluctuations show a diverging peak at $T_R > 0$. Moreover, the roughening transition temperature obtained from the step energy and the bond energy fluctuation are in good agreement.

The step energy, E_{step}, can be defined as the energy difference between a surface with one step and the same surface without such a step (Leamy and Gilmer 1974; Swendsen 1977; Swendsen 1978)

$$E_{step} \equiv \frac{1}{L}[\langle\mathcal{H}\rangle(\text{one step}) - \langle\mathcal{H}\rangle(\text{no steps})] \tag{5.1}$$

In our simulations of the three-dimensional nonequilibrium SOS model, a step on

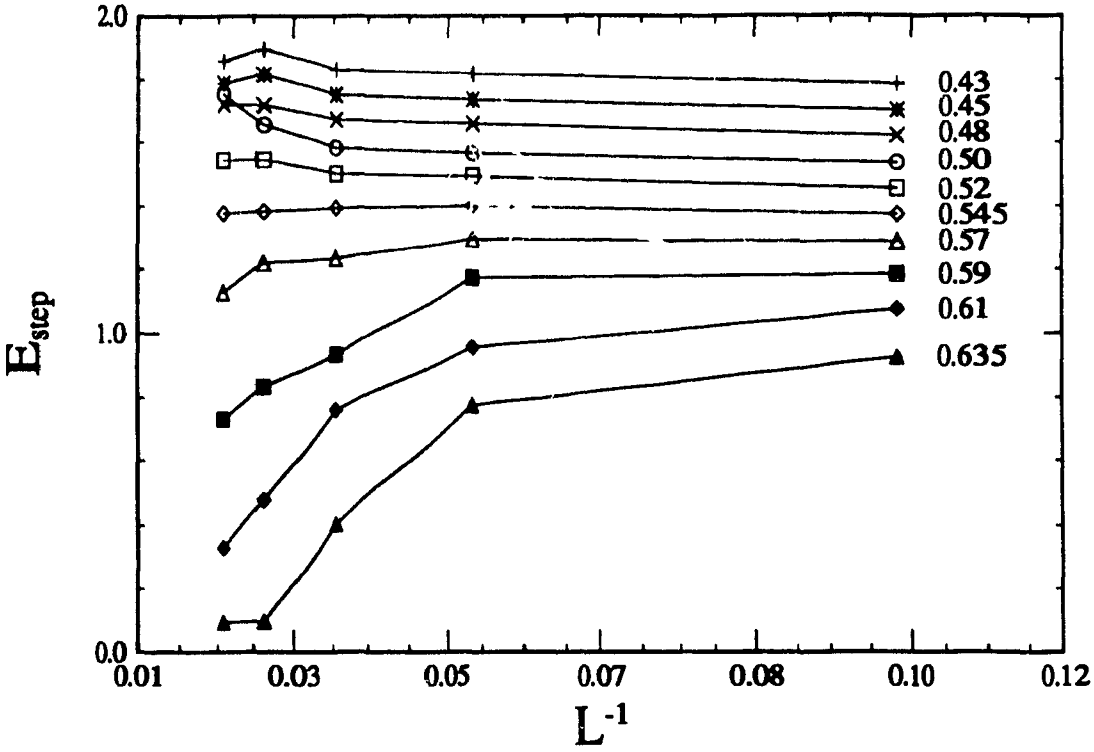

Figure 5.5: Step free energy E_{step} vs L for various temperatures for $\lambda_a = 0.4$. The temperature at which the curve changes its bending direction is the roughening temperature T_R

the surface $\vec{x} = (x_1, x_2)$ can easily be created by maintaining periodic boundary condition in, say, the x_1-direction, while applying a screw boundary condition in the x_2-direction (the growth is in the y-direction). The height of the step can also be adjusted, although we chose it to be unity.

For $T < T_R$, one should obtain a nonzero value of E_{step} which increases with lattice size. On the other hand, for $T > T_R$, E_{step} should decrease and ultimately vanishes as $L \to \infty$. We have simulated systems of edge length $L = 10$ to 50 for various temperatures. The asymmetric growth rate λ_a was fixed at 0.4. The simulations were run with and without a step for 2×10^5 Monte Carlo steps. In Fig. 5.5, E_{step} for different temperatures as a function of L is shown.

As anticipated, for different T, the curves bend upward or downward, showing a smooth phase at low temperatures and a rough phase at high temperatures. We find $T_R \approx 0.55$. Furthermore, plotting E_{step} as a function of temperature for various sizes a transition of E_{step} from a large value to a much smaller one is visible. Note also

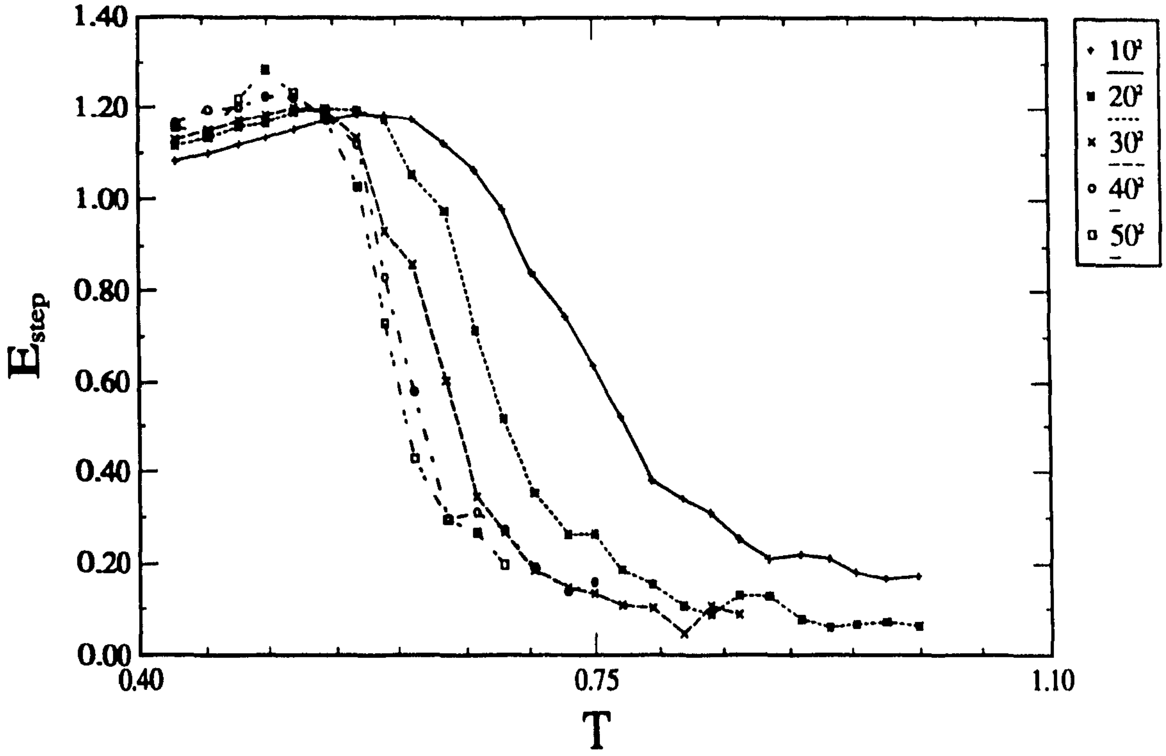

Figure 5.6: Step free energy E_{step} vs T for various system sizes with $\lambda_a = 0.4$. The temperature at which the curves dip down is the roughening temperature T_R

the sharpening of the transition as L increases, and the curves' common intersection point at $T_R = 0.55$ (Fig. 5.6).

We also studied the bond-energy fluctuations defined as

$$C \equiv \frac{1}{L^2T^2}(\langle \mathcal{H}^2 \rangle - \langle \mathcal{H} \rangle^2). \tag{5.2}$$

In equilibrium, this gives the specific heat. Fig. 5.7 shows C as a function of the temperature for several driving forces λ_a. C is strongly peaked for nonzero λ_a at a finite T, and from inspection of configurations, its peak corresponds to the roughening transition. Thus we interpret the peak position as $T_R(\lambda, L)$, which shifts to lower temperatures as λ is increased (see the insert in Fig. 5.7).

In contrast, there is no anomaly in the specific heat for roughening of an equilibrium interface (Weeks and Gilmer 1979; Weeks 1980), although there is a small bump close to T_R (Swendsen 1977; Swendsen 1978). This bump is actually consistent with the form of the step free energy for the equilibrium systems. Note that as λ_a

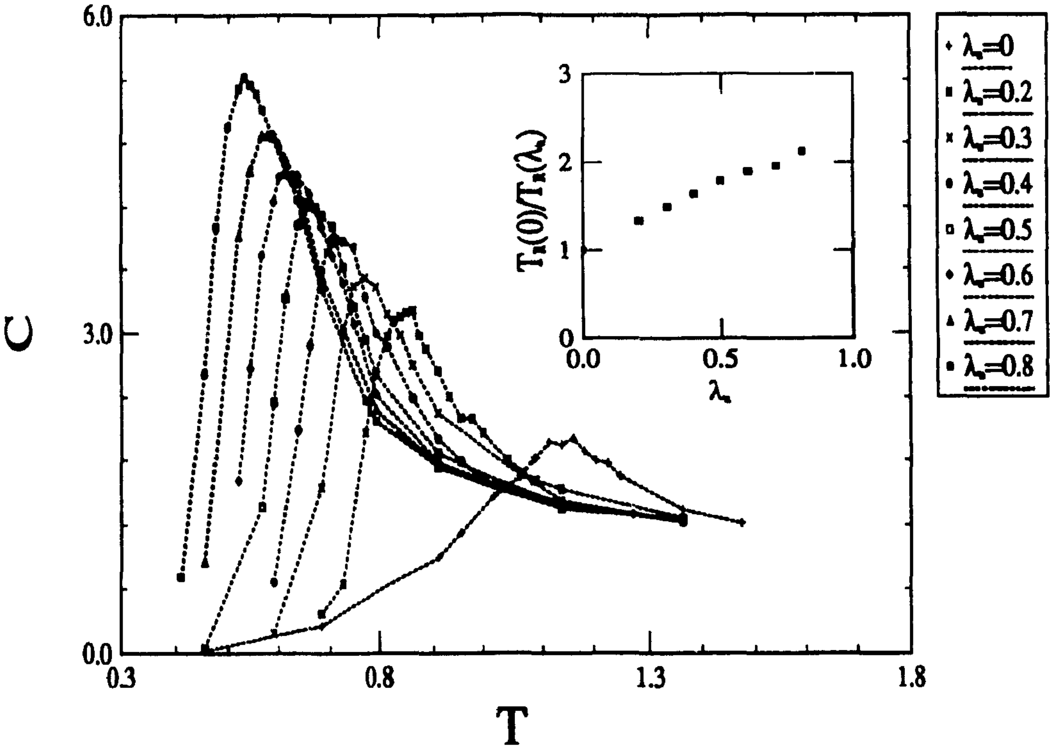

Figure 5.7: Fluctuations in the energy bond vs T for various values of the driving force λ_a. The position of the peak is interpreted as being the nonequilibrium roughening temperature.

increases, the peak position of C shifts to lower temperatures. This implies one can go from the smooth to the rough phase by increasing the driving force at a given temperature, as seen qualitatively for the discrete KPZ model in the previous subsection. This feature has also been observed experimentally (Dougherty and Gollub 1988). The inset to Fig. 5.7 shows a fit to $T_R(\lambda) \sim T_R(0)/(1+\mathcal{O}(\lambda))$, motivated by the equation of motion, where $T_R(0) = 1.24$ is the equilibrium roughening transition temperature for the SOS model (Weeks and Gilmer 1979).

An important issue is to determine if $T_R(\lambda, L)$ is nonzero as $L \to \infty$. To estimate the nature of possible singular behavior in C, in the absence of theory which includes the effect of the nonlinearity, we have followed standard treatments for *second-order* transitions. We make the finite-size scaling ansatz,

$$C \sim L^{\alpha/\nu} F(|T - T_R| L^{1/\nu}) \tag{5.3}$$

and fit to find α and ν. These are not equilibrium exponents since C could depend

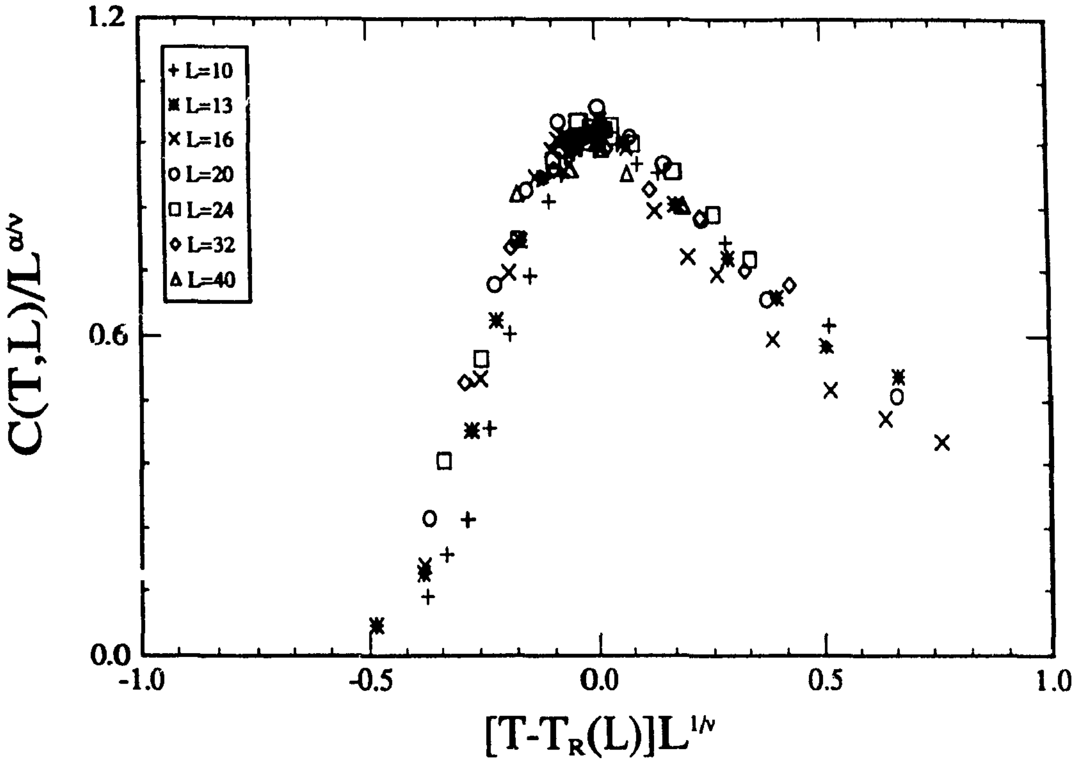

Figure 5.8: Finite size scaling plot of the energy bond fluctuations for $\lambda_a = 0.4$ for various system sizes.

on the dynamical universality class (Sun, Guo and Grant 1989). We also caution that such a procedure is not appropriate for the equilibrium case ($\lambda_a = 0$) since, as mentioned above, the equilibrium roughening transition is of infinite order. We believe that an ultimate validation of this ansatz can only come from further study of the nature of the nonequilibrium phase transition. In any case, from the data collapse shown in Fig. 5.8 for $\lambda_a = 0.4$, our ansatz is self-consistent, and we estimate $\alpha/\nu \approx 0.5$, and $\nu \approx 1.5$.

The transition temperature in the hydrodynamic limit is then estimated taking the equivalent of the thermodynamic limit and using

$$T_R(L) = T_R(L \rightarrow \infty) + \mathcal{O}(1/L^{1/\nu}), \tag{5.4}$$

which gives $T_R(L \rightarrow \infty) \approx 0.54$. This value agrees very well with that from the step-energy data discussed above. Indeed, the consistency of the results for the step energy E_{step}, and the bond-energy fluctuations C, gives us confidence in interpreting our data in terms of a transition occurring at a nonzero temperature.

5.2 Discussion

To conclude this section, we give arguments to clarify the nature of the transition. Some of our remarks are implicit in the earlier work of Gilmer and Weeks (Gilmer 1982; Weeks and Gilmer 1979; Weeks 1980), and Saito (Saito 1978; Saito 1980). We expect that, for a system of any large size, a kinetic roughening transition at nonzero temperature occurs, and that this nonzero temperature is intimately connected to the relevance of bubbles in the KPZ equation.

Layered growth in the smooth phase can occur, unless layers themselves are thermally unstable, or further ledges appear in an amount that contributes to the width of the interface in the hydrodynamic limit. At low T, one must determine the time scales for the speed at which a ledge grows, and for the appearance of a new nucleated ledge. For small fields (i.e., small driving forces) in systems of finite size, the time scale for growth is algebraic, while that for nucleation is exponentially small in the external field. They are thus very well separated and the ledge will sweep through the system before any appreciable nucleation event has the time to occur. Hence we expect that layer-by-layer growth is possible for a significant time regime in a finite-size system, at low T in a small field.

The question of the hydrodynamic limit, $t \to \infty$, $L \to \infty$ is more subtle. Consider Fig. 5.9, where we show an interface growing layer-by-layer in the smooth faceted phase (perhaps with screw boundary conditions as mentioned above).

As we discussed in the introduction, it can be useful to look down from the top of the facet. One then sees that the low-temperature one-block excitations of layered growth in three-dimensional driven growth are equivalent to the low-temperature fluctuations of *two-dimensional* driven growth, as described by the KPZ equation. Those fluctuations are not sufficient to destroy coexistence in the two-dimensional KPZ equation, since $W/L \to 0$ as $t, L \to \infty$. Therefore we do not expect them to

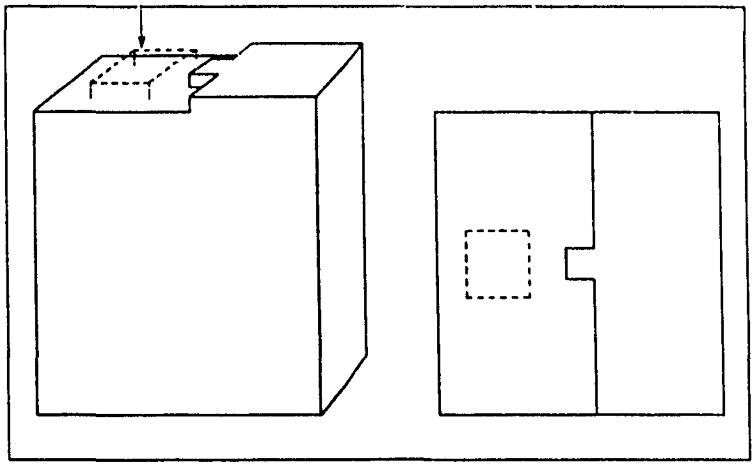

Figure 5.9: a) Global view of a stepped interface in a three dimensional Ising model. The dashed line represents a nucleating bubble. b) Top view of the same interface.

destroy layer-by-layer growth at low temperatures in the three-dimensional system

Nevertheless, one must also consider the possibility of large nucleated ledges. Note that the rate of appearance of such ledges, which could destroy growth in the smooth phase, is essentially independent of dimension of space for $d > 2$. Thus the argument below applies to $d \geq 3$. In Fig. 5.9, the rate of appearance of new layers is independent of whether they appear on the top or bottom ledge. So consider only the bottom, as shown by the dotted lines. Then one sees that ledges on ledges correspond to the droplet fluctuations occurring on very long time scales τ, rendering the two-dimensional KPZ equation irrelevant, as discussed in Section 2. (Note that the time scales for the two-dimensional droplet fluctuations are not well separated from the time scales for three-dimensional droplet fluctuations from Eq. 2.77.). Thus, we expect any definition of the hydrodynamic limit for the KPZ equation to also be consistent with a kinetic roughening transition at nonzero temperature, when a finite energy gap is introduced. Nevertheless, we cannot rule out the possibility that we are in a crossover regime, and that there really is no transition in the thermodynamic limit.

Some complementary analytic work on this issue has been done by Hwa *et al.* (Hwa, Kardar and Paczuski 1991). To the best of our knowledge, it is unfortunately not known how to define a metastable state in the hydrodynamic limit. Finally, we note that the order of the transition is not clear. Although nucleation of ledges would be a signature of a first-order transition, if the hydrodynamic limit requires the presence of long-range forces to suppress droplet-like fluctuations, the transition could occur at the spinodal curve, a line of second-order phase transitions.

In any event, existing experiments (Dougherty and Gollub 1988), as well as our simulation data, seem to suggest the kinetic roughening transition occurs at a nonzero temperature for a given driving force, in the hydrodynamic limit. We expect that a consistent definition can therefore be found for that limit. It should also be noted that the existence of the hydrodynamic limit for the transition from smooth to rough, or rough to rough interfaces for $d > 3$ has been implicitly assumed in other studies (Kardar, Parisi and Zhang 1986; Medina et al. 1989) (our comments concerning nucleation on the $(d-1)$-dimensional substrate are essentially independent of dimension for $d > 2$).

Chapter 6

Conclusion

6.1 Summary and Discussion

We have studied the nature of interfaces during driven growth. The Kardar-Parisi-Zhang equation was derived from the Langevin equations for a system with a non-conserved scalar order parameter, for the cases where an external field is present, and where an asymmetric coupling to a conserved variable exists.

We then numerically integrated the nonlinear stochastic differential equation proposed by Kardar, Parisi and Zhang, and used Monte Carlo simulation to study a nonequilibrium solid-on-solid model. We established that these models share the same dynamic universality class, in both two and three dimensions, by analyzing crossover behavior, and estimating asymptotic scaling exponents.

For the nonequilibrium SOS model, evidence of a kinetic roughening transition was found. In particular, our data can be naturally and self-consistently interpreted in terms of such a transition occurring at nonzero temperature. Moreover, this transition seems to be stronger than the equilibrium roughening which is of Kosterlitz-Thouless type. In order to establish this, however, further study is required. For example, it would be interesting to study the analytic behavior of the step free energy close to the transition point. Such a study would certainly allow for the precise determination of the order of the transition. Finally, the results of this paper, in particular the kinetic roughening transition in driven interfacial growth, are experimentally accessible by many methods. In our opinion, such a study would be of considerable interest.

References

Allen, S. and Cahn, J. 1979. *Act. Metall.*, **27**, 1085.

Amar, J. and Family, F. 1989. *Phys. Rev. A*, **41**, 3399.

Baiod, R., Kessler, D., Ramanlal, P., Sander, L., and Savit, R. 1988. *Phys. Rev. A*, **38**, 3672.

Bak, P., Tang, C., and Wiesenfeld, K. 1988. *Phys. Rev. A*, **38**, 364.

Bausch, R., Dohm, V., Janssen, H., and Zia, R. 1981. *Phys. Rev. Lett.*, **47**, 1837.

Becker, R. and Döring, W. 1935. *Ann. der Phys.*, **24**, 719.

Bilgram, J., Firmann, M., and Hürlimann, E. 1989. *J. Crys. Growth*, **96**, 175.

Bovier, A., Fröhlich, J., and Glaus, U. 1986. *Phys. Rev. B*, **34**, 6409.

Boyanovsky, D. and Cardy, J. 1983. *Phys. Rev. B*, **27**, 5557.

Brézin, E., LeGuillou, J., and Zinn-Justin, J. 1974. *Phys. Rev. B*, **10**, 892.

Buff, F., Lovett, R., and Stillinger, F. 1965. *Phys. Rev. Lett.*, **15**, 621.

Burgers, J. 1974. *The Nonlinear Diffusion Equation*. Riedel, Boston.

Burton, W., Cabrera, N., and Frank, F. 1951. *Phil. Trans. R. Soc. A*, **243**, 299.

Caginalp, G. 1989. *Phys. Rev. A*, **39**, 5887.

Caginalp, G. 1990. *IMA J. Appl. Math.*, **44**, 77.

Chakrabarti, A. and Toral, R. 1989. *Phys. Rev. B*, **40**, 11419.

Chang, L. and Ploog, K., editors 1985. *Molecular Beam Epitaxy and Heterostructures*. Martinus Nijhoff, Dordrecht.

Chui, S. and Weeks, J. 1976. *Phys. Rev. B*, **14**, 4978.

Chui, S. and Weeks, J. 1978. *Phys. Rev. B*, **40**, 733.

Collins, J. and Levine, H. 1985. *Phys. Rev. A*, **31**, 6119.

Devillard, D. and Stanley, H. 1989. *Physica A*, **160**, 298.

Dougherty, A. and Gollub, J. 1988. *Phys. Rev. A*, **38**, 3043.

Eden, M. 1961. In Neyman, F., editor, *Proceedings of the Fourth Berkeley Symposium on Mathematical Statistics and Probability, Vol. IV*, Berkeley. University of California Press.

Edwards, S. and Wilkinson, D. 1982. *Proc. Roy. Soc. London A*, **381**, 17.

Family, F. and Vicsek, T. 1985. *J. Phys. A*, **18**, L75.

Forrest, B. and Tang, L. 1990. *Phys. Rev. Lett.*, **64**, 1405.

Forster, D., Nelson, D., and Stephen, M. 1977. *Phys. Rev. A.*, **16**, 732.

Fox, R. 1990. Preprint.

Franck, J. and Jung, J. 1986. *Physisca. D*, **23**, 259.

Furutsu, K. 1963. *J. Res. Nat. Bur. Standards*, **67D**, 303.

Gallet, F., Balibar, S., and Rolley, E. 1987. *J. Phys. (Paris)*, **48**, 369.

Gibbs, J. 1948. *Collected Works.* Yale, New Haven.

Gilmer, G. 1982. In Vanselow, R. and Howe, R., editors, *Chemistry and Physics of Solid Surfaces*, volume 35 of *Springer Series in Chemical Physics.* Springer, Heidelberg.

Grant, M. 1988. *Phys. Rev. B*, **37**, 5705.

Grant, M. and Gunton, J. 1983. *Phys. Rev. B*, **28**, 5496.

Grant, M. and Gunton, J. 1984. *Phys. Rev. B*, **29**, 6266.

Grossmann, B., Guo, H., and Grant, M. 1990. *Phys. Rev. A.*, **41**, 4195.

Grossmann, B., Guo, H., and Grant, M. 1991a. *Phys. Rev. A.*, **43**, 1727.

Grossmann, B., Guo, H., and Grant, M. 1991b. *Mat. Res. Soc. Proc.* in press.

Guggenheim, E. 1945. *J. Chem. Phys.*, **13**, 253.

Gunton, J. and Droz, M. 1983. In *Introduction to the Theory of Metastable and Unstable States*, volume 183 of *Lectures Notes in Physics.* Springer, Berlin.

Gunton, J., San Miguel, M., and Sahni, P. 1983. volume 8 of *Phase Transitions and Critical Phenomena.* Academic, London.

Guo, H., Grossmann, B., and Grant, M. 1990a. *Phys. Rev. Lett.*, **64**, 1262.

Guo, H., Grossmann, B., and Grant, M. 1990b. *Phys. Rev. A*, **41**, 7082.

Harris, R. and Grant, M. 1990. *J. Phys. A*, **23**, L567.

Heyraud, J. and Métois, J. 1984. *Phys. Rev. Lett.*, **52**, 1009.

Hohenberg, P. and Halperin, B. 1977. *Rev. Mod. Phys.*, **49**, 435.

Huse, D. and Henley, C. 1985. *Phys. Rev. Lett.*, **54**, 2708.

Hwa, T., Kardar, M., and Paczuski, M. 1991. *Phys. Rev. Lett.*, **66**, 441.

Jackson, K. and Miller, C. 1977. *J. Cryst. Growth*, **40**, 169.

Jasnow, D. 1986. volume 10 of *Phase Transitions and Critical Phenomena*. Academic Press, London.

Jörgensen, L., Harris, R., and Grant, M. 1989. *Phys. Rev. Lett.*, **63**, 1693.

José, J., Kadanoff, L., Kirkpatrick, S., and Nelson, D. 1977. *Phys. Rev. B.*, **16**, 1217.

Jullien, R. and Botet, R. 1985. *J. Phys. A*, **18**, 2279.

Kardar, M. 1985. *Phys. Rev. Lett.*, **55**, 2923.

Kardar, M., Parisi, G., and Zhang, Y. 1986. *Phys. Rev. Lett.*, **56**, 889.

Kardar, M. and Zhang, Y. 1987. *Phys. Rev. Lett.*, **58**, 2087.

Katz, S., Lebowitz, J., and Spohn, H. 1983. *Phys. Rev. B*, **28**, 1655.

Kawasaki, K. and Ohta, T. 1982a. *Prog. Theor. Phys.*, **67**, 147.

Kawasaki, K. and Ohta, T. 1982b. *Prog. Theor. Phys.*, **68**, 129.

Kim, J. and Kosterlitz, J. 1989. *Phys. Rev. Lett.*, **62**, 2289.

Kossel, *N*. 1927. *Nachr. Ges. Wiss. Göttingen*, **Mathemat./Physikal Klasse S**, 135.

Kosterlitz, J. 1974. *J. Phys. C*, **7**, 1046.

Kosterlitz, J. and Thouless, D. 1974. *J. Phys. C*, **6**, 1181.

Krug, J. and Spohn, H. 1990. *Solids far from Equilibrium: Growth, Morphology and Defects*. To be published.

Leamy, H. and Gilmer, G. 1974. *J. Crys. Growth*, **24/25**, 499.

Leung, K., Mon, K., Vallès, J., and Zia, R. 1988. *Phys. Rev. Lett.*, **61**, 1744.

Liu, D. and Plischke, M. 1988. *Phys. Rev. B*, **38**, 4781.

Maurer, J., Boissou, P., Perrin, B., and Tabeling, P. 1989. *Europhys. Lett.*, **8**, 67.

Mazor, A., Srolovitz, D., Hagan, P., and Bukiet, B. 1988. *Phys. Rev. Lett.*, **60**, 424.

Meakin, P. 1987. *J. Phys. A*, **20**, L1113.

Meakin, P., Jullien, R., and Botet, R. 1986. *Europhys. Lett.*, **1**, 609.

Meakin, P., Ramanlal, P., Sander, L., and Ball, R. 1986. *Phys. Rev. A*, **34**, 5091.

Medina, E., Hwa, T., Kardar, M., and Zhang, Y. 1989. *Phys. Rev. A*, **39**, 3053.

Mon, K., Wansleben, S., Landau, D., and Binder, K. 1988. *Phys. Rev. Lett.*, **60**, 708.

Müller-Krumbhar, H. 1979. *Monte Carlo Methods in Statistical Physics*, volume 43. Springer-Verlag, Berlin.

Nattermann, T. and Renz, W. 1988. *Phys. Rev. B*, **38**, 5184.

Nelson, D. and Kosterlitz, J. 1977. *Phys. Rev. Lett.*, **39**, 120.

Novikov, E. 1965. *Sov.. Phys. JETP*, **20**, 1290.

Nozières, P. and Gallet, F. 1987. *J. Phys. (Paris)*, **48**, 353.

Pavlovska, A. and Nemow, D. 1977. *J. Cryst. Growth*, **39**, 346.

Plischke, M. and Rácz, Z. 1985. *Phys. Rev. A*, **32**, 3825.

Plischke, M., Rácz, Z., and Liu, D. 1987. *Phys. Rev. A*, **35**, 3485.

Rottmann, C. and Wortis, M. 1984. *Phys. Rev. B*, **29**, 328.

Rottmann, C., Wortis, M., Heyraud, J., and Métois, J. J. 1984. *Phys. Rev. Lett.*, **52**, 1009.

Saito, Y. 1978. *Z. Phys. B*, **32**, 75.

Saito, Y. 1980. *Ordering in Strongly Fluctuating Condensed Matter Systems.* Plenum, New York.

Sun, T., Guo, H., and Grant, M. 1989. *Phys. Rev. A. Rapid Communications*, **40**, 6763.

Swendsen, R. 1977. *Phys. Rev. B*, **15**, 5421.

Swendsen, R. 1978. *Phys. Rev. B*, **17**, 3710.

Van Beijeren, H. and Nolden, I. 1987. In Schommers, W. and Blackhagen, P. V., editors, *Structure and Dynamics of Surfaces*, volume 43 of *Topics in Current Physics*. Springer-Verlag, Berlin.

Vossen, J. and Kern, W., editors 1978. *Thin Film Processes.* Academic, New York.

Weeks, J. 1980. *Ordering in Strongly Fluctuating Condensed Matter Systems.* Plenum, New York.

Weeks, J. and Gilmer, G. 1979. *Adv. Chem. Phys.*, **40**, 157.

Wolf, D. and Kertész, J. 1987a. *J. Phys. A*, **20**, L257.

Wolf, D. and Kertész, J. 1987b. *Europhys. Lett.*, 4, 651.

Wolf, P., Gallet, F., Balibar, S., Rolley, E., and Nozières, P. 1985. *J. Phys. (Paris)*, **46**, 1987.

Zabolitzky, J. and Stauffer, D. 1986. *Phys. Rev. A*, **34**, 1523.

Zia, R. 1984. *Statistical and Particle Physics: Common Problems and Techniques.* SUSSP Publications, Edinburgh.

Zia, R. 1990. Private communication.